The Cellular Composition of Neurogenic Periventricular Zones in the Adult Zebrafish Forebrain

Benjamin W. Lindsey,[1] Audrey Darabie,[1] and Vincent Tropepe[1,2]*

[1]Department of Cell and Systems Biology, University of Toronto, Toronto, Ontario, M5S 3G5, Canada
[2]Centre for the Analysis of Genome Evolution and Function, University of Toronto, Toronto, Ontario, M5S 3G5, Canada

ABSTRACT

A central goal of adult neurogenesis research is to characterize the cellular constituents of a neurogenic niche and to understand how these cells regulate the production of new neurons. Because the generation of adult-born neurons may be tightly coupled to their functional requirement, the organization and output of neurogenic niches may vary across different regions of the brain or between species. We have undertaken a comparative study of six (D, Vd, Vv, Dm, Dl, Ppa) periventricular zones (PVZs) harboring proliferative cells present in the adult forebrain of the zebrafish (*Danio rerio*), a species known to possess widespread neurogenesis throughout life. Using electron microscopy, we have documented for the first time the detailed cytoarchitecture of these zones, and propose a model of the cellular composition of pallial and subpallial PVZs, as well as a classification scheme for identifying morphologically distinct cell types. Immunolabeling of resin-embedded tissue confirmed the phenotype of three constitutively proliferating (bromodeoxyuridine [BrdU]+) cell populations, including a radial glial-like (type IIa) cell immunopositive for both S100β and glutamine synthetase (GS). Our data revealed rostrocaudal differences in the density of distinct proliferative populations, and cumulative labeling studies suggested that the cell cycle kinetics of these populations are not uniform between PVZs. Although the peak numbers of differentiated neurons were generated after ~2 weeks among most PVZs, niche-specific decline in the number of newborn neurons in some regions occurred after 4 weeks. Our data suggest that the cytoarchitecture of neurogenic niches and the tempo of neuronal production are regionally distinct in the adult zebrafish forebrain. J. Comp. Neurol. 520:2275–2316, 2012.

INDEXING TERMS: neurogenesis; proliferation; ultrastructure; adult neural stem/progenitor cells; comparative; cell cycle; zebrafish

Adult neurogenesis occurs in well-circumscribed regions of the mature vertebrate brain. This process is initiated by the proliferation of stem and/or progenitor cells, which over time generate new neurons and glia. Adult neurogenesis is regulated, in part, through the interaction between neurogenic cells and neighboring cells that are present within their immediate microenvironment, or niche. Moreover, the niche itself may be largely unique in terms of its cellular composition, degree of plasticity, and the molecular factors maintaining it as an active site of adult neurogenesis in different regions of the brain or at different times during development. For instance, studies in the adult rodent brain show differences in the time course of neuronal differentiation, and the neuronal subtypes that arise from the subependymal zone (SEZ; also referred to as the subventricular zone [SVZ]) of the forebrain lateral ventricles or the subgranular zone (SGZ) of the hippocampal dentate gyrus (reviewed in Zhao et al., 2008).

These findings support the notion of niche-specific regulation at the cellular and molecular levels. Despite significant advances using rodent models, many nonmammalian vertebrates offer the opportunity to explore the regulation and composition of the neurogenic niche in both homologous structures as well as within novel

Grant sponsor: Natural Sciences and Engineering Research Council of Canada (NSERC); Grant number: 298525.

*CORRESPONDENCE TO: Vincent Tropepe, Ph. D., Department of Cell and Systems Biology, University of Toronto, 25 Harbord Street, Toronto, Ontario, M5S 3G5, Canada. E-mail: v.tropepe@utoronto.ca

Received October 20, 2011; Revised December 13, 2011; Accepted January 24, 2012
DOI 10.1002/cne.23065
Published online February 9, 2012 in Wiley Online Library (wileyonlinelibrary.com)

neuroanatomical loci where this trait is absent in mammals (Zupanc, 2001). Understanding how adult neurogenic niches are differentially regulated across vertebrate species will be an essential step in gaining a fundamental understanding of the functional significance of this conserved trait (Lindsey and Tropepe, 2006).

Studies of the mouse SEZ and SGZ niches have been seminal in constructing a detailed model of the cellular organization of the adult neurogenic niche and continue to serve as a basis for comparison as the stem cell niches of additional species are described (Doetsch et al., 1997; Seri et al., 2004). Serial reconstructions of the SEZ using electron microscopy have demonstrated the presence of five main cell type within this niche: glial fibrillary acidic protein (GFAP)-expressing neural stem cells (type B1), astrocytes (type B2), transiently amplifying progenitor cells likely committed to a neuronal fate (type C), and migrating neuroblasts (type A), all of which reside beneath a continuous layer of ependymal cells (type E) that lines the ventricle (Doetsch et al., 1997). Subsequent experiments confirmed that type B1 astrocytic cells were the resident adult neural stem cell within the SEZ niche (Doetsch et al., 1999).

Functional evidence supporting this view has come from studies using transgenic mice expressing herpes simplex virus thymidine kinase (tk) from the GFAP promoter that were exposed to the antiviral agent ganciclovir, resulting in the selective ablation of dividing tk-expressing cells (Sofroniew and Vinters, 2010). In vitro analysis of the cell lineage progression from type B cells to type A following ablation of GFAP-expressing cells showed the loss of stem cell-derived neurospheres, revealing the relationship and sequential dependence of the cell types within the niche upon one another (Morshead et al., 2003). The cellular composition of the hippocampal SGZ has similarly been described, demonstrating a lineage originating from radial glia-like stem cells through an intermediate proliferative stage (type D1) giving rise to committed neuronal progenitors (type D2) that over time differentiate into immature granule interneurons (type D3; Seri et al., 2001, 2004; Steiner et al., 2006). More recently, the importance of the proximity of vasculature to cell types within the niche for trophic support has been highlighted (Tavazoie et al., 2008), in particular for type B1 cells that have been shown to extend a process onto centrally localized blood vessels (Mirzadeh et al., 2008).

It has become clear that pronounced differences exists in the organization of the SEZ niche of vertebrates. This is true even among mammalian species arising from different orders. The SEZ of macaques, marmosets, and humans all possess a structurally distinct three-layer organization, comprising a continuous ependymal lining adjacent to the lateral ventricles, a middle hypocellular GAP layer, and a lateralmost astrocyte-ribbon layer (Gil-Perotin et al., 2009; Kam et al., 2009; Sawamoto et al., 2011). The hypocellular layer is absent in rodents, however, and thus far appears to be restricted to primates, although the significance of this layer remains unknown. Variations in cell types have also been observed. For instance, unlike the SEZ of most mammalian species studied, no type C cells were detected in the macaque SEZ (Gil-Perotin et al., 2009), a finding more closely related to the proliferative ventricular zone of reptiles and birds. Moreover, tanycytes present in neurogenic niches have only been reported in rodents (Doetsch et al., 1997).

Studies of the periventricular zone of reptiles and birds have revealed that even though anatomically homologous cell types comprise the wall of the lateral ventricle, these nonmammalian neurogenic niches lack type C cells and are generally characterized by the absence of a continuous layer of ependymal cells, in contrast to mammals (Perez-Sanchez et al., 1989; Perez-Canalles and Garcia-Verdugo, 1996; Font et al., 2001; Garcia-Verdugo et al., 2002). Furthermore, adult mammalian species share an SEZ and a distinct rostral migratory stream, although in humans the rostral migratory stream appears to gradually disappear after birth and is absent in adults (Sanai et al., 2011). Some evidence suggests that this migratory stream may also exist in birds (Rousselot and Nottebohm, 1995) and zebrafish (Adolf et al., 2006; Marz et al., 2010; Kishimoto et al., 2011), but has yet to be observed in any reptilian species studied to date. Given the differences identified between the SEZ of mammalian and nonmammalian animals to date, it is likely that niche organization and the cell–cell interactions that together determine its

Abbreviations

BrdU	bromodeoxyuridine
D	dorsal telencephalic area
Dc	central zone of D
Dd	dorsal zone of D
DEL	dorsal ependymal lining
DiV	diencephalic ventricle
Dl	lateral zone of D
Dm	medial zone of D
Dp	posterior zone of D
GF	growth fraction
GS	glutamine synthetase
Ppa	anterior part of parvocellular preoptic nucleus
PVZ	periventricular zone
SEM	scanning electron microscopy
SEZ	subependymal zone
SGZ	subgranular zone
TelV	telencephalic ventricle
TEM	transmission electron microscopy
V	ventral telencephalic area
Vd	dorsal nucleus of V
Vp	postcommissural nucleus of V
Vs	supracommisural nucleus of V
VS	ventricular surface
Vv	ventral nucleus of V

neurogenic capacity demonstrate significant variation among species.

Within the last decade the zebrafish (*Danio rerio*) has gained popularity as a model for adult neurogenesis owing to its robust neurogenic capacity throughout the mature brain. Early work revealed that numerous different neuroanatomical regions across the central nervous system (CNS) harbor mitotic cell populations (Zupanc et al., 2005), and more recently that nearly 50% of these cells differentiate to give rise to newborn adult neurons (Hinsch and Zupanc, 2007). A number of these proliferative niches are localized within distinct neuroanatomical regions adjacent to the brain ventricles (periventricular zone) similar to rodents, birds, and reptiles (Garcia-Verdugo et al., 2002). Within the forebrain, two regions surrounding the telencephalic ventricle have been suggested to be homologues to the hippocampus and amygdala of the mammalian forebrain (Wullimann and Rink, 2002; Salas et al., 2006), making the zebrafish an attractive model from a comparative standpoint.

The periventricular zone (PVZ) of the adult zebrafish includes several of the most active sites of neurogenesis throughout the forebrain. Separate studies have highlighted a strong dichotomy between the pallial and subpallial division of the rostral half of the adult forebrain in both glial phenotypes and the expression of various transcription factors of developmental importance. These studies have revealed that the PVZ is endowed with both slow and fast cycling cell populations, arising from a radial glia-like adult neural stem/progenitor cell (Adolf et al., 2006). Most recently, a classification scheme based on detailed immunohistochemical (Marz et al., 2010) and clonal analysis (Rothenaigner et al., 2011) has presented three types of cycling progenitor cells, types II, IIIa, and IIIb, as well as a nondividing glial type I cell (Marz et al., 2010). Moreover, the pallial–subpallial divisions of rostral forebrain PVZs has illustrated that progenitors express, and may be regulated by, different transcription and growth factors such as fibroblast growth factors (Adolf et al., 2006; Ganz et al., 2010). Nonetheless, despite a growing number of studies examining adult zebrafish telencephalic forebrain PVZs, we are still far from understanding some of the most fundamental questions, including the anatomical boundaries of these neurogenic compartments, their ultrastructural composition, and how this cellular organization might differ between distinct pallial and subpallial PVZs within the same species. The many sites of continuous neurogenesis in the zebrafish brain offer the opportunity to consider whether the composition and maintenance of the niche are governed by a set of similar cellular components or whether niche-specific environmental differences play a role in the neurogenic output of the niche.

The present study investigates the cellular composition of six distinct neurogenic PVZs in the adult zebrafish forebrain. By using a combination of immunohistochemistry, scanning, and transmission electron microscopy, we reveal the detailed cellular organization of these zones. Additionally, we examine differences in the cell cycle kinetics of niche-specific proliferative populations and compare the timeline of neuronal differentiation for each. The results reported here are compared with recent immunohistochemical studies documenting the putative progenitor cells within the adult zebrafish forebrain in order to broaden our understanding of the phenotype of cells composing these neurogenic PVZs. Our results provide a foundation for comparative studies of the cellular regulation between different neurogenic niches.

MATERIALS AND METHODS

Animals

Adult wild-type (AB) zebrafish (*Danio rerio*) of both sexes were obtained from our laboratory population and housed in a recirculation system (Aquaneering, San Diego, CA) under a 14:10 light–dark cycle at 28°C. All water chemistry parameters (pH, conductivity, nitrate, ammonia) were monitored daily. Fish were between 9 and 12 months old and were fed a diet of granular food (ZM Medium; ZM, Winchester, UK) and brine shrimp. Zebrafish were sacrificed by using an overdose of 0.4% tricaine methanesulfonate until all movement and respiration ceased. Immediately thereafter, the sex, total length (mm), and weight (g) of each fish was determined. Measurements from ~200 zebrafish yielded an average total length of 33.92 ± 2.56 mm and an average weight of 0.413 ± 0.136 g. Handling procedures were done in accordance with the policies set forth by the University of Toronto and the Canadian Council for Animal Care (CCAC).

BrdU administration

Animals were anesthetized in a solution of 0.04% tricaine diluted in facility water until movement and respiration slowed, and then injected intraperitoneally with a 10 mM bolus of bromodeoxyuridine (BrdU; Sigma, St. Louis, MO) diluted in 1X phosphate-buffered saline (PBS; pH 7.4) at a volume of 50 μL/g body weight fish (Zupanc et al., 2005) to detect proliferating cells in the S-phase of the cell cycle. Following injection, fish were monitored in a recovery tank until respiration and swimming returned to normal, and then transferred back to their housing tank until sacrifice.

Perfusion and fixation

Following sacrifice, animals were transcardially perfused through the ventricle of the heart to clear blood from brain vasculature and improve tissue fixation. For immunohistochemistry (IHC) on cryosectioned tissue, ice-cold 1X PBS was perfused by using a Model II Plus Syringe Pump (Harvard Apparatus, Dover, MA) until all effluent was clear, followed by 10 ml of ice-cold 4% paraformaldehyde (PFA) diluted in PBS. For transmission (TEM) and scanning (SEM) electron microscopy, ice-cold 0.1 M Sorenson's phosphate buffer (pH 7.4) was perfused followed by 10 ml of either 3% glutaraldehyde (GLUT) for ultrastructural analysis, or 0.1% GLUT/4% PFA for immuno-TEM labeling (EM grade, Electron Microscopy Sciences, Ft. Washington, PA). Thereafter, the braincase was removed and placed in fresh fixative for 3 hours at 4°C, after which time the brain was excised and placed in fresh fixative overnight at 4°C. For all electron microscopy analyses the forebrain was separated from midbrain at the level of the rostral optic tectum before being placed in fixative. For SEM analysis, forebrain hemispheres were additionally separated along the midline for visualization of the medial ventricular surface.

Cryosectioning

Brain tissue was cryoprotected in ascending sucrose solutions before being placed in 30% sucrose overnight at 4°C. Tissue was infiltrated with a 2:1 solution of 30% sucrose/O.C.T. Compound (Tissue-Tek, Sakura, Torrance, CA) for 30 minutes at room temperature, before being cryoembedded en bloc at −20°C. Brains were serially sectioned at 20 μm intervals by using a Leica Cryostat (Model CM3050), and sections were collected onto Superfrost Plus slides (VWR, Chicago, IL), and stored at −80°C until IHC labeling.

Immunohistochemistry

Cryosections were briefly postfixed in 4% PFA, blocked for 1 hour, and incubated in primary antibody overnight at 4°C (Table 1). For BrdU labeling, antigen retrieval was performed by immersing sections in 10 mM sodium citrate buffer (pH 6.0) for 30 minutes at 65°C and incubating in 1 M hydrochloric acid for 1 hour at 37°C to denature the double-stranded DNA. For HuC/D and γ-tubulin labeling, antigen retrieval was carried out by incubating sections in 50 mM Tris Buffer (pH 8.0) for 30 minutes at 65°C. The next day, sections were incubated in one of the following Alexa Fluor-conjugated secondary antibody (Jackson ImmunoResearch, West Grove, PA) for 2 hours at 37°C: goat-anti-rat, goat-anti-mouse, or goat-anti-rabbit Cy3 (1:400) or Cy2 (1:200). Nuclear staining was performed by using a 1% solution of Hoechst 33258 applied

TABLE 1.

Primary antibodies used for immunohistochemical labelling

Name	Immunogen	Manufacturer (cat. #)	Host	Type	Dilution	Target Phenotype
Bromodeoxyuridine (BrdU)	BU1/75(ICR1) – clone	Serotec (MCA2060)	Rat	Monoclonal (IgG2a)	1:1000	All dividing cells in S-phase
Bromodeoxyuridine (BrdU)	BMC 9318 - clone	Roche (11170376001)	Mouse	Monoclonal (IgG_1)	1:100	All dividing cells in S-phase
Anti-Human Neuronal Protein HuC/HuD(HuC/D)	Aa 240-251 of human HuD	Molecular Probes (16A11)	Mouse	Monoclonal (IgG_{2b+k})	1:400	All neurons
Polysialic Acid Neural Cell Adhesion Molecule (PSA-NCAM)	Viable Meningococcus group B (strain 355)	Millipore (MAB5324)	Mouse	Monoclonal (IgM)	1:800	Newly differentiated migrating neurons
Glutamine Synthetase (GS)	Glutamine synthetase purified from sheep brain	Millipore (MAB302)	Mouse	Monoclonal (IgG_{2a})	1:800	Astrocytes/radial glia
S100β	S100 isolated from cow brain	Dako Cytomation (Z0311)	Rabbit	Polyclonal	1:800	General glia, including ependyma
CalbindinD-28k	Purified rat calbindin D-28	SWANT (CB-38a)	Rabbit	Monoclonal	1:600	Calbindin containing neurons
Tyrosine Hydroxylase (TH)	Tyrosine hydroxylase purified from PC12 cells	Millipore (MAB318)	Mouse	Monoclonal ($IgG1_k$)	1:400	Adrenergic neurons
Pax-6	Peptide (QVPGSEPDMSQYWPRLQ) derived from the C-terminus of the mouse Pax-6 protein	Covance (PRB-278P)	Rabbit	Polyclonal	1:100	Stem/progenitor cells
SOX-2	Synthetic peptide corresponding to amino acids 113-127 of human, mouse and rat SOX-2	StemCell Technologies (01438)	Rabbit	Polyclonal	1:400	Stem/progenitor cells
γ-tubulin (tubg1)	Recombinant protein fragment containing a sequence corresponding to a region within amino acids 3-154 of tubg1	GeneTex (GTX124352)	Rabbit	Polyclonal	1:500	Ciliary basal bodies

to sections for 15 to 20 minutes. All double-labeling protocols were performed sequentially, and brain sections were mounted in 100% glycerol for imaging.

Primary antibody characterization

Anti-BrdU

The mouse (Roche Diagnostics, Indianapolis, IN) and rat (Serotec, Bicester, UK) monoclonal anti-BrdU antibodies label the nucleus of cells in the S-phase of the cell cycle, by recognizing BrdU incorporated into single-stranded DNA, attached to a protein carrier, or free BrdU (manufacturer's technical information; Wang et al., 2006; Silvestroff et al., 2010). Both antibodies have been shown to successfully label the nuclear profile of BrdU+ mitotic cells in the adult zebrafish brain (Adolf et al., 2006; Grandel et al., 2006; Ganz et al, 2010). Rat anti-BrdU does not cross-react with thymidine but does react weakly with chlorodeoxyuridine, whereas mouse anti-BrdU shows minimal cross-reactivity with iodouridine (manufacturer's technical information). Positive labeling of both antibodies was originally tested in zebrafish gut tissue, an area shown to be highly proliferative (Crosnier et al., 2005), before IHC labeling in the adult forebrain. Negative controls performed by using non-BrdU–injected zebrafish or by omitting the primary antibody, showed no BrdU+ labeling in the brain. Based on the above, we were confident that anti-BrdU only labeled nuclei incorporating BrdU into newly synthesized, single-stranded DNA.

Anti-HuC/D

The anti-human neuronal protein HuC/HuD (HuC/D) monoclonal antibody (Molecular Probes, Eugene, OR) was raised against the human HuD peptide QAQRFRLDNLLN (Marusich et al., 1994). The Hu antigen is an RNA-binding protein of the embryonic lethal abnormal visual (Elav) family that is specific to neuronal proteins of the Elav family members HuC, HuD, and Hel-N1 and is expressed most intensely in the perikaryal region of neurons but can also be detected in neuronal nuclei (Yang et al., 2010; Marusich et al., 1994; manufacturer's technical information). Numerous studies of the zebrafish brain have employed this marker to identify resident and newly derived populations of neuronal cells (Zupanc et al., 2005; Grandel et al., 2006; Pelligrini et al., 2007; Topp et al., 2008; Zupanc et al., 2009; Rothenaigner et al., 2011).

Anti-PSA-NCAM

The anti-polysialic acid–neural cell adhesion molecule (PSA-NCAM) monoclonal antibody (Millipore, Bedford, MA) detects a single band of 180 kDA (Rougon et al., 1986). PSA is a long, linear homopolymer that is attached to NCAM, displays the greatest level of expression in precursor cells during early development and is known to promote their migration following cell division (manufacturer's technical information). PSA-NCAM has been shown to be a reliable marker for the detection of young, migrating neurons in the postnatal and adult brain of mammals (Seki and Arai, 1995; Doetsch et al., 1999), and more recently the mature forebrain of zebrafish (Adolf et al., 2006; Chapouton et al., 2010; Marz et al., 2010).

Anti-GS

The anti-GS (glutamine synthetase) monoclonal antibody (Millipore) was purified from sheep brain and its enzymatic activity makes it an ideal marker of astrocytes (manufacturer's technical information). Additionally, glutamine synthetase is considered an important enzyme in the recycling of the neurotransmitter glutamate (manufacturer's technical information). Recently, glutamine synthetase has been documented in the periventricular zone of the adult zebrafish brain as a marker of radial glial cells (Grupp et al., 2010).

Anti-S100β

The anti-S100β polyclonal antibody (Dako, Carpinteria, CA) labels S100β strongly, with little to no reactivity with other variants of S100 proteins tested based on Western blotting of purified human recombinant S100 proteins (manufacturer's technical information). S100 is a multigene family of low molecular weight calcium-binding proteins, comprising 19 members that are differentially expressed in a large number of cell types, with S100β being most abundant in glial cells of the central and peripheral nervous system (manufacturer's technical information). Anti-S100β has been used as a general glial marker (Wainwright et al., 2004) in the proliferation zones of the adult zebrafish brains, and we obtained a similar pattern of labeling as shown previously during in vivo and in vitro studies (Grandel et al., 2006; Kaslin et al., 2009; Marz et al., 2010; Rothenaigner et al., 2011).

Anti-calbindin

The anti-calbindin monoclonal antiserum (Swant, Bellinzona, Switzerland) was produced against recombinant rat calbindin D-28k, with this calcium-binding protein recognized as a single band of approximately 27–28 kDa in immunoblots (manufacturer's technical information). The CB protein has been used as a reliable marker of subpopulations of neurons both in the enteric nervous system (Uyttenbroek et al., 2010) and in the adult brain (Zupanc et al., 2005; Castro et al., 2006) of zebrafish. Presently, only a predicted protein sequence is available for zebrafish calbindin D-28k (XP 001341604; http://www.ncbi.nlm.nih.gov; Uyttenbroek et al., 2010).

Anti-TH

The anti-tyrosine hydroxylase (TH) monoclonal antibody (Millipore) specifically recognizes an epitope on the outside of the regulatory N-terminus, and is used to identify neuronal subpopulations having dopaminergic or noradrenergic phenotypes (manufacturer's technical information). The pattern of immunostaining seen in our study is in agreement with previous labeling studies of TH-immunoreactive cells in the vertebrate forebrain (Grandel et al., 2006; Dimitrov and Usdin, 2010).

Anti-Pax6

The anti-Pax6 polyclonal antibody (Covance, Princeton, NJ) was generated from the peptide sequence QVPGSEPDMSQYWPRLQ derived from the C-terminus of the mouse Pax6 protein and purified on a peptide affinity column (manufacturer's technical information; Roesch et al., 2008). The peptide sequence is highly conserved among Pax6 of various species, making this a useful marker for studying cell populations in the brain during early and postnatal development (manufacturer's technical information). The last 17 amino acids of the peptide sequence show 100% identity between mouse and zebrafish Pax6a, and greater than 88% identity with Pax6b (Ensembl). This polyclonal antibody is therefore likely capable of detecting both endogenous Pax6a and Pax6b proteins. The *Pax6* gene encodes a transcription factor that contains a paired domain and a homeodomain, is involved in peripheral and CNS development, and has been shown to be expressed in stem/progenitor cells (Sakurai and Osumi, 2008). Pax6 is required for the multipotent state of retinal progenitor cells (Marquardt et al., 2001), and the expression patterns of *pax6a* in the teleostean forebrain (Wullimann and Rink, 2002) and *pax6a* and *pax6b* in the neurogenic zones of the mature zebrafish forebrain (Adolf et al., 2006) have recently been documented.

Anti-SOX2

The anti-SOX2 polyclonal antibody (Stem Cell Technologies, Singapore) was generated by using a synthetic peptide sequence corresponding to amino acids 113–127 of human, mouse, and rat Sox2, and is a useful marker for the detection of undifferentiated neural cells in the central nervous system, which have stem cell-like characteristics (manufacturer's technical information). The amino acid sequence 113–127 used to generate this antibody shows 100% identity between mouse and zebrafish (Ensembl). This marker has been previously used to successfully examine populations of neural stem/progenitor markers in the developing and adult mouse brain within the SGZ of the dentate gyrus (Tseng et al., 2010).

Anti-γ-tubulin

The anti-tubg1 polyclonal antibody (GeneTex, Irvine, CA) was derived from a recombinant protein fragment containing a sequence corresponding to a region within amino acids 3–154 of γ-tubulin (manufacturer's technical information). Zebrafish neurons and embryos were used as positive control tissues to confirm the expected labeling pattern of this antibody, localized specifically to the basal body of cilia similar to other γ-tubulin antibodies (Mirzadeh et al., 2008, 2010).

Demarcating the periventricular zones

Many of the proliferative/neurogenic niches in the adult zebrafish forebrain are situated adjacent to the telencephalic and diencephalic ventricles, and are localized within a subregion of distinct neuroanatomical nuclei that line the lumen. A process of eversion (an outward bending) occurs in teleostean fishes such as the zebrafish, unlike evagination of the distal walls of the prosencephalic vesicle during early mammalian brain development, which results in the formation of internal forebrain ventricles (Broglio et al., 2005). The eversion process in teleosts gives rise to two solid forebrain hemispheres divided by a midline ventricle, which extends a short distance dorsolaterally as a narrow lumen beneath a thin ependymal lining. The properties of these neurogenic compartments contain the trademark features of a typical adult neurogenic niche, namely, resident proliferating cell populations that harbor the potential to give rise to adult-born neurons. Because the zebrafish brain undergoes eversion during telencephalic hemisphere development (Wullimann and Rink, 2002), resulting in many neurogenic niches positioned next to the forebrain ventricles, in this study we refer to each of the six niches under investigation as periventricular zones (PVZs). For example, a neurogenic niche present within the dorsal telencephalic area (D) would be referred to as the "PVZ of D."

To identify the PVZs in the adult zebrafish forebrain with the greatest density of proliferation, animals ($n = 10$) were sacrificed 2 hours after a 10-mM injection of BrdU. Cryosections of the forebrain between cross-sectional levels 50–107 according to the adult zebrafish brain atlas (Wullimann et al., 1996) were immunostained to visualize BrdU. For each section, all BrdU+ cells were counted within each region of the brain, and the resulting mean was calculated by region across all brains. The number of BrdU+ cells per forebrain region was compared statistically to determine regions with the greatest levels of cell proliferation. The localization of BrdU+ cells in these regions in combination with ultrastructural observations of the position of morphologically distinct cell types was next used to demarcate the lateral aspect of

PVZs opposite the ventricle and in relation to the deeper parenchymal region, in order to obtain the total surface area of each. Surface area (μm^2) was calculated by tracing along the boundaries of each PVZ in maximum projection confocal images by using Leica Application Suite Advanced Fluorescence Lite 2.3.0 proprietary software. The mean number of BrdU+ cells per PVZ at each rostrocaudal level was then normalized to the estimated total number of cells calculated in a separate set of age-matched animals (n = 6) stained with Hoechst 33258.

Cell cycle kinetics

Previous work has demonstrated the presence of both fast and slow proliferating cell populations in distinct neurogenic niches of the pallial and subpallial regions of the adult zebrafish telencephalon (Adolf et al., 2006). Here, a cumulative labeling protocol based on the method of Nowakowski et al. (1989) was used to examine in detail the cell cycle kinetics between anatomically defined neurogenic PVZs. This method has been successfully applied to the SEZ of the adult mouse brain (Morshead and van der Kooy, 1992), the developing mouse brain (Kim and Shen, 2008), and most recently the zebrafish retina (Wong et al., 2010). By injecting BrdU at regular intervals over time and then by using BrdU immunohistochemistry, it is possible to determine the maximum labeling index LI_M (or growth fraction [GF]), known as the proportion of cells that comprise the proliferating population, in addition to the corresponding time at which the maximum number of BrdU+ cells are labeled (T_M), the length of the cell cycle (T_C), and the length of the DNA-synthesis phase (T_S). Two assumptions are made when using this protocol. First, the proliferative cells within each distinct PVZ are assumed to be a single population, asynchronously distributed across the various stages of the cell cycle. Second, each population is undergoing a steady-state growth phase.

Zebrafish 10 months of age were injected one to seven times (n = 5/group) beginning at 08:00 with a 1 mM bolus of BrdU in 2-hour increments for up to 12 hours, and sacrificed 30 minutes following the last injection. For each injection group, the total numbers of BrdU+ cells across three to four brain sections within the boundaries of each PVZ were counted and averaged across animals. Mean values at each time point were next plotted for each PVZ by using GraphPad Prism 5.04 proprietary software to examine the line of best fit. The notion that after a finite number of BrdU injections all proliferating cells in the population should be labeled, resulting in the GF and the commencement of a plateau at which time no additional cells take up BrdU, suggests that the data should fit a one-phase exponential association model. However, given the toxicity effects of BrdU on cell survival with continuous exposure (Kee et al., 2002; Taupin, 2007), in fitting these data, we considered that following the plateau phase of the curve, cell death may occur. Therefore, the preferred fit of our data to a first (linear) or second (quadratic) order polynomial using regression analysis by least squares fitting was compared for each PVZ by using the above software. When the preferred model was a linear regression, the last data point was considered the minimum GF, and this value was used to estimate cell cycle parameters. In the event that neither model fit the data with confidence, the possibility of two distinct mitotic populations within the PVZ was investigated by fitting the data to a third order polynomial (cubic). When a plateau could be observed, the first time point when the slope of the curve approached 0 was taken as the GF and the start of the plateau. All data points prior to and including the GF were then replotted to a linear regression to determine cell cycle parameters. By using the equations slope = GF/T_C, and $Tm = T_C - T_S$, we could then calculate T_C and T_S. For all graphs the 95% confidence interval bands are shown.

Immunohistochemical experiments

For all sets of markers the percentage of co-labeled BrdU+ cells among the total mitotic cell population sampled within each PVZ was quantified. Four to six animals were examined for each set of markers with the exception of qualitative observations made by using markers for cilia and vasculature, for which only two to three animals were used.

Characterization of periventricular zones

Immunohistochemistry was used to compare differences in the phenotype of mitotically active cell populations across PVZs, in addition to the presence of ciliated cells and vasculature. The phenotype of mitotic cells was examined 2 hours post-BrdU injection by double-labeling with BrdU and Pax6, S100β, GS, or HuC/D antibodies. To identify cells displaying cilia along the ventricular surface, whole-mount preparations of forebrain hemispheres and cross-sectional images were labeled with γ-tubulin and counterstained with Hoechst 33258. A *Tg[flk1:gfp]* transgenic zebrafish line that specifically labels the endothelial cells of the vasculature was used to assess the presence of vessels within niches (A kind gift from Dr. Ian Scott, University of Toronto, Canada).

Neuronal and glial differentiation and cell migration

In order to track the time course of differentiation of BrdU+ cells to mature neuronal or glial phenotypes between PVZs, we injected zebrafish with BrdU and sacrificed animals after 1, 2, or 4 weeks. To investigate the time course of BrdU+ cell differentiation, we first

TABLE 2.

Morphological details of design-based stereology used during cell counting

	Periventricular zone					
Variable	*D*	*Vd*	*Vv*	*Dm*	*Dl*	*Ppa*
Bromodeoxyuridine						
Rostrocaudal boundaries*	50–60	50–85	60–85	71–107	71–107	92–107
Sampling frequency	every 4th sec.	every 4th sec.	every 4th sec.	every 4th sec.	every 4th sec.	every 4th sec.
Mean # of sections sampled/brain	6.4	12.1	9.3	12.3	11.7	6.33
# of biological samples	10	10	10	10	10	10
z-stack optical sections (μm)	1	1	1	1	1	1
Hoechst 33258						
Rostrocaudal boundaries*	50–60	50–85	60–85	71–107	71–107	92–107
Sampling frequency	1 hem/sec. x2	1 hem/sec. x2	1 hem/sec. x2	1 hem/sec. x2	1 hem/sec. x2	1 hem/sec. x2
Mean # of sections sampled/brain	2	2	2	2	2	2
# of biological samples	7	7	7	7	7	7
z-stack optical sections (μm)	1	1	1	1	1	1
Co-labelling						
Rostrocaudal boundaries*	50–60	50–60	60	71–85	98–107	98–107
Sampling frequency	1 hem/sec. x2	1 hem/sec. x2	1 hem/sec. x2	1 hem/sec. x2	1 hem/sec. x2	1 hem/sec. x2
Mean # of sections sampled/brain	2	2	2	2	2	2
# of biological samples	4–6	4–6	4–6	4–6	4–6	4–6
z-stack optical sections (μm)	0.5	0.5	0.5	0.5	0.5	0.5

*Rostrocaudal boundaries listed refer to cross-sectional levels based on the adult zebrafish brain atlas (Wullimann et al., 1996)

examined the percentage of BrdU+/PSA-NCAM+ cells within PVZs 1 and 2 weeks after BrdU injection. Newly derived populations immunoreactive for BrdU/HuC/D were investigated at all three time points (1, 2, and 4 weeks), in addition to a separate set of animals examined 2 hours post-BrdU injection that served as a negative control group. Four weeks post-BrdU injection the differentiated phenotype of BrdU+ cells was assessed by IHC by using the following sets of markers: BrdU/GS, BrdU/calbindin, and BrdU/TH. A separate zebrafish transgenic line *Tg[dlx5a/6aIG:gfp]* (n = 3) was examined 10 months following a single pulse of BrdU to detect the presence of BrdU+/dlx5a/6aIG+ cell populations. The *Tg[dlx5a/6aIG:gfp]* transgene expression has been shown to mark γ-aminobutyric acid (GABA)ergic neurons within the embryonic and larval brain (MacDonald et al., 2010; Souza et al., 2011).

To next assess the migration of differentiating proliferative cells, the distance of BrdU+ cells from the ventricle in individual PVZs was measured following 2-hour, 4-week, and 10-month chase periods by using Leica Application Suite Advance Fluorescence Lite 2.3.0 proprietary software. For each zone and time point, a minimum of n = 6 BrdU+ cells were randomly sampled within each brain. Distance measurements were taken from the center of BrdU+ nuclei to the edge of the ventricle or pial surface (Dl). In the PVZ of D, only BrdU+ cells along the midline were measured.

Cell counting and imaging

All imaging of immunostained tissue was performed by using a Leica TCS SP5 confocal microscope. Cell counting experiments were carried out in order to obtain a representative estimate of the number of positively single- or co-labeled cells within respective PVZs across tissue sections (variables summarized in Table 2). The purpose here was not to estimate the total number of positive cells within the entire rostrocaudal neuraxis of each niche. For BrdU labeling alone, a minimum of every fourth section was examined through the rostrocaudal axis of the forebrain, and all BrdU+ cells were counted within each region of the brain. Cell counts for nuclear labeling of Hoechst 33258 and double-labeling experiments were sampled from a single hemisphere on a minimum of two separate cryosections within the boundaries of each PVZ from each biological sample at the respective rostrocaudal level. For all IHC labeling, z-stacks of 0.5–1 μm were created from 20 μm immunolabeled cryosections at 40× (BrdU, Hoechst 33258) or 100× (double-labeling) magnification. The position of PVZs examined for IHC prevented the possible bias of "lost caps" during unbiased virtual counting, because all forebrain regions were located rostral to the optic tectum and caudal to the olfactory bulbs (Schmitz and Hof, 2005). As a result, it was not necessary to introduce a guard zone because cryosectioning was done throughout the entire rostrocaudal neuroaxis of each intact brain.

Cell counting was accomplished by counting through the z-stack using the optical disector principle (West, 1999; Geuna, 2005) with Leica Application Suite Advance Fluorescence Lite 2.3.0 proprietary software. The optical depth of all z-stacks ranged between 14 and 20 μm. During cell counting, positively labeled nuclei were used as the characteristic point for BrdU, Hoechst 33258, Pax6,

Sox2, TH, calbindin, and *Tg[dlx5a/6aIG:gfp]*, whereas cytoplasmic labeling was used for S100β, GS, PSA-NCAM, and HuC/D as newly labeled cells came into focus within the counting frame through the depth of the tissue section. To confirm co-labeling of antibody markers, z-stacks taken at 100× magnification were further examined by using orthogonal sectioning. All images shown are maximum projections, with the exception of images of orthogonal views used as evidence for co-labeling, and were adjusted for brightness and contrast by using Adobe Photoshop 7.0 software.

Scanning electron microscopy

Scanning EM was performed to examine the ventricular wall en face for the presence of ciliated cells. Following perfusion and fixation, brain hemispheres (n = 6) were rinsed with 0.1 M Sorenson's phosphate buffer and then dehydrated through an ascending ethanol series, before being infiltrated in a second ascending series of 100% ethanol and hexamethyldisilizane (HMDS) and placed in fresh HMDS overnight. Specimens were mounted on stubs, sputter-coated with gold–palladium for 50 seconds (SCD050, Bal-Tec, Los Angeles, CA), visualized with a Hitachi S-2500 scanning electron microscope, and imaged by using Quartz PCI software.

Transmission electron microscopy

Transmission EM was used to characterize the ultrastructural composition of PVZs. Following overnight fixation of forebrains (n = 7 D, Vd, Vv, Dm, Ppa; n = 4 Dl) in 3% GLUT, specimens were rinsed in 0.1 M Sorenson's phosphate buffer and postfixed for 2 hours with 1% osmium tetroxide. Thereafter, tissue was rinsed and dehydrated through an ascending ethanol series, and then infiltrated with an ascending series of 100% ethanol and Spurr's epoxy resin. The next day, tissue was infiltrated with fresh Spurr's resin twice over a 6-hour period and then flat-embedded and polymerized at 65°C overnight. Using a Leica EM UC6 ultramicrotome, 1 μm semithin sections and 100 nm ultrathin sections were taken at the corresponding rostrocaudal level of each PVZ. At each level, semithin sections collected onto glass slides were stained with 0.035% Toluidine Blue/Methylene Blue diluted in methanol, whereas ultrathin sections were collected onto copper grids for TEM imaging. Ultrathin sections were stained with 3% uranyl acetate in 50% methanol for 45 minutes, followed by Reynold's lead citrate for 10 minutes, and then dried overnight. Imaging was done by using a Hitachi H-7000 transmission electron microscope and AMT Image Capture Engine Software (Version 5.44.599).

To first examine the overall ultrastructural organization of PVZs, low-magnification TEM images (2–4 K) were taken at rostrocaudal levels 60 (D, Vd, Vv), 85 (Dm), and 98 (Dl, Ppa). These images were used to mark the borders of each PVZ for subsequent analysis of cell types and cell frequencies between niches. For detailed morphological analysis of the different cell types composing PVZs, a minimum of three cells of each type having morphologically unique ultrastructural features, from each PVZ and across all forebrains, was sampled. When only a few cells of a given morphology could be observed within the confines of the PVZ, all cells identified were analyzed. To characterize cell types, the following features were examined: nucleus: contour, color, chromatin organization, number of nucleoli, length of long and short axis of the nucleus (short axis taken at half the long axis); cytoplasm: percentage, color, presence of mitochondria, cilia, microvilli, vacuoles, lipid droplets, dense bodies; localization of cell types; and cell–cell contacts. By using these criteria, the morphological profile and frequency of each cell type within each PVZ and as a percentage of all cells examined were calculated. Based on the morphological features revealed, a model representing the cellular organization of PVZs and a classification scheme of the distinct cell types making up the different niches were established.

TEM immunohistochemistry

To determine the molecular phenotype of cells identified at the ultrastructural level, two labeling protocols were employed. To identify mitotic cells and those having a glial phenotype, we injected zebrafish (n = 2) with a 10 mM bolus of BrdU twice over a 4-hour period, before processing the forebrain for embedding in LR White hydrophilic resin (Electron Microscopy Sciences). In brief, tissue was washed in 0.1 M Sorenson's phosphate buffer following perfusion and fixation and then dehydrated in an ascending ethanol series beginning with 70% ETOH at 4°C and terminating in 100% ETOH at −20°C. Tissue was next infiltrated in an ascending series of LR White: 100% ETOH over a 2-day period at −20°C. Forebrains were then placed in a silicone mold filled with LR White and 0.5% benzoin methyl ether. The mold was covered with Aclar film and placed in a Leica automatic freeze substitution unit. The LR White was polymerized with UV light for 48 hours at −10°C followed by 24 hours at 20°C. At the corresponding level of each PVZ, 500 nm semithin sections were collected onto glass slides and 80 nm ultrathin sections were collected onto formvar-coated nickel grids for subsequent IHC labeling.

For BrdU labeling, tissue was first pretreated with 2 M HCl for 20 minutes to denature the double-stranded DNA. For postembedding labeling of all antibodies, tissue was rinsed with distilled water and incubated in 1% bovine

serum albumin (BSA) for 30 minutes. Tissue was next incubated in mouse-anti-BrdU (1:20), rabbit-anti-S100β (1:160), or mouse-anti-GS (1:80) primary antibody diluted in incubation buffer for 1 hour. Thereafter, sections were incubated in the appropriate anti-mouse or anti-rabbit IgG secondary antibody conjugated to 10-nm gold diluted in incubation buffer for 2 hours. Tissue was then postfixed in 2% GLUT for 10 minutes, stained with 2% aqueous uranyl acetate for 2.5 minutes, and finally stained with lead citrate for 30 seconds. For each antibody, one set of grids was processed without primary antibody as a negative control, whereas in another set contrast staining was omitted to better visualize gold particles in positively labeled tissue. All imaging was done as described for TEM analysis.

To label neurons at the ultrastructural level, a preembedding protocol was used. This protocol was additionally employed to further assess cell types having a glial phenotype. Following fixation, forebrains ($n = 6$) were embedded en bloc in a 15% solution of agar. Tissue was cut into 80-μm-thick sections through the rostrocaudal axis by using a Leica Vibratome (VT12005) and floated onto ice-cold 1X PBS buffer and stored at 4°C until staining. IHC was carried out by using a mouse-anti-GS (1:100) or mouse-anti-HuCD (1:400) primary antibody in conjunction with an anti-mouse/rabbit, horseradish peroxidise (HRP)/3,3′-diaminobenzidine (DAB) detection kit as per the manufacturer's protocol (ab64264; Abcam, Boston, MA). Labeled sections were then stored in 0.1 M Sorensen's phosphate buffer before processing with Spurr's resin for electron microscopy as described previously. Ultrathin sections were stained only with uranyl acetate for 20 minutes before TEM imaging.

Between 5 and 15 ultrathin sections were surveyed for each antibody marker across PVZs. All cell types positively labeled for specific markers were examined following both labeling protocols; cell types immunonegative for markers were not analyzed in detail. The morphology of immunopositive cells was then correlated with our initial classification of the distinct cell types making up the different PVZs under investigation.

Statistical analysis

All values are expressed as mean ± standard deviation. Differences in pairs of means were assessed by using independent-samples t-tests. Multiple mean comparisons were validated by using a one-way ANOVA, with Tukey's HSD post hoc tests applied when significance was present. Samples were considered significant at $P \leq 0.05$. All statistical analyses were performed by using SPSS Statistics 17.0 and graphs created by using SigmaPlot 11.0, Microsoft Excel 2003, or GraphPad Prism 5.04 proprietary software.

RESULTS

Variation in the relative size of the proliferative cell population along the rostrocaudal axis exists within distinct periventricular zones

To initially determine the most proliferative neuroanatomical regions of the adult zebrafish forebrain between rostrocaudal levels 50–107 (Wullimann et al., 1996), BrdU labeling was used to mark cells in the S-phase of the cell cycle following a single 2-hour BrdU injection. By counting dividing cells in 20 μm sections throughout the rostrocaudal axis of 11 different regions, we found six distinct loci having a significantly higher number of BrdU+ cells than all others examined (one-way ANOVA, Tukey's HSD post hoc test), including D, Vd, Vv, Dm, Dl, and Ppa (Fig. 1A–C). In contrast, we noted that the central zone of the dorsal telencephalon (Dc) was nearly void of mitotic cells (Fig. 1C), demonstrating a general lack of proliferative populations residing within the central parenchyma of the forebrain. However, our analyses did not rule out the possibility of parenchymal neurogenesis, and further studies are required to examine this issue more rigorously. Among the six highly proliferative regions, D had a significantly higher absolute number of BrdU+ cells compared with other regions, localized within the rostral forebrain. The ventral nucleus of V (Vv) had the second greatest number of BrdU+ cells and was significantly higher than Dm, where the least number of BrdU+ cells were detected. Proliferating cell populations were localized adjacent to the telencephalic (D, Vd, Vv, Dm, Dl) or diencephalic (Ppa) ventricles, comprising only a small fraction of each neuroanatomical region (Figs. 1A,B, 3). Very few BrdU+ cells were seen more than three to four cell diameters from the ventricle 2 hours post-BrdU injection, with almost no cells observed in the deeper parenchyma of these regions. Given the well-circumscribed ventricular position of the proliferating cells within these neuroanatomical regions, we hereafter will refer to these highly proliferative regions as periventricular zones.

We next asked whether the relative number of BrdU+ cells varied along the rostrocaudal axis of each PVZ. By normalizing the number of BrdU+ cells to the estimated total cell population within the surface area of each defined region, we were able to quantify the percentage of BrdU+ cells. These experiments yielded three main observations. First, there exists significant variation in the relative number of BrdU+ cells at different rostrocaudal levels in the PVZ of Vd, Vv, Dl, and Ppa, but not D or Dm (Fig. 2C,I; one-way ANOVA, Tukey's HSD post hoc test; Fig. 2). In Vd and Vv, a drastic decrease in the size of the mitotic population occurs caudal to cross-sectional level 60 (Fig. 2F), whereas the opposite trend is seen in Dl and

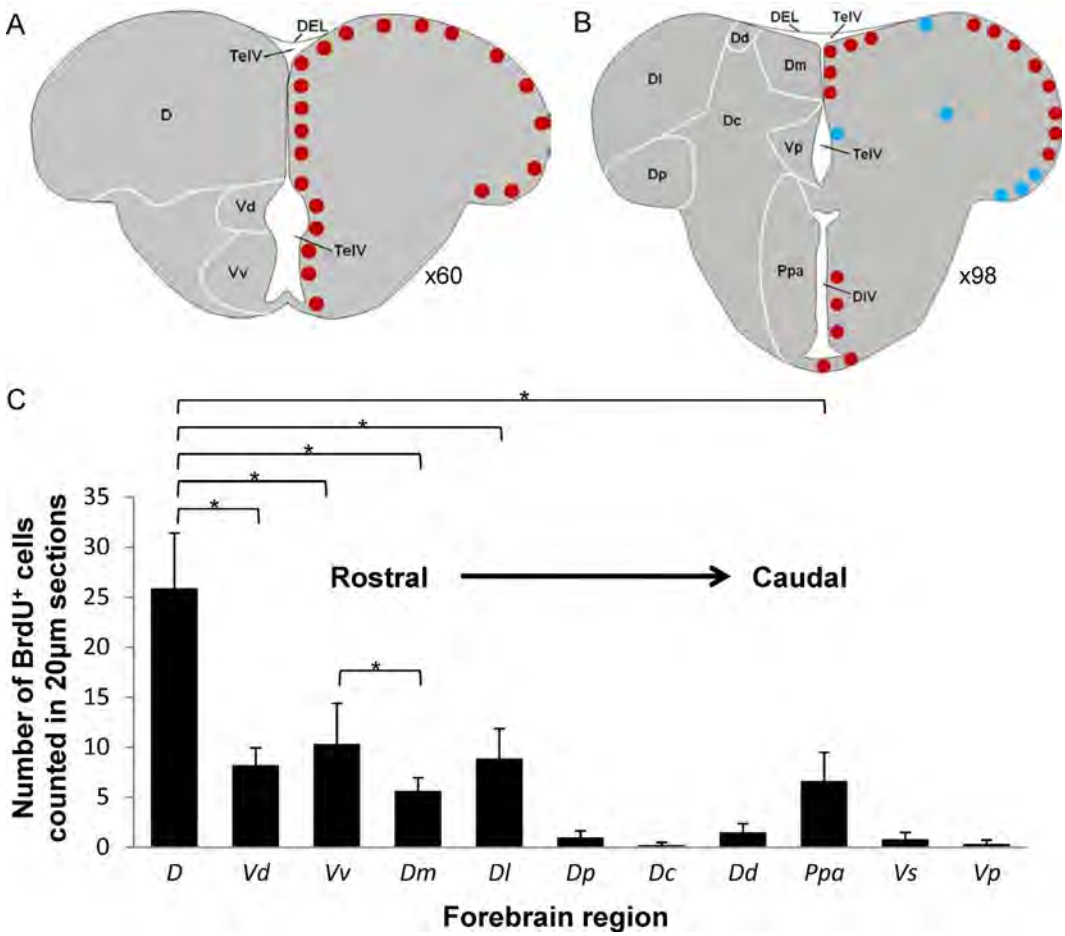

Figure 1. Bromodeoxyuridine-positive labeling examined across 11 neuroanatomical regions in the adult zebrafish forebrain used to determine the major proliferation zones. **A,B:** Schematics depict the location of BrdU+ cells along the border of the ventricle at two rostrocaudal levels (×60, ×98) that include the specific regions investigated (Vs not shown). Red dots indicate regions with significantly higher levels of BrdU+ labeling following a 2-hour pulse-chase compared with regions with blue dots as per the graph in C. **C:** Total number of BrdU+ cells counted through the entire rostrocaudal axis for each region in 20 µm cryosections. The number of BrdU+ cells in the proliferation zones of D, Vd, Vv, Dm, Dl, and Ppa were significantly greater than all other zones examined, and thus for clarity no indication of significance is denoted on the graph for these comparisons. Significance (*) was determined by using one-way ANOVA and Tukey's HSD post hoc tests ($P \leq 0.05$). For abbreviations, see list.

Ppa, resulting in a gradual increase in the size of the BrdU+ population from the rostral- to caudalmost level (Fig. 2L,O). Second, our surface area estimates showed widespread variation in the overall size of each of these six PVZs, with the order from largest to smallest being D, Dl, Ppa, Dm, Vv, Vd (Table 3). However, there was no correlation between the total surface area and the number of BrdU+ cells in each PVZ. Third, our normalized data demonstrated that the BrdU+ cell population accounts for only a small fraction of the total cell population within PVZs (Fig. 2C,F,I,L,O); those comprising the largest percentage of the overall cell population were observed in Vd (10.59%, level ×50) and Vv (9.74%, level ×60), which also had the smallest estimated surface area (Table 3). All subsequent experiments were done at the rostrocaudal levels and within the neuroanatomical boundaries of each PVZ where the highest density of BrdU+ cells was reported, as shown schematically in Figure 3.

Cell cycle parameters vary between periventricular zones

To assess whether the difference in the size of the BrdU+ cell population across different PVZs was related to differences in cell cycle kinetics, we performed a BrdU cumulative labeling experiment. Zebrafish were intraperitoneally injected with a 1 mM bolus of BrdU at 2-hour intervals over a 12-hour period, and separate groups of fish were sacrificed every 2 hours, 30 minutes after the last injection. Preliminary experiments confirmed that our

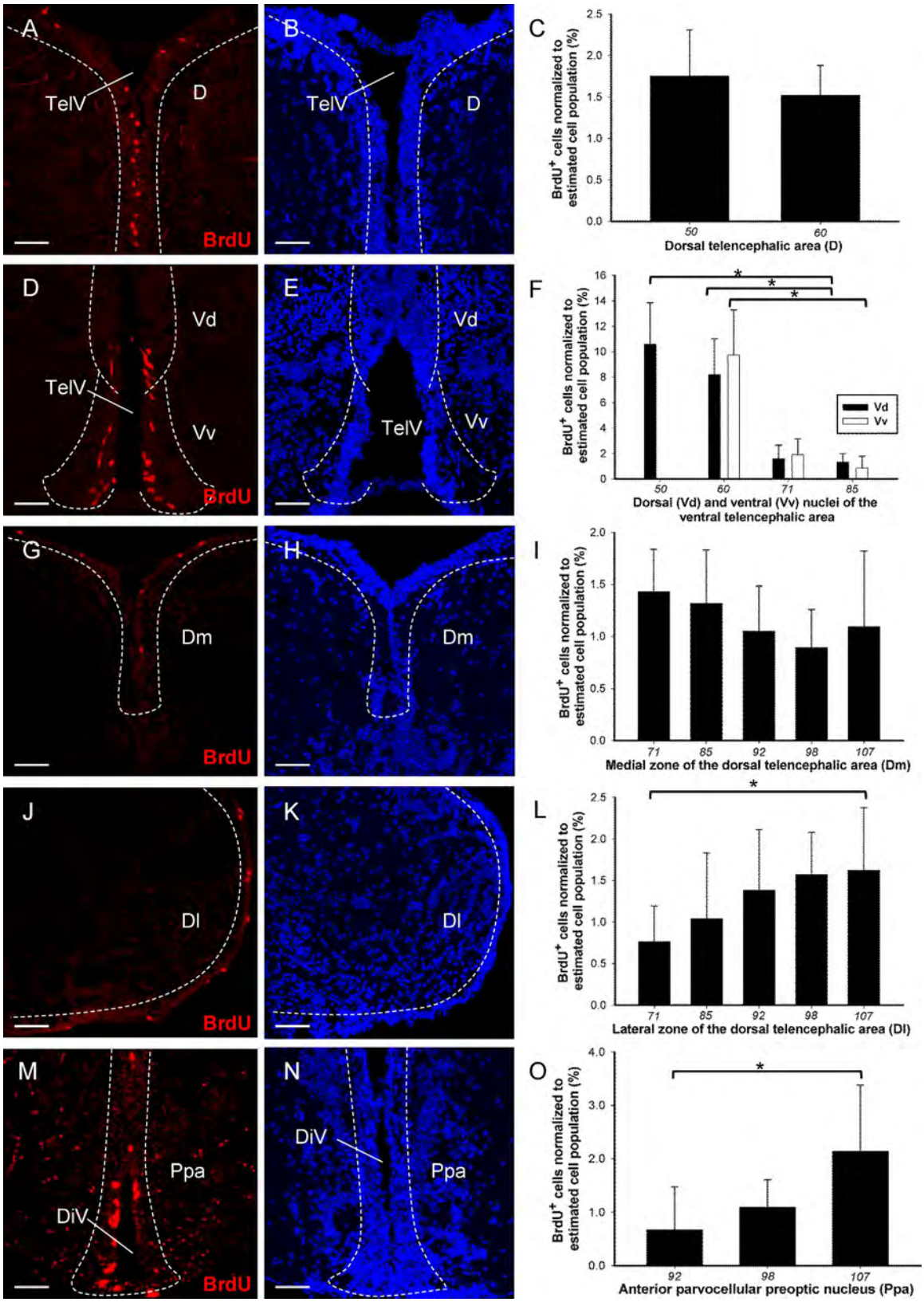
A
TelV
D
BrdU
B
TelV
D
C
BrdU+ cells normalized to estimated cell population (%)
2.5
2.0
1.5
1.0
0.5
0.0
50
60
Dorsal telencephalic area (D)
D
Vd
TelV
Vv
BrdU
E
Vd
TelV
Vv
F
BrdU+ cells normalized to estimated cell population (%)
16
14
12
10
8
6
4
2
0
*
*
*
Vd
Vv
50
60
71
85
Dorsal (Vd) and ventral (Vv) nuclei of the ventral telencephalic area
G
Dm
BrdU
H
Dm
I
BrdU+ cells normalized to estimated cell population (%)
2.0
1.5
1.0
0.5
0.0
71
85
92
98
107
Medial zone of the dorsal telencephalic area (Dm)
J
Dl
BrdU
K
Dl
L
BrdU+ cells normalized to estimated cell population (%)
2.5
2.0
1.5
1.0
0.5
0.0
*
71
85
92
98
107
Lateral zone of the dorsal telencephalic area (Dl)
M
Ppa
DiV
BrdU
N
DiV
Ppa
O
BrdU+ cells normalized to estimated cell population (%)
4.0
3.0
2.0
1.0
0.0
*
92
98
107
Anterior parvocellular preoptic nucleus (Ppa)

Figure 2

method of injection could be sustained over the 12-hour period, and that the multiple doses of BrdU used for this experiment were not toxic to the animals (data not shown). The cumulative labeling method allowed us to estimate the growth fraction (GF), which is the length of time taken for the entire proliferative population to take up BrdU (T_M), the length of the cell cycle (T_C), and the S-phase (T_S), by comparing the best fit of our data to first-, second-, or third-order polynomial equations. Over the injection period, all proliferating cells in the S-phase of the cell cycle will incorporate BrdU; however, upon re-entry into the S-phase these cells would not be counted as newly BrdU+ cells. Therefore, assuming the injection period is long enough, at a specific time point, only previously labeled BrdU+ cells would comprise the cell population leading to the GF and plateau phase of the best fit curve. In the event that the 12.5-hour cumulative labeling period used here was insufficient to mark all proliferating cells, we would expect to see a linear regression as the best fit to all data points.

Our results show clearly that the cell cycle parameters differ across regionally distinct PVZs. Representative confocal images of BrdU+ cells 30 minutes following the first injection and when the percentage of BrdU-labeled cells reached its maximum (i.e., the first time point when the plateau is reached = GF) are shown in Figure 4. The results of all cell cycle parameters based on a single population model are given in Table 4. The D, Vv, Dm, and Dl data were best fit to a linear regression model by using the least squares method (Fig. 4A,G,J,M), suggesting a single proliferative population, but having yet to reach a plateau. The continuous increase in BrdU- labeled cells beyond the 12-hour cumulative labeling endpoint of this study prevented us from accurately determining the GF and total cell cycle and S-phase lengths. Thus, we reasoned that across these PVZs the last time point assayed at 12.5 hours could be interpreted only as the minimum GF, with the PVZ of D, Dm, and Dl having a minimum GF of between 3.2 and 4.3% compared with the GF of 28.76% seen in Vv (Table 4).

The Ppa and Vd cumulative labeling data were found to best fit quadratic and cubic polynomial regression models, respectively. In the PVZ of Ppa (Fig. 4P–R), the beginning of the plateau was observed ~6.5 hours after the first BrdU injection (red dot), resulting in a maximum GF of 4.35%. By using the first four data points that fit a linear model ($R^2 = 0.4603$, $y = 1.401 + 0.477x$; Table 4), we were able to estimate the total cell cycle length to be 11 hours with an S-phase length of 4.5 hours. Unlike the apparent single population of cells seen in the PVZ of Ppa, Vd showed evidence of two separate mitotic populations (Fig. 4D–F). The data for this zone conformed most closely to a third-order polynomial, with the curve having three distinct phases. Between 0.5 and 4.5 hours, the number of BrdU+ cells can be seen to steadily increase, after which time a plateau could be noted extending until ~8.5 hours after the first BrdU injection. We interpret the time elapsed between 0.5 and 8.5 hours to represent the first mitotic population within the PVZ of Vd, with 4.5 hours marking the GF (red dot), calculated to be 13.62%. By fitting the first three data points to a linear model ($R^2 = 0.7289$, $y = 5.624 + 1.820x$), we obtain a total cell cycle length of 7.48 hours and S-phase length of 2.98 hours for this first population in Vd (Table 4). A putative second proliferative population can be seen commencing 8.5 hours after the first BrdU injection and increasing toward our last time point at 12.5 hours, although our cumulative labeling period would need to be extended to definitively assess the kinetics of this putative second population. Overall, these data clearly indicate that the size of proliferative populations and their cell cycle characteristics are relatively non-uniform between PVZs.

Figure 2. Bromodeoxyuridine-positive cells normalized to the total cell population at separate rostrocaudal levels across the six proliferation zones having the greatest number of BrdU+ cells (D, Vd, Vv, Dm, Dl, Ppa). **A,D,G,J,M:** Location of BrdU+ cells (red) in each zone at the rostrocaudal level where most BrdU+ labeling was observed, indicating the level of the PVZ niche. **B,E,H,K,N:** Hoechst 33258 staining at corresponding levels for each PVZ niche showing the density of the cell population where BrdU+ labeling is observed. **C,F,I,L,O:** Percentage of BrdU+ cells normalized to the estimated total cell population throughout different levels of the rostrocaudal axis of the proliferation zones. The level at which the proliferation zones displayed the greatest number of BrdU+ cells was considered the level of the PVZ niche for that neuroanatomical region, with this rostrocaudal level examined specifically in subsequent experiments. Brackets denote a significant difference in the percentage of BrdU+ cells between rostrocaudal levels within the same proliferation zone. Significance (*) was determined by using one-way ANOVA and Tukey's HSD post hoc tests ($P \leq 0.05$). In F, for clarity only a subset of significantly different comparisons are shown graphically. However, a significant difference was reported between Vd at cross-sectional levels 50/60 and levels 71/85, and Vv at cross-sectional level 60 compared with both 71/85. White dashed lines demarcate the boundaries of PVZs within each neuroanatomical region, used to estimate the surface area and total population size to normalize BrdU+ cell counts. In all images dorsal is up. See also Table 3 for estimates of the total cell population comprising PVZs. For abbreviations, see list. Scale bar = 50 μm in A,B,D,E,G,H,J,K,M,N.

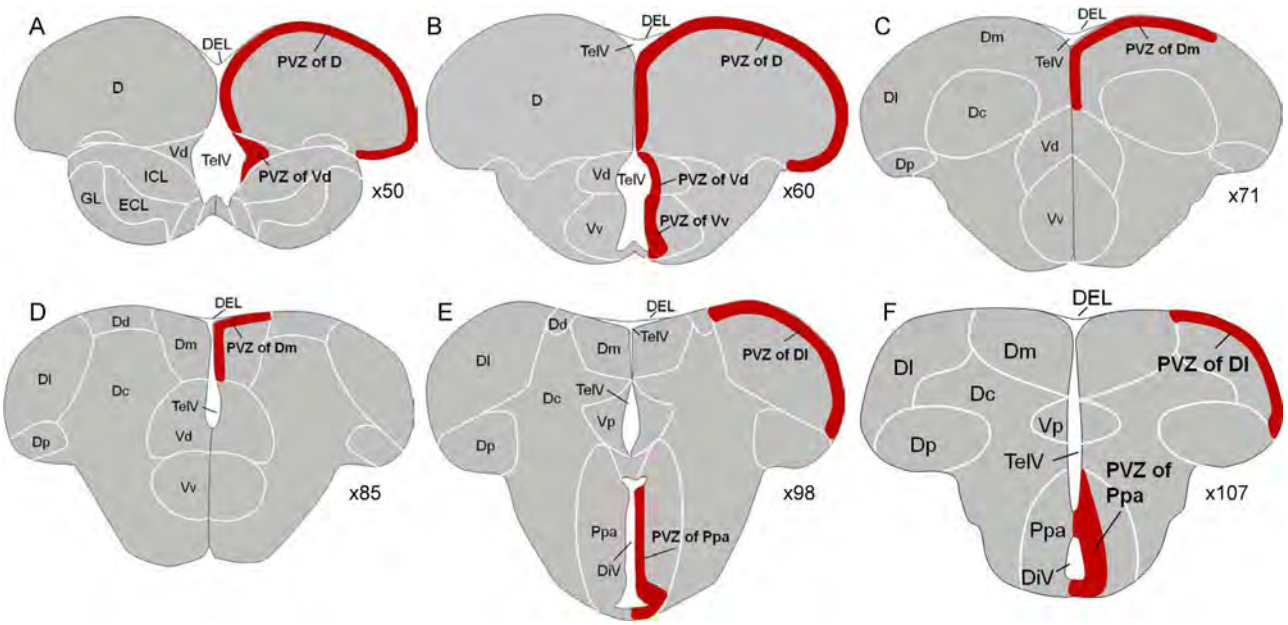

Figure 3. A–F: Schematic drawings showing the six PVZs in red in relation to the larger neuroanatomical forebrain region in which they are located, at the rostrocaudal levels where the highest level of BrdU-positive cells were observed. Note that the position of PVZs is consistently localized adjacent to the ventricles at all levels, and that the size of each PVZ differs considerably. Some PVZs spanned two rostrocaudal levels, including the PVZ of D, Vd, Dm, and Dl. All subsequent experiments were examined only at these rostrocaudal levels, and within the neuroanatomical boundaries shown here. GL, glomerular layer of olfactory bulb; ECL, external cellular layer of olfactory bulb including mitral cells; ICL, internal cellular layer of olfactory bulb. For other abbreviations, see list. See also Table 3 for surface area estimates of each PVZ.

TABLE 3.

Estimated surface area and BrdU+ cell population size of periventricular zones (PVZ)

Rostrocaudal cross-sectional level studied	*D*		*Vd*		*Vv*	*Dm*		*Dl*		*Ppa*	
	x50	x60	x50	x60	x60	x71	x85	x98	x107	x98	x107
Estimated PVZ surface area (μm^2)	44 624	53 693	4807	3244	5848	18 905	11 703	20 447	23 711	18 489	15 675
Mean number of $BrdU^+$ cells 2 hours post injection	26.2	26.05	17.46	10.45	21.54	8.4	4.97	11.41	11.67	5.52	10.35
Estimated cell population of PVZ	1493	1712	165	128	221	587	378	726	720	506	484
$BrdU^+$ cells of total cell population (%)	1.75	1.52	10.59	8.19	9.74	1.43	1.32	1.57	1.62	1.09	2.14

Ciliated cells and distinct populations of BrdU+ glia vary by periventricular zone between pallial and subpallial regions and are in proximity to the surrounding vasculature

To gain insight into the general features previously shown to be characteristic of other vertebrate niches studied along the ventricular wall (Alvarez-Buylla and Lim, 2004; Morrison and Spradling, 2008; Shen et al., 2008), we used a combination of scanning EM and confocal microscopy to examine the presence of ciliated cell populations, glial phenotypes, and vasculature within PVZs. To first identify the presence of ciliated cells, we separated the forebrain hemispheres and processed the tissue for SEM to look at the ventricular zone en face (Fig. 5A–C). At the dorsalmost aspect of the forebrain, the dorsal ependymal lining (DEL) can be seen covering the entire rostrocaudal aspect of D and Dm (Fig. 5A). From our scanning EM preparations, we noted that the DEL does not continue ventrally along the ventricle, but rather bridges the two hemispheres dorsally, as expected. When PVZs along the rostrocaudal axis were surveyed, a small number of ciliated cells were observed, displaying one to three cilia extending into the ventricle from the tip of cells or seen individually arising between adjacent cells from a deeper cell layer (Fig. 5B,C). Variations in surface topography of cells between PVZs or within different regions of the same zone were also observed; however, this was not examined in detail. The presence of ciliated cell populations observed at the SEM level was further corroborated

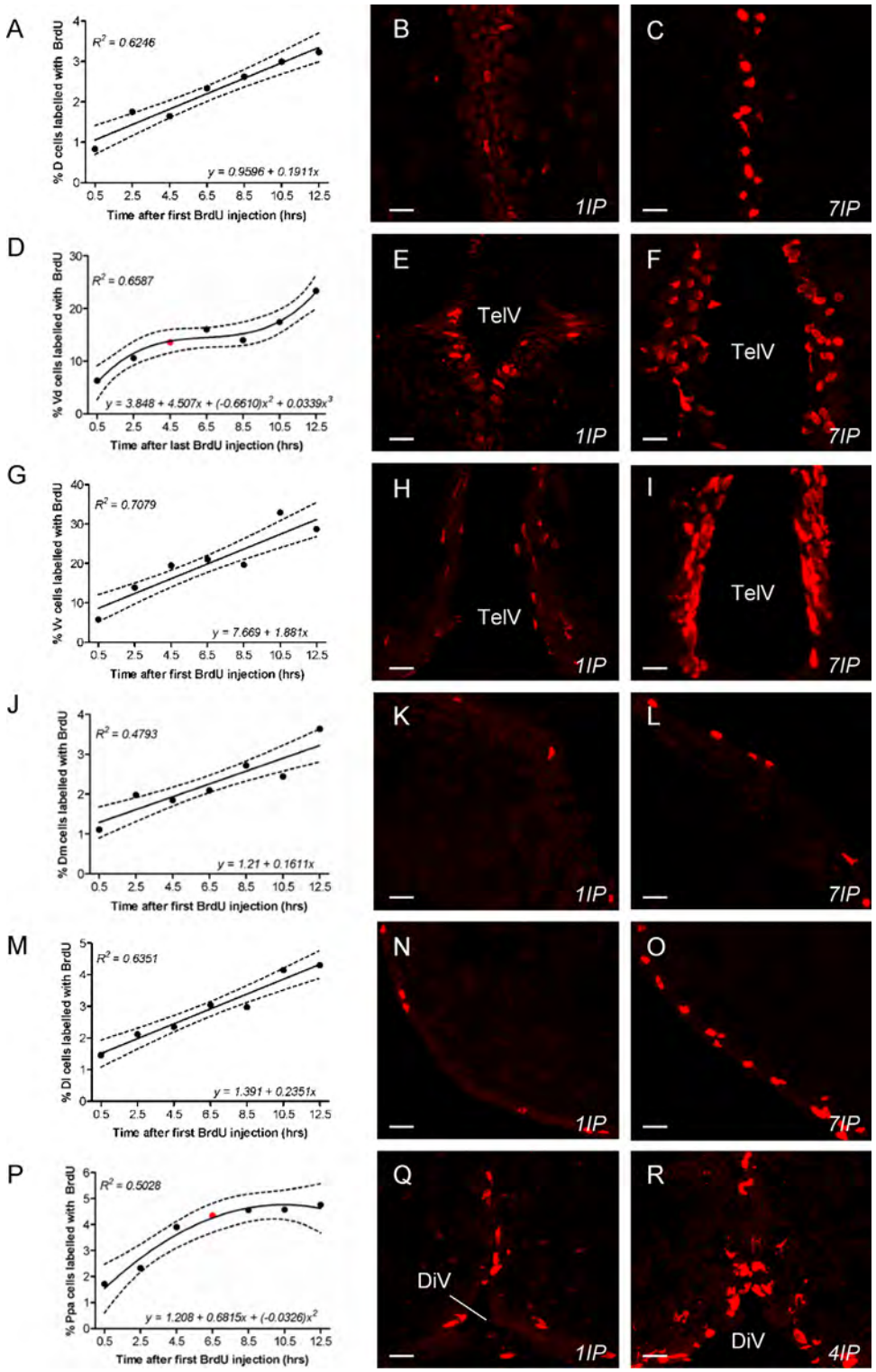

Figure 4. Cumulative BrdU-positive labeling over a 12-hour injection period demonstrating variation in the cell cycle kinetics of proliferative populations across the six PVZs of interest. **A,D,G,J,M,P:** Percentage of BrdU+ labeled cells fitted to the best linear or nonlinear (quadratic, cubic) model plotted over the injection period. On all graphs the 95% confidence bands (black dotted lines) and R-squared value for the best fit model are noted. Red dots denote the commencement of the plateau phase of a single cell population, with all data points from here prior replotted to a linear regression and used to calculate the maximum growth fraction of the population (GF_M), in addition to the total length of the cell cycle (T_C) and S-phase (T_S). When the line of best fit was a linear regression and continued to increase beyond the end of the 12.5-hour injection period (A,G,J,M), the GF_M could not be determined, and therefore only the minimal growth fraction for the population could be interpreted from the graph. In D, note the presence of two possibly separate proliferative cell populations, the first ranging from 0.5 to 4.5 hours and the second beginning at 8.5 hours. B,C,E,F,H,I,K,L,N,O,Q,R: For all graphs the corresponding confocal images of the number of BrdU+ cells for each niche 30 minutes after the first injection (**B,E,H,K,N,Q**) and at the time point when the estimated maximum or minimum growth fraction (**C,F,I,L,O,R**) was reached are shown. See also Table 4 for values of cell cycle parameters calculated for each PVZ. In all images dorsal is up. Scale bar = 8 μm in B,C,E,F,H,I,K,L,N,O.

TABLE 4.

Cell cycle parameter estimates following a 12.5 hour BrdU cumulative labelling study

	D	*Vd*	*Vv*	*Dm*	*Dl*	*Ppa*
Growth fraction (%)	3.23*	13.62**	28.76*	3.637*	4.304*	4.348
Time at $BrdU^{+}$ cell maximum (hrs)	12.5	4.5	12.5	12.5	12.5	6.5
Cell cycle length (hrs)	16.90	7.484	15.29	22.58	18.31	11.00
S-phase length (hrs)	4.402	2.984	2.79	10.08	5.81	4.50

*Indicates that the cell population only reached a minimum growth fraction after 12.5 hours

**Denotes the growth fraction of the first of two putative subpopulations of proliferative cells in Vd

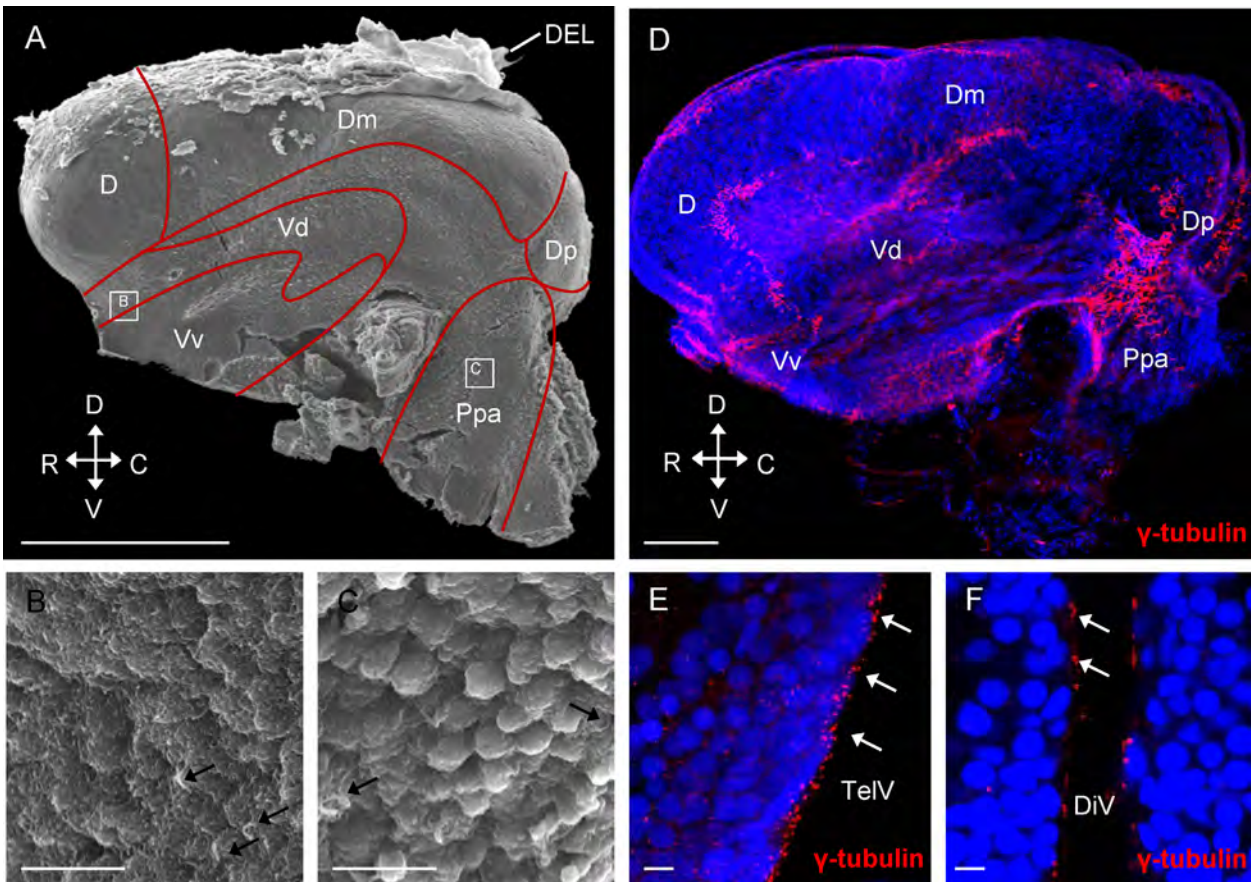

Figure 5. Evidence of ciliated cell types along the ventricular surface of the adult zebrafish forebrain. **A–C:** Scanning electron microscopy showing an en face view of the ventricular surface of a single forebrain hemisphere. Red lines demarcate the general boundaries of the major neuroanatomical regions in which PVZs are situated, seen along the ventricular surface. White boxes in A correspond to higher magnification images seen in B and C displaying evidence of ciliated cells (white) extending from the apical cell surface into the lumen (black arrows). **D:** Whole-mount preparation of a single forebrain hemisphere stained with γ-tubulin (red) to label the basal bodies of cilia and counterstained with Hoechst 33258. The orientation is the same as in A. Note the orientation of images in A and D along the dorsoventral (D–V) and rostrocaudal (R–C) axes. **E,F:** Images showing γ-tubulin+ staining (white arrows) similar to D, but viewed in cross section along the surface of the telencephalic (TelV) and diencephalic (DiV). In all images dorsal is up. DEL, dorsal ependymal lining. Scale bar = 270 μm in A; 10.5 μm in B,C; 100 μm in D; 8 μm in E,F.

by whole-mount IHC of the forebrain ventricular surface labeled with the antibody against γ-tubulin. Figure 5D shows γ-tubulin+ labeling (red) in discrete regions of the ventricular wall, with several of these regions overlapping with the PVZs of interest. Labeling with γ-tubulin provided additional evidence that ciliated cell populations contained ciliary basal bodies on the apical cell membrane facing the ventricle or localized at the ventricular midline (Fig. 5E,F).

To identify the phenotype of cells composing PVZs, zebrafish were injected with BrdU and sacrificed 2 hours later for co-labeling with BrdU and the glial markers

S100β or GS, or BrdU and the putative stem/progenitor markers Pax6 or Sox2, for comparisons between niches. BrdU+/S100β+ cells made up nearly 10% or more of the cell population sampled in all PVZs (Fig. 6A–C). A statistically significant difference in this population was noted between Dm and Ppa (one-way ANOVA; Tukey's HSD post hoc test), with Dm having nearly 40% of cells BrdU+/S100β+. Although BrdU+/S100β+ cell populations were seen in all six PVZs, those having the highest percentage of co-labeled cells were localized in the pallial zones (D, Dm, and Dl). Unlike the consistent finding of BrdU+/S100β+ cells throughout all PVZs, BrdU+/GS+ cells were absent from both the subpallial Vv and Ppa (Fig. 6D–F). This result is due to the general absence of GS+ labeling in Vv, as well as within the ventral aspect of Ppa. The lack of GS+ labeling in Vv helps to demarcate the boundary between Vd (which displays GS+ labeling) and Vv. Despite an overall statistically significant effect between PVZs (one-way ANOVA), the high degree of variation between samples from a single zone did not allow for accurate post hoc tests to be performed. From our analysis, we show, however, that the PVZ where the greatest population of BrdU+/GS+ resided was D (25%). The pattern of BrdU+/GS+ labeling seen here suggests that this cell population resides primarily in the pallial PVZs of the zebrafish forebrain, but also includes the subpallial zone of Vd.

Stem/progenitor markers Pax6 and Sox2 showed sparse labeling throughout most niches, compared with cycling glial populations. Pax6+ cells were often localized adjacent to the PVZ boundaries of Vd and Vv, whereas some degree of labeling could additionally be seen within niches of D (mainly along the midline), Dm, Dl, and Ppa (Fig. 6G). However, from cell counting of BrdU+/Pax6+ cells across forebrain PVZs, co-labeled cells were only rarely observed (Fig. 6H). The above labeling pattern demonstrates that the Pax6 antibody used here may be detecting both Pax6a and Pax6b cell populations in a regionally specific manner, consistent with previous observations (Wullimann and Rink, 2002; Adolf et al., 2006). Similarly to Pax6 labeling, few BrdU+/SOX2+ cells were detected across any of the six PVZs (Fig. 6I). These data suggest that dividing Pax6+ and Sox2+ periventricular cells are sparse among PVZs, although these markers may be useful to identify putative stem/progenitor cells, which are typically thought to be rare among the population of niche cells.

Finally, to examine the location and degree of vascularization of PVZs, we used a *Tg[flk1:gfp]* transgenic zebrafish line, which marks the endothelial cells of the brain vasculature. Although the degree to which vasculature infiltrated each zone varied, they were all in close proximity to surrounding vessels. Qualitative observations showed that the PVZs of D, Vd, and Ppa were most highly vascularized compared with Vv, Dm, and Dl (Fig. 6J–L). Nevertheless, Dl and Ppa (Fig. 6K,L) appeared to possess the greatest density of vessels adjacent to the neuroanatomical boundaries of the niche.

Ultrastructural characterization of PVZs reveals pallial and subpallial variation in the cytoarchitecture and differences in the frequency of distinct cell types

We performed a detailed morphological study in order to compare the cytoarchitectural composition of six PVZs in the zebrafish forebrain. All zones bordered the telencephalic (D, Vd, Vv, Dl, Dm) or diencephalic (Ppa) ventricle medially along the dorsoventral axis of the forebrain, and were composed of several distinct cell types. Lateral to the ventricle, the deeper layers of each zone terminated with one or more layers of neurons or in the adjacent parenchyma. The first complete cell layer composed exclusively of neurons was considered the lateralmost boundary of each zone, with this layer not included as part of the PVZ. Varying degrees of vasculature could be seen in the form of venules and arterioles and these were noted when appropriate. Periventricular zones were studied at the following rostrocaudal cross-sectional levels to investigate the ultrastructural organization and cell types composing each niche: D, Vd, Vv (×60), Dm (×85), and Dl and Ppa (×98). A summary of the characteristic features of the distinct cell types comprising PVZs is listed in Table 5, whereas the frequency of each cell type across zones is noted in Table 6. When multiple cell types shared some, but not all, features, cells were divided into subtypes. When cell types could not be determined but were present in the niche, they were classified as unknown.

Dorsal telencephalic area (D)

The PVZ of D encompassed the greatest surface area (Table 3) and ran medially along the dorsoventral axis of the telencephalic ventricle, terminating at Vd, which marked the ventralmost position of the pallial zone. A continuous dorsal ependymal lining (DEL) composed of a single cell layer of classical ependymal cells could be seen spanning the roof of the telencephalic ventricle at the level of the PVZ of D and Dm (Figs. 7A, 8A, 11A,B) and continuing a short distance laterally along both hemispheres (Fig. 11C), before being replaced by a thin layer of squamous epithelial cells. The DEL appeared to form an ependymal-like sheath covering the entire dorsal surface of the forebrain (Fig. 5A), although in many cases the DEL went undetected because it is lost during specimen preparation. Ependymal cells were typically cuboidal to low cuboidal, displaying clumps of heterochromatin

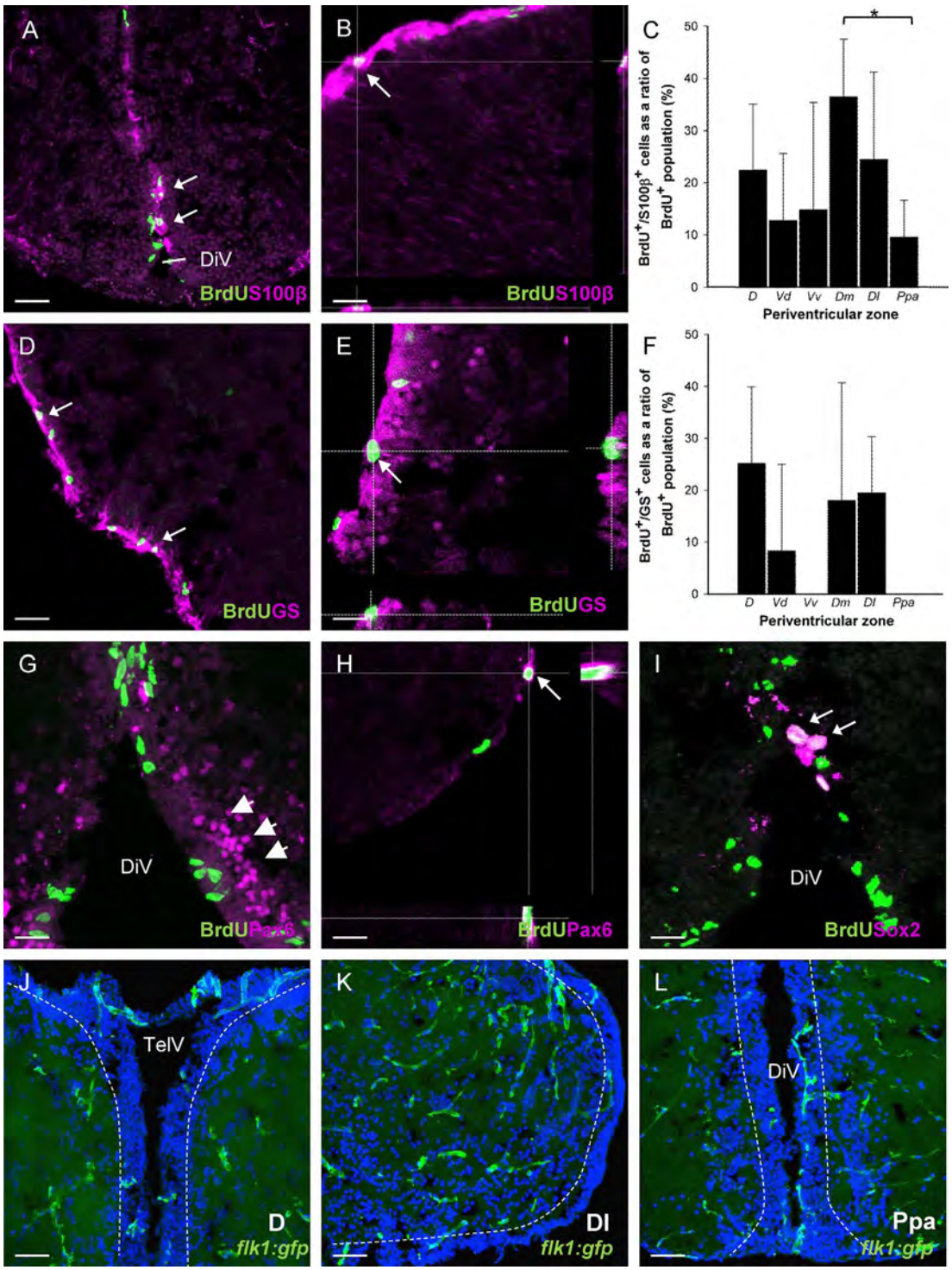

Figure 6. Characterization of BrdU-positive glial populations 2 hours post-BrdU injection and localization of vasculature compared between PVZs. **A–C:** BrdU+/S100β+ co-labeling (A,B) quantified (C) following a single BrdU injection. In C, note the smaller size of this population in the PVZ of Vd, Vv, and Ppa. **D–F:** BrdU+/GS+ co-labeling (D,E) quantified (F) following a single BrdU injection. In F, note the absence of BrdU+/GS+ cells in the PVZ of Vv and Ppa. Significance (*) was determined by using one-way ANOVA and Tukey's HSD post hoc tests ($P \leq 0.05$). **G,H:** BrdU+/Pax6- (G) and BrdU+/Pax6+ cells (H) cells detected in PVZs. In most cases Pax6+ cell populations were observed near the border of the PVZ (G, white arrowheads), and only rarely were dividing Pax6+ cells observed (H). **I:** One of few BrdU+/Sox2+ cells detected across PVZs. In A–I, white arrows and cross-hairs in orthogonal views denote examples of positively co-labeled cells. **J–L:** Localization of vasculature (green, flk1:gfp) in relation to Hoechst 33258-labeled cells (blue) in PVZs; examples are provided for the PVZ of D (J), Dl (K), and Ppa (L). White dashed lines demarcate the border of PVZs. In all images dorsal is up. GS, glutamine synthetase. For other abbreviations, see list. Scale bar = 40 μm in A,D,J,K,L; 10 μm in B,E,H,I.

TABLE 5.

Morphological features of cell types identified in adult forebrain periventricular zones

Sample Size	Ependyma n=30	Type IIa n=113	Type IIb n=17	Type III n=52	Type IVa n=88	Type IVb n=26	Type V n=43	Neurons (VI) n=51
NUCLEI								
Contour	elliptical; elongate ± some invag.	ovoid; irregular ± shallow invag.	ovoid; irregular	elongate; irregular ± invag.	ovoid; irregular ± invag.	elongate; irregular ± deep invag.	ovoid; irregular	ovoid
Long axis (μm)	4.39 ± 1.39	5.79 ± 1.34	5.15 ± 1.32	5.73 ± 1.96	5.28 ± 1.43	4.37 ± 1.10	3.47 ± 1.22	5.96 ± 0.94
Short axis (μm)	2.04 ± 0.65	3.49 ± 1.03	3.06 ± 0.97	2.66 ± 0.88	2.36 ± 0.79	2.38 ± 0.70	1.88 ± 0.56	4.84 ± 1.01
Chromatin	clumped hetero; evenly distributed	evenly distributed; non-clumped	reticulated; non-clumped	evenly distributed; non-clumped	reticulated; clumped hetero.	reticulated; clumped hetero.	reticulated; hetero. peripheral	mainly dispersed; some clumped
Color	light	light-medium	medium-dark	medium	dark	dark	dark	light-medium
Nucleoli	1–2	1–2	none visible	1–2	1–2; seldom visible	1–2; seldom visible	1; seldom visible	1
CYTOPLASM								
Percentage/colour	abundant/light	abundant/light	abundant/light	scant/light	scant/medium	scant/medium	scant/dark	intermediate/ light
Mitochondria	many	many	few	few	few	few	few	intermediate
Cilia	few to many	none	many	no	no	many	no	no
Microvilli	many; bulbus	few-intermediate	intermediate-many	no	no	intermediate	no	no
Vacuoles	many; large	many; small	few	no	no	no	no	some; small
Lipid droplets	yes	yes	yes	0–1	no	0–1	no	no
Dense bodies	no	yes	yes	no	no	no	no	no
LOCALIZATION	DEL (D & Dm only)	VS	VS (Ppa only)	VS and deeper layers	VS and deeper layers	VS (mainly Ppa)	1+ cell layers deep to VS	1–2 cell layers deep to VS
CELL CONTACTS	Ependymal cells	Types II-VI	Type IIa, Type VI	Types II-VI	Types II-VI	Types II-VI	Types II-VI	Types II-VI

Invag., invagination; hetero., heterochromatin; DEL, dorsal ependymal lining; VS, ventricular surface

TABLE 6.

Frequency of cell types in periventricular zones (% total N sampled)

	Ependyma	Type IIa	Type IIb	Type III	Type IVa	Type IVb	TypeV	Neurons	Unknown	N cells/PVZ
D	1.85	32.45	0	0.53	31.93	0.26	1.58	29.29	2.11	379
Vd	0	18.89	0	8.52	40.74	0	2.22	29.63	0	270
Vv	0	0.35	0	20.74	56.38	0	0.53	21.63	0.35	564
Dm	13	29.33	0	2	8.33	0	1.67	44.33	1.33	300
Dl	0	28.70	0	8.70	22.61	0	0.87	31.30	7.83	115
Ppa	0	19.17	3.56	2.57	24.90	5.93	1.38	41.11	1.38	506
%total/cell type	2.16	18.46	0.84	8.01	34.02	1.45	1.31	32.33	1.41	2134

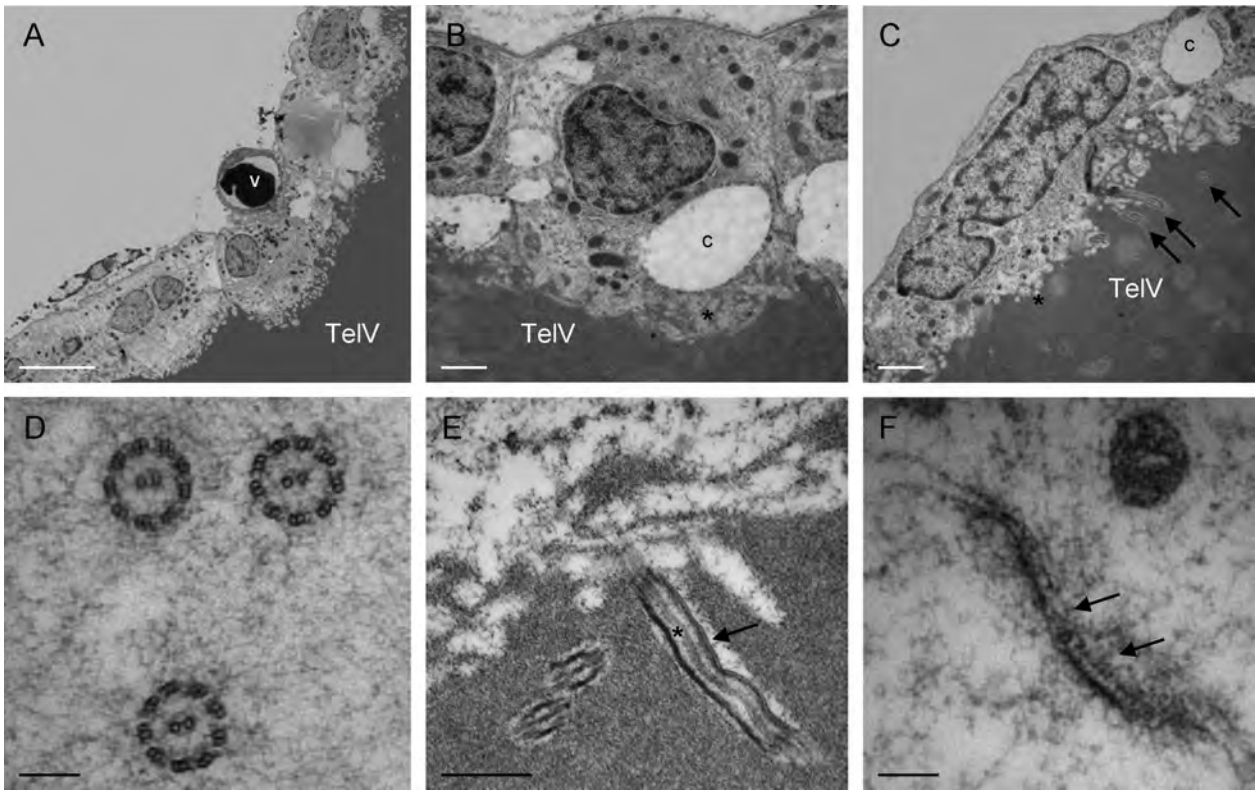

Figure 7. Ultrastructural organization of the dorsal ependymal lining (DEL) above the pallial PVZs of D and Dm. **A–D:** A single row of characteristic ependymal cells (A) are seen enclosing the dorsal aspect of the telencephalic ventricle (TelV) and displaying a cuboidal (B) to low cuboidal (C) conformation. These cells contained clumped heterochromatin, numerous bulbus microvilli (asterisk), and many mitochondria and vacuoles dispersed throughout the cytoplasm. In several cells large capillaries (c) could be seen coursing through the cytoplasm (B,C). Cilia can be seen extending from the apical cell surface (C, black arrows), having a typically 9+2 microtubule arrangement in cross sections (D). **E:** In longitudinal section both the peripheral (black arrow) and central (asterisk) microtubules can be detected. **F:** Adjacent ependymal cells contacted one another via junctional complexes (black arrow). See also Table 5 for additional morphological features of ependymal cells, and Table 6 for the frequency of ependymal cells across PVZs. In all images dorsal is up. v, vessel. Scale bar = 4 μm in A; 1 μm in B,C; 500 nm in E; 100 nm in D,F.

throughout an elliptical to elongated nucleus (Fig. 7B,C). Abundant, lightly stained cytoplasm contained numerous mitochondria, with several cilia and bulbus microvilli projecting into the lumen at the apical surface. Cilia were composed of a 9+2 arrangement of microtubules, which were easily recognizable in both cross sections and longitudinal sections (Fig. 7D,E). Capillaries were often found tightly interspersed among ependymal cells near the apical surface (Fig. 7B,C), in addition to the presence of darkly staining lipid droplets within the cytoplasm. Junctional complexes could be seen joining the membrane of adjacent ependymal cells, as shown in Figure 7F. These ependymal cells were localized exclusively to the roof of the telencephalic ventricle and were not observed elsewhere across any of the PVZs.

Laterally, the PVZ of D extended around the entire perimeter of the pallium, beneath a thin layer of squamous epithielial cells, ending at the lateral olfactory tract. For

ultrastructural analysis, the medial portion of D was studied in most detail; the greatest heterogeneity of cell types was observed in this niche (Fig. 8B–D). At the dorsalmost aspect of the midline of D, this zone often consisted of a single layer of cells having a modified ependymal-like appearance (Fig. 8A, type IIa). Type IIa cells had an ovoid

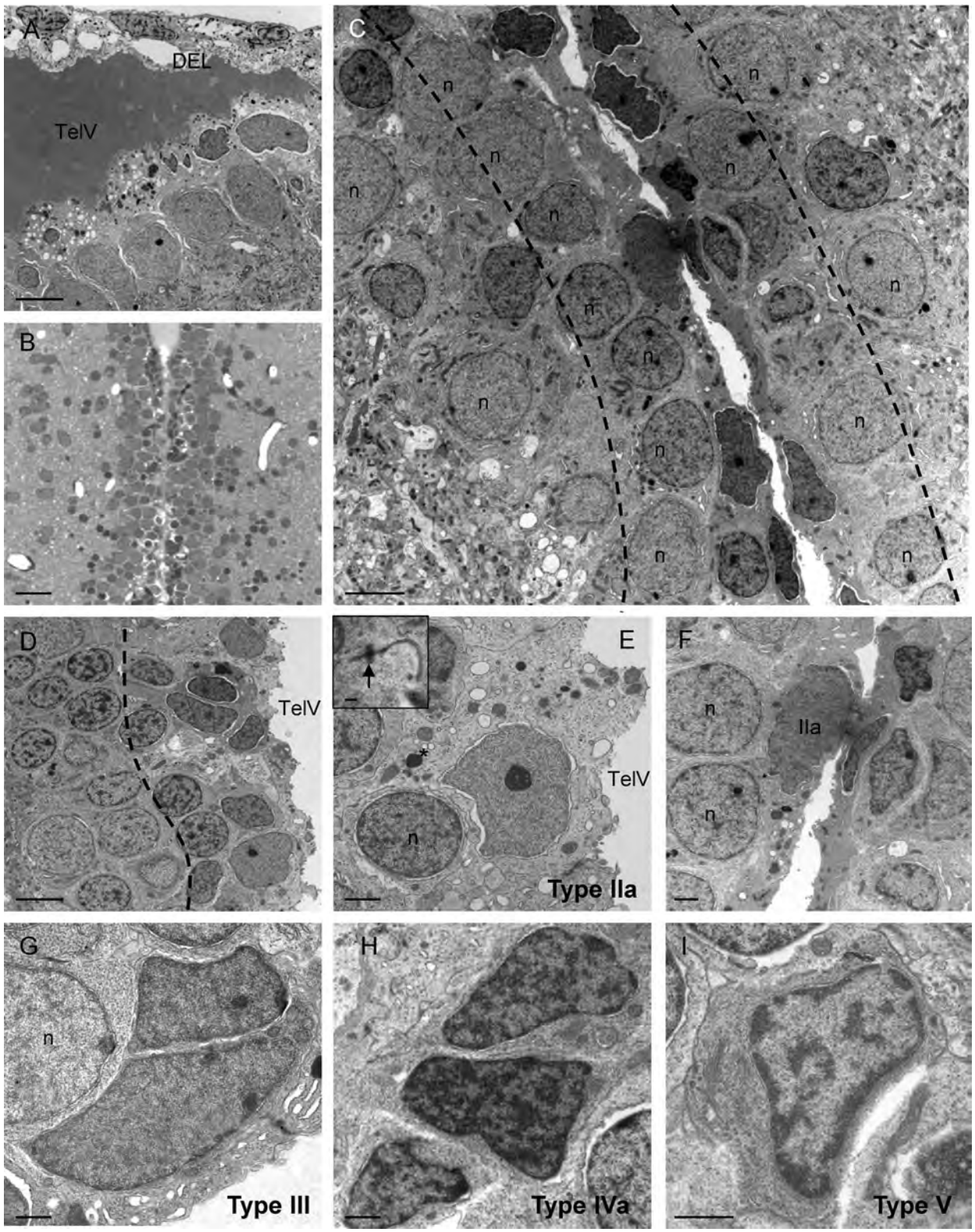

Figure 8. (Legend on page 2296.)

or irregular nuclear contour with mostly evenly distributed, lightly stained chromatin, with one to two large nucleoli easily identified within the nucleus (Fig 8E). At times the long axis of the nucleus could be seen oriented parallel to the midline ventricle (Fig. 8F). Similar to ependymal cells, the cytoplasm was abundant and lightly stained and often extended along the luminal surface. In some cases, cytoplasmic processes of type IIa cells situated at the lumen could be seen extending into the deeper cell layers of the PVZ and terminating in the parenchyma (see Fig. 11E), reminiscent of radial glia (Gotz et al., 2002). Cytoplasmic organelles included numerous mitochondria and small vacuoles, lipid droplets, and dense bodies. Unlike ependymal cells, however, no cilia were seen projecting from the apical cell surface, although often a small number of microvilli were present. Type IIa cells made contacts with all cell types and were abundant across nearly all PVZs, with the exception of Vv, where these cells only contributed to 0.35% of the population (Table 6). Both type IIa and IIb (see PVZ of Ppa) could be seen bound to adjoining cells of similar or different morphologies via tight and intermediate junctions, including desmosomes (Fig. 8E, inset).

As the PVZ of D extended ventrally adjacent to the midline telencephalic ventricle, an increasing number of different cell morphologies was observed (Fig. 8C,D). Here, the PVZ expanded to two to three cell layers deep and abutted one or more layers of neurons laterally (Fig. 8D). In addition to the type IIa cells described previously, three distinct cell morphologies were identified. Type III cells were distinguished by their elongated or irregular nucleus, with shallow to deep invaginations and evenly distributed medium staining chromatin containing one to two prominent nucleoli (Fig. 8G). These cells contained limited electrolucent cytoplasm with few visible organelles; only a small number of mitochondria or vacuoles was typically observed. Type III cells were least populous in the PVZ of D, comprising only 0.53% of the cell population (Table 6). Type IVa cells were easily distinguished from type III cells by their darkly staining, highly reticulated chromatin structure of varying degrees of clumped heterochromatin, and the rare presence of visible nucleoli. The cytoplasm of type IVa cells was typically darker than that of type III and contained very few visible organelles (Fig. 8H). The cytoplasm of both type III and type IVa cells intimately conformed to the shape of the nucleus, which for type IVa cells was most highly variable, taking on either an ovoid or irregular shape. Type IVa cells were the most abundant cell type across all PVZs (34.02%), followed by type IIa (18.46%), both of which could be seen localized at the ventricular surface or within the deeper layers of PVZs.

The final cell type identified in the PVZ of D was classified as type V. Type V cells were the smallest in size (LA: 3.47 μm ± 1.22; SA: 1.88 μm ± 0.56) and the least frequent of the cell types present throughout PVZs. These cells were primarily characterized by the large percentage of darkly staining heterochromatin localized to the periphery of their nucleus, which had an ovoid to slightly irregular shape (Fig. 8I). The color of the cytoplasm of type V cells was similar to or darker than that of type IVa cells, scant, and often contained only a few mitochondria. Type V cells were never located at the lumen, but rather were observed one or more cell layers deep to the ventricular surface, and were situated adjacent to all other cell types.

Dorsal zone of the ventral telencephalon (Vd)

The PVZ of Vd comprised the smallest estimated surface area compared with all other niches examined (Table

Figure 8. Ultrastructural organization of the pallial PVZ of D. **A:** Mid-dorsal image showing the dorsal ependymal lining (DEL) enclosing the roof of the telencephalic ventricle (TelV) and the large modified ependymal-like cells lining the lumen. **B–D:** Semithin (B) and high (C,D) magnification images showing the midline region of the PVZ of D that was studied in detail at the ultrastructural level. Note the heterogeneity of cell types forming a one- to three-cell-layer-deep PVZ (C,D) on either side of the TelV with a number of putative neurons at the lateral border of the PVZ. Black dashed lines denote the lateral boundaries of the PVZ. **E:** A single type IIa cell distinguished by its abundant, light staining cytoplasm, with numerous vacuoles and mitochondria, dense bodies (asterisk), and evenly distributed chromatin with a single large nucleolus, situated at the ventricular surface. The profile of a putative neuron can be seen at the basal surface of the cuboidal shaped type IIa cell. Inset displays a tight junction (desmosome) seen between adjacent type IIa cells (black arrow). **F:** Type IIa cell observed with the long axis of the nucleus oriented parallel to the lumen, with its cytoplasm dividing adjacent neurons from the ventricular space. **G:** Two adjacent type III cells distinguished by their elongated to irregular nucleus with evenly distributed chromatin, one to two visible nucleoli, and minimal cytoplasm containing few organelles. A putative neuron can be seen at the basal surface of these cells. **H:** Three adjacent type IVa cells characterized by their often irregular nucleus with variable degrees of dark staining, reticulated chromatin, and scant cytoplasm containing few organelles. type IVa cells were often seen in clusters. **I:** A single type V cell recognized by its small size and medium-darkly staining minimal cytoplasm, with a large proportion of heterochromatin localized to the periphery of the nucleus. These cells were typically located in the deeper layers of the PVZ and were the most infrequent cell type detected. See also Table 5 for additional morphological features of type IIa, type III, type IVa, and type V cells, and Table 6 for the frequency of cell types within the PVZ of D. In all images dorsal is up. n, neuron. Scale bar = 4 μm in A,C,D,F; 10 μm in B; 1 μm in E,G–I; 150 nm in inset in E.

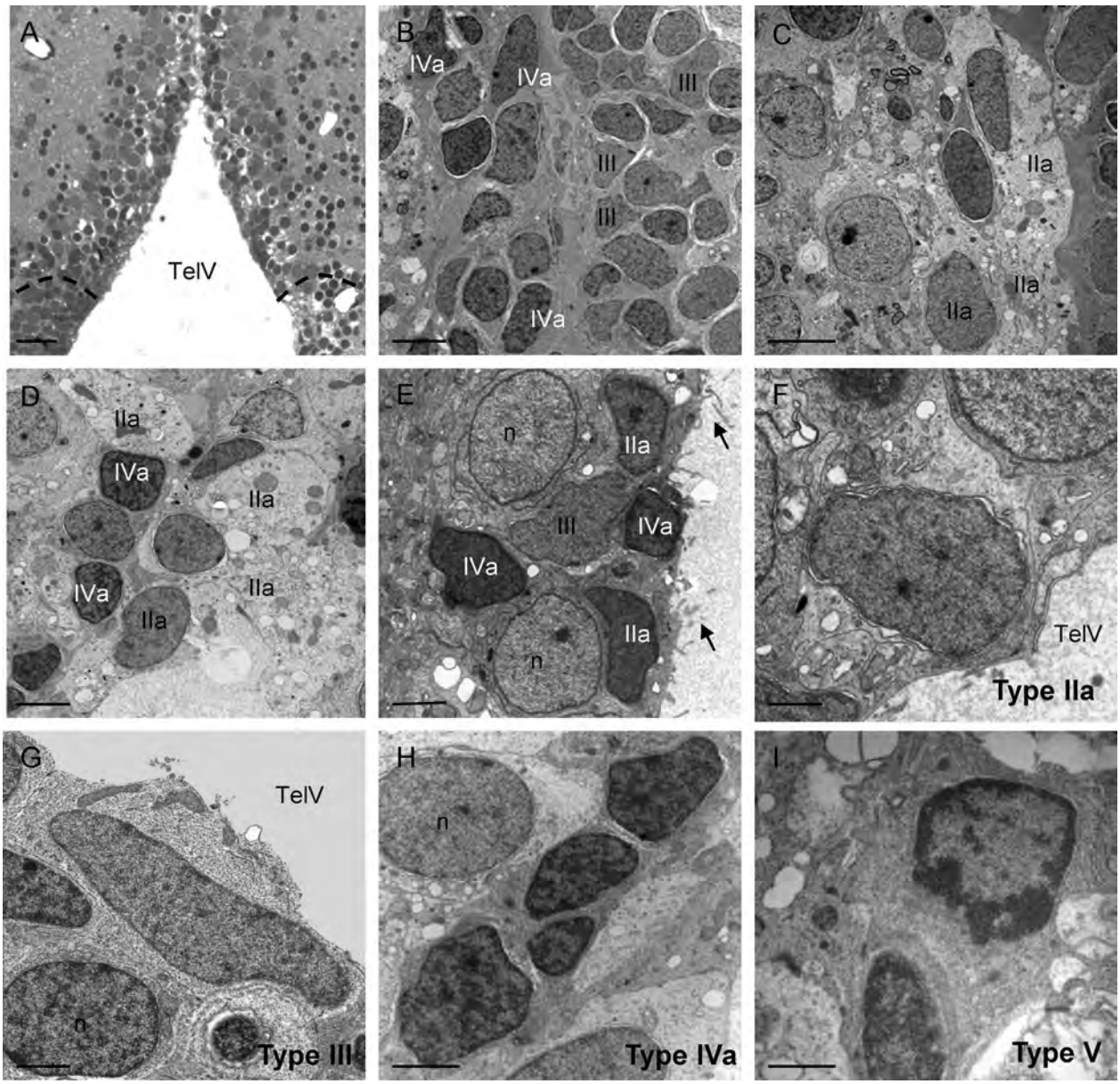

Figure 9. Ultrastructural organization of the subpallial PVZ of Vd. **A:** Semithin image showing the density of cell types composing this PVZ adjacent to the large telencephalic ventricle (TelV) and the ventral border (black dashed lines) with the dorsal aspect of the PVZ of Vv. **B,C:** A mixture of type IIa, type III, and type IVa cells are evident beginning at the dorsalmost aspect of the PVZ of Vd before the ventricle enlarges. **D:** A greater density of type IIa cells was detected as the TelV began to enlarge. **E:** Representative image of the three primary cell types comprising the PVZ of Vd adjacent to the lumen. Note the presence of microvilli extending from the apical surface of type IIa cells (black arrows). **F–I:** Profiles of the morphology of type IIa (F), type III (G), type IVa (H), and type V (I) cells in the PVZ of Vd. See also Table 6 for the frequency of cell types within the PVZ of Vd. In all images dorsal is up. n, neuron. Scale bar = 10 μm in A; 4 μm in B,C,D,H; 2 μm in E,G; 1 μm in F,I.

3). The dorsalmost aspect of this zone marked the beginning of the medial subpallial zone where the telencephalic ventricle (TelV) began to enlarge from an initially compressed pallial midline ventricle (Fig. 9A). Multiple cell types could be seen two to three layers deep, forming the dorsal region of this zone, including type IIa, type III, and type IVa (Fig. 9B,C). This region of Vd was largely dominated by numerous type IIa cells, identified by their abundant, lightly staining cytoplasm (Fig. 9D). Moving ventrally, the number of cell layers comprising the PVZ expanded to three to four; in addition, a greater number of rows of neurons divided the lateral boundary of this zone from the parenchyma. An increasingly heterogeneous population of cell types were observed as the PVZ extended toward the junction with Vv (Fig. 9E–I; see Fig. 9A for the ventral boundary of Vd with Vv). Type IVa cells

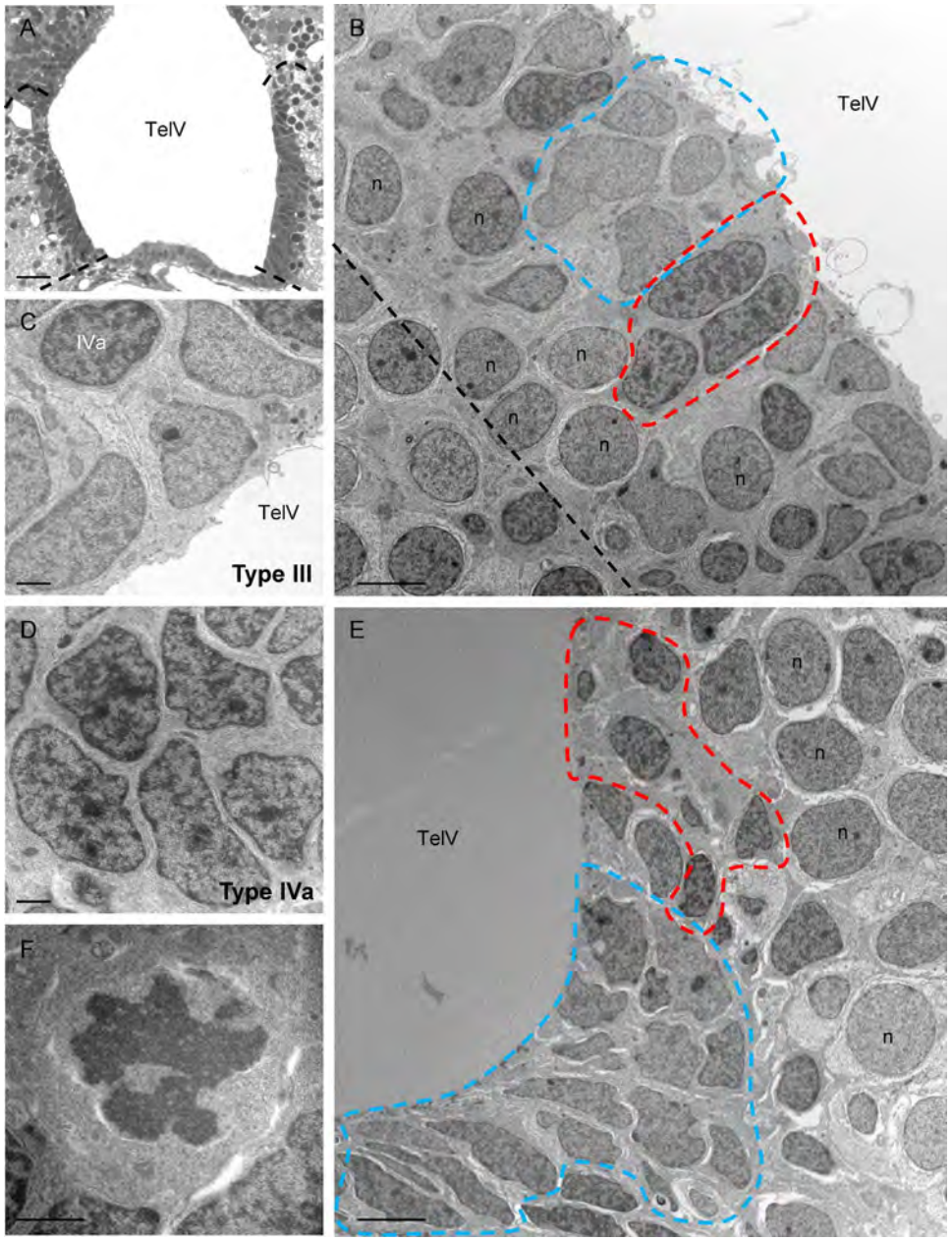

Figure 10. Ultrastructural organization of the subpallial PVZ of Vv. **A:** Semithin image showing the density of cells making up the PVZ of Vv along the telencephalic ventricle (TelV) and the dorsal and ventral borders (black dashed lines) of this zone. Note that the floor of the TelV is not considered part of this PVZ. **B:** High-magnification image illustrating approximately four to five cell layers composing this PVZ along the lateral walls of the TelV and made up primarily of type III (blue dashed lines) and type IVa (red dashed lines) cells. Black dashed line demarcates the lateral extent of the PVZ. **C,D:** Clusters of type III (C) and type IVa (D) displaying their characteristic evenly distributed or reticulated chromatin, respectively. **E:** The morphological profiles of these two cell types composed nearly the entire PVZ of Vv, in addition to neurons. Blue and red dashed lines in E are the same as in B. The irregular and elongated nuclear profile of type III cells is most evident at the ventrolateral corners of the PVZ of Vv. **F:** A mitotic cell detected adjacent to the TelV that appears to be in late prophase. See also Table 6 for the frequency of cell types within the PVZ of Vv. In all images dorsal is up. n, neurons. Scale bar = 10 μm in A; 4 μm in B,E; 1 μm in C,D,F.

made up the greatest population of cells (Fig. 9H; 40.74%) in this niche, whereas type V cells were far less frequent (Fig. 9I; 2.2%). The ventralmost aspect of Vd was located where the telencephalic ventricle had reached its greatest width and began to narrow, and an increasing number of darkly stained cells lined the lumen (type IVa), marking the beginning of the PVZ of Vv (boundary seen in Fig. 9A).

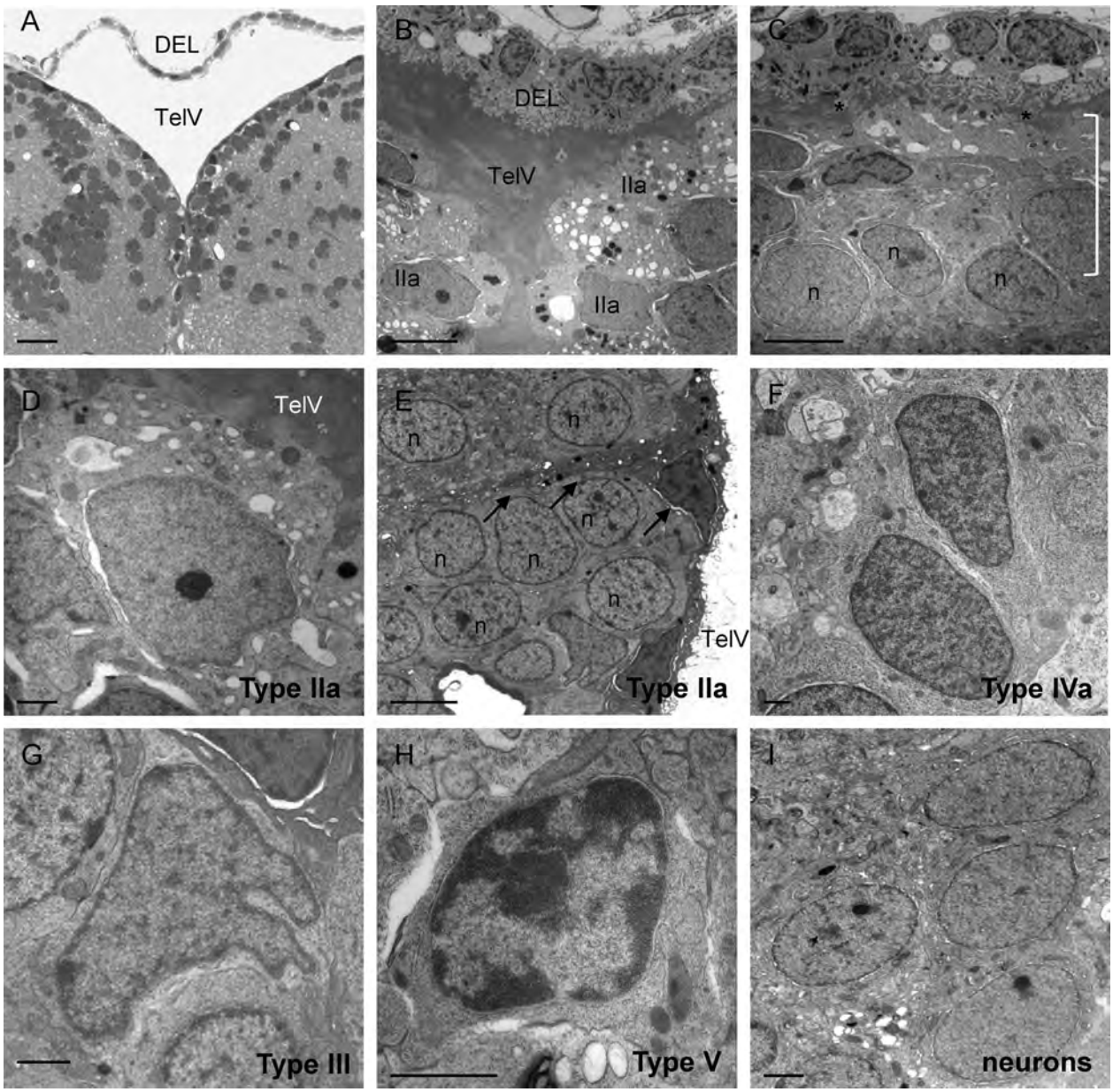

Figure 11. Ultrastructural organization of the pallial PVZ of Dm. **A,B:** Semithin (A) and high (B) magnification images showing the dorsal aspect of the PVZ of Dm and the single layer of ependymal cells enclosing the telencephalic ventricle (TelV) and forming the dorsal ependymal lining (DEL). Similar to the PVZ of D, type IIa cells can be seen lining this zone in B. **C:** Dorsolateral zone of the PVZ of Dm displaying the DEL extending laterally along one hemisphere and enclosing the remnants of the TelV (*). Only one to two cell layers comprise this PVZ beneath the ventricle dorsally (white bracket). **D,E:** Representative type IIa cells situated at the lumen. In E, notice the cytoplasmic processes of a type IIa cell extending into the deeper layers of the PVZ (black arrows), interspersed among neurons. **F–I:** Nuclear profiles of the morphology of type IVa (F), type III (G), and type V (H) cells, and neurons (I) composing the PVZ of Dm. Note the highly invaginated nature of type III cells in G. See also Table 6 for the frequency of cell types within the PVZ of Dm. In all images dorsal is up. n, neurons. Scale bar = 10 μm in A; 4 μm in B,C,E; 1 μrm in D,F,G,H,I.

Ventral zone of the ventral telencephalon (Vv)

The PVZ of Vv extended ventrally from the border of Vd, and along the telencephalic ventricle, ending at the ventralmost corners of the lumen (Fig. 10A). The floor of the ventricle was not considered part of this niche, because immunostaining experiments revealed the absence BrdU+ proliferating cells. The greatest number of cell layers extending laterally into the surrounding parenchyma was located in the PVZ of Vv, typically ranging from two to five layers deep (Fig. 10B,E). This zone was dominated by type III (Fig. 10C; 20.74%) and type IVa (Fig. 10D; 56.38%) cells that could be seen intermingled with neurons (Fig. 10B), or densely clustered together displaying characteristic irregular nuclear contours toward

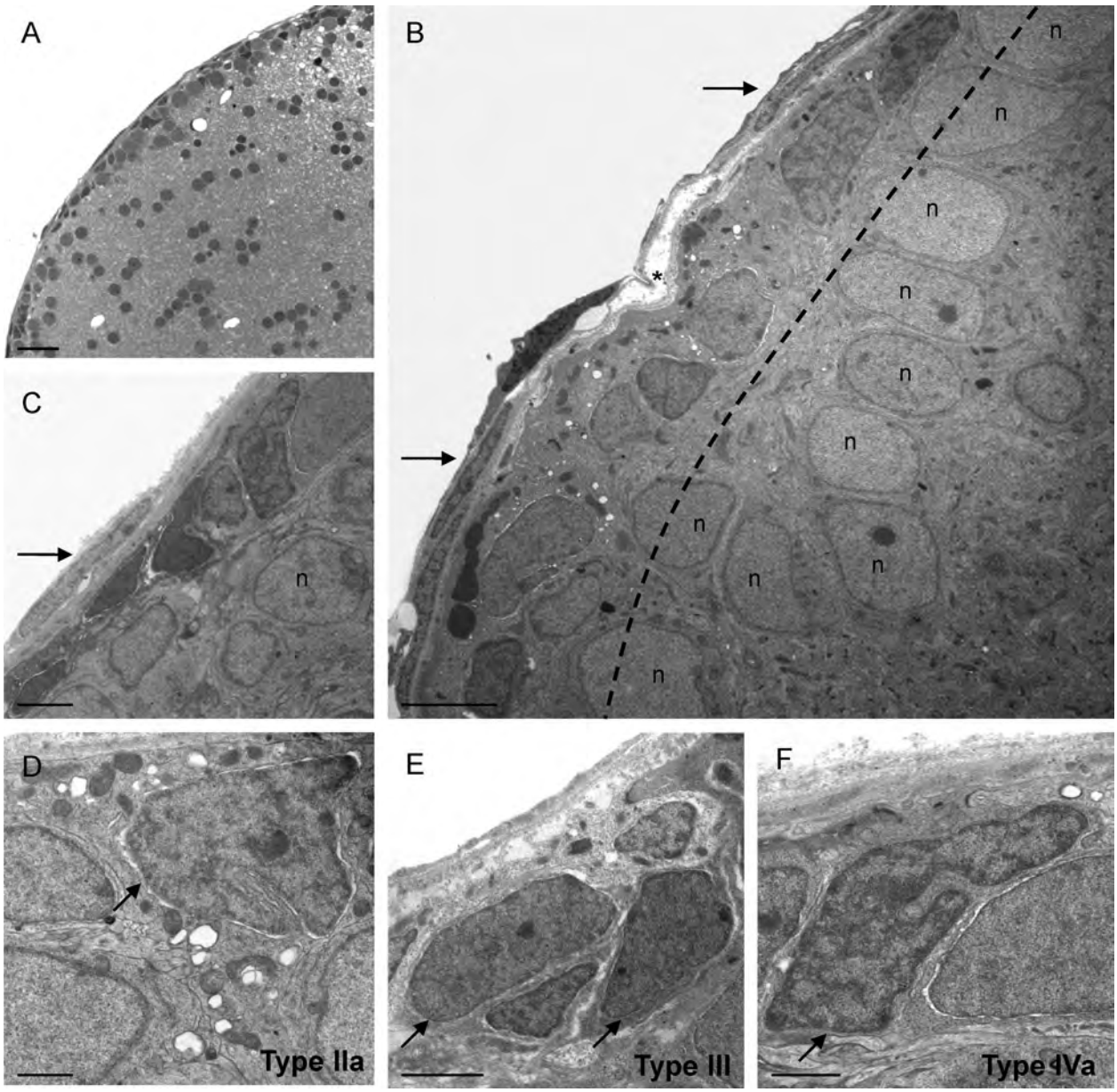

Figure 12. Ultrastructural organization of the pallial PVZ of Dl. **A–C:** Semithin (A) and high (B,C) magnification images displaying the one- to two-cell-layer-thick PVZ of Dl covered by a thin epithelial lining at the outer surface of the hemisphere (black arrows in B,C). Clusters or rows of neurons separating the PVZ from the parenchyma can also be seen. In B the lateral extension of the telencephalic ventricle (*) is seen beneath the epithelial lining. Black dashed lines denote the boundary of the PVZ of Dl. **D–F:** Morphological profiles of the major cell types composing the niche of Dl, including type IIa (D), type III (E), and type IVa (F). Black arrows indicate the cell type of interest in each image. See also Table 6 for the frequency of cell types within the PVZ of Dl. In all images dorsal is up. n, neurons. Scale bar = 10 μm in A; 4 μm in B; 2 μm in C,E; 1 μm in D,F.

the ventrolateral edges of this zone (Fig. 10E). In contrast, the smallest percentage of type V cells (0.53%) was detected in this niche. Neurons demarcating the lateral boundary could be readily identified by their large, ovoid nuclei in this zone (Fig. 10E). Within the PVZ of Vv, a small number of mitoses were identified, typically localized at or near the ventricular surface (Fig. 10F).

Medial zone of the dorsal telencephalon (Dm)

The PVZ of Dm was lined dorsally by cuboidal ependymal cells (DEL) that bridged both forebrain hemispheres and continued laterally a short distance (Fig. 11A–C), similar to the PVZ of D described above. Along the dorsal aspect of the forebrain, this zone extended laterally beneath the ependymal lining and luminal space, and consisted of only one to two cell layers (Fig. 11C). Ventrally this niche

lined the telencephalic ventricle until it came into contact with the dorsal boundary of Vd. Type IIa cells (Fig. 11D,E; 29.33%) and type IVa cells (Fig. 11F; 8.33%), and a small number of type III and type V cells (Fig. 11G,H) comprised the PVZ of Dm. Figure 11E shows an example of the cytoplasm of a type IIa cell (arrows) as it extends its

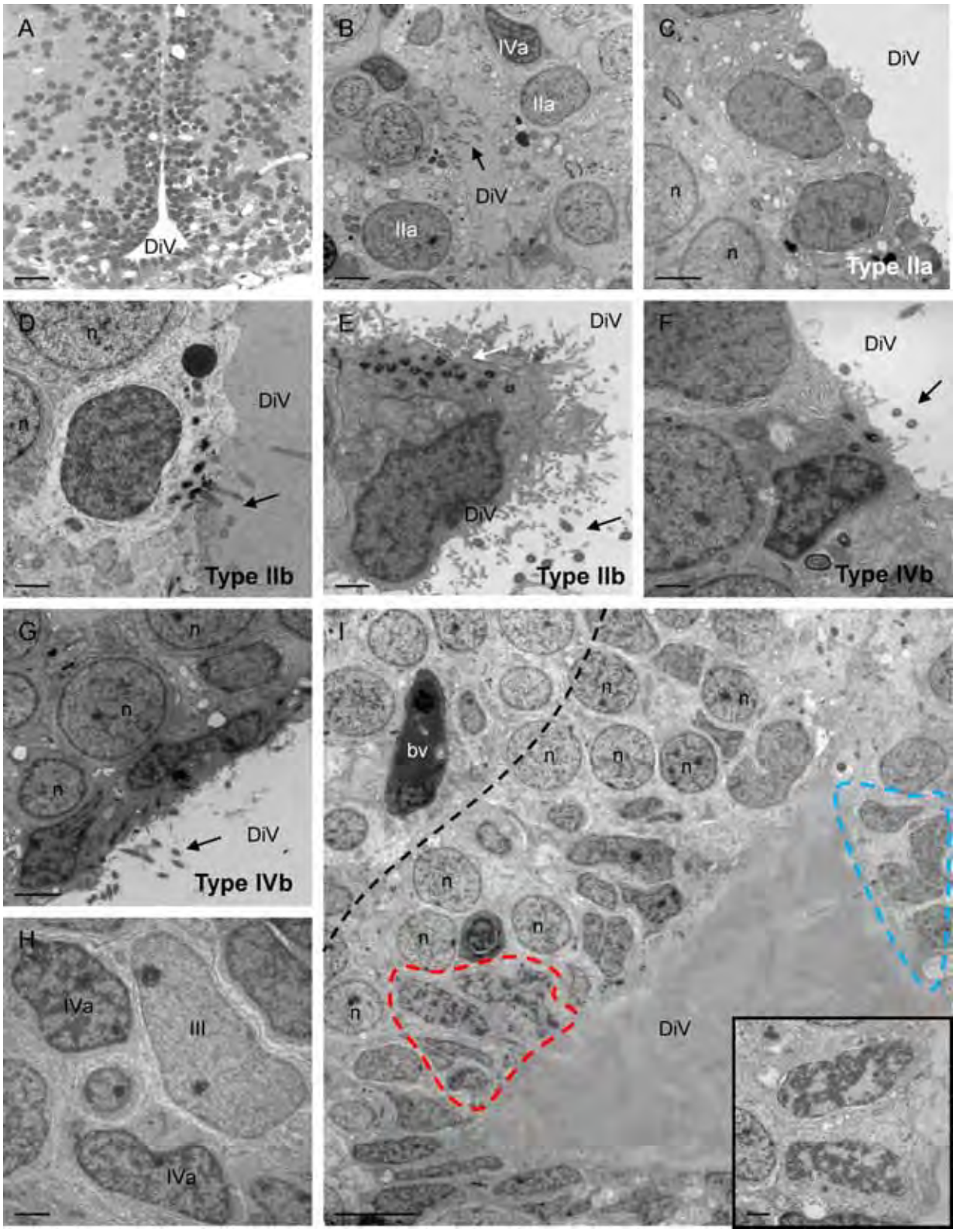

Figure 13. (Legend on page 2302.)

processes both along the ventricular surface as well as into the deeper cell layers of this zone, while coursing between adjacent neurons. The PVZ of Dm had the greatest percentage of neurons localized within any of the six PVZs examined (44.33%), with one to three layers of neurons generally marking the niche boundary (Fig. 11I).

Lateral zone of the dorsal telencephalon (Dl)

The PVZ of Dl was situated along the dorsal lateral region of the forebrain, beneath a single layer of squamous epithelial cells (Fig. 12A–C, arrows). A small amount of luminal space beneath the epithelial cells could be seen in some preparations representing the continuation of the telencephalic ventricle (Fig. 12B, asterisk). No ependymal cells were present in this region. The dorsal boundary of Dl was the dorsal zone of D (Dd), whereas its lateral boundary followed the contour of each hemisphere until the posterior zone of D (Dp) was reached. Typically this PVZ was only one to two cell layers deep (Fig. 12B,C), similar to that of Dm, although it had the second highest estimated surface area (Table 3). However, in contrast to Dm, a more heterogeneous mixture of cell types was present in this niche. These included type IIa (Fig. 12D), type III (Fig. 12E), and type IVa (Fig. 12F), all representing nearly 10% or greater of the total cell population of this zone. Infrequently, type V cells were found, whereas a considerable number of neurons made up nearly a third of the cell population of this PVZ.

Parvocellular preoptic nucleus, anterior part (Ppa)

The PVZ of Ppa extended dorsoventrally along the walls of the diencephalic ventricle within the subpallial zone of the forebrain (Fig. 13A). The number of cell layers composing this zone generally increased from two to four along the dorsoventral axis, and most resembled the organization described in the subpallial PVZ of Vv (Fig. 10D). However, the PVZ of Ppa encompassed the greatest diversity of distinct cell types, including two additional multiciliated cell types not previously detected in other niches. These ciliated cells were most commonly observed in the dorsal aspect of this niche (Fig. 13B), with fewer observed ventrally.

The first of these cell types shared many morphological features with type IIa cells (Fig. 13C), and as a result were classified as type IIb cells. Type IIb cells were most easily distinguished from type IIa cells (Fig. 13C) by the presence of many cilia (9+2 microtubules) projecting into the lumen from the apical cell surface (Fig. 13D,E). Type IIb cells comprised 3.56% of the cell population of the PVZ of Ppa. These cells had ovoid or irregular nuclei; however, their chromatin had a significantly darker, and more reticulated appearance compared with type IIa, and lacked any visible nucleoli. Moreover, despite the abundant cytoplasm of type IIb cells, it contained fewer mitochondria and vacuoles compared with type IIa. However, lipid droplets, dense bodies, and microvilli were commonly observed. Type IIb cells were localized only at the surface of the diencephalic ventricle and made contacts with adjacent type type IIa cells and neurons.

The second ciliated cell type identified within the PVZ of Ppa was most closely related in morphological profile of type IVa cells (Fig. 13H), and as such was referred to as type IVb (Fig. 13F,G). Type IVb cells had much the same heterochromatin organization and variation in nuclear contour as type IVa cells; however, they generally contained more cytoplasm surrounding the nucleus, although this was still far less than seen in ependymal cells, type IIa or IIb cells. The distinguishing characteristic of type IVb cells was its highly ciliated nature, and microvilli extending from the apical surface into the lumen, localized exclusively at the ventricular surface. In the PVZ of Ppa, type IVb cells consisted of 5.93% of the cell population.

Figure 13. Ultrastructural organization of the subpallial PVZ of Ppa. **A:** Semithin image showing the density of cells composing this PVZ situated along the diencephalic ventricle (DiV). **B:** Image showing the rich heterogeneity of cell types within the dorsal zone of the PVZ of Ppa, including two ciliated cell types not previously described in any other PVZs examined. The black arrow shows cilia extending into the ventricle. **C–E:** Type IIa (C) and type IIb cells observed in the PVZ of Ppa. Type IIb cells (D,E) had darker and slightly more reticulated chromatin compared with type IIa cells, with multiple microvilli and cilia (black arrows) extending into the DiV, and a lesser number of organelles present in the cytoplasm. **F,G:** Multiciliated type IVb cells detected in the PVZ of Ppa. Compared with type IVa cells (H), the morphological features of type IVb cells included cilia, a slightly greater number of organelles within the cytoplasm, and clumped/reticulated heterochromatin similar to type IVa cells. Both multiciliated type IIb and type IVb cells were predominantly seen in the dorsal zone of the PVZ of Ppa, with few detected in the ventral zone of Ppa. **H:** Morphological profiles of type III and type IVa cells that, along with neurons, composed nearly all the ventral zone of the PVZ of Ppa as illustrated in I. **I:** Overview of the cytoarchitecture of the ventral zone of the PVZ of Ppa. The black dashed line denotes the lateral boundary of the PVZ of Ppa, and the blue and red dashed lines show clusters of type III and type IVa cells, respectively, composing this ventral zone of Ppa. The inset displays two newly divided daughter cells seen at the ventricular surface. See also Table 5 for additional morphological features of type IIb and type IVb cells, and Table 6 for the frequency of cell types within the PVZ of Ppa. In all images dorsal is up. n, neuron; bv, blood vessel. Scale bar = 10 μm in A; 2 μm in B,C,G; 1 μm in D,E,F,H, inset in I; 5 μm in I.

TABLE 7.

Immuno-TEM labelling of morphologically distinct cell types (% cells analyzed)

	# Cells analyzed	Type IIa	Type IIb	Type III	Type IVa	Type IVb	Type V	Neurons	Unknown
BrdU	95	26.3	N.D.	26.3	21.1	N.D.	–	–	15.8
S100β	46	50	4.3	13	32.6	N.D.	–	–	–
GS	57	91.2	N.D.	–	–	N.D.	–	–	8.8
HuC/D	152	–	–	–	–	–	–	100	–

N.D. indicates that the morphological profile of the cell type was not detected in LR White sections. Dash (-) denotes the cell type was not labelled with the antibody

More ventrally along the PVZ of Ppa, the number of cell layers composing the niche increased, similar to the PVZ of Vv. Only a few ciliated type IIb and IVb cells were seen in this region; this ventral region of Ppa was made up of mainly type III and type IVa cells, along with neurons (Fig. 13I). Thus, it appeared that the dorsal zone of Ppa was composed of a more heterogeneous mixture of cell types, whereas ventrally, as the lumen enlarged, only two cell types comprised this PVZ. A notable difference between the niche of Ppa and that of Vv was that the ventral floor of the diencephalic ventricle was proliferative and was therefore included as part of the PVZ (Fig. 13I). Within the ventral portion of this zone of Ppa, several mitotic events were also detected at the luminal surface (Fig. 13I, inset).

Immunohistochemical labeling of morphologically distinct cell types reveals the phenotype of three proliferative cell populations within periventricular zones

To further confirm the phenotype of the different cells composing forebrain PVZs, immunolabeling experiments were performed at the EM level on resin-embedded tissue (Table 7). For all markers, immunonegative cell types were observed, but were not examined in detail in this particular analysis. Positive antibody labeling of cells was visualized by using either 10 nm gold particles or DAB labeling. When gold particles were used, one or more sections were left unstained for each marker to better visualize positive labeling. Sections encompassing rostral (D, Vd, Vv) and caudal (Dm, Dl, Ppa) PVZs were labeled with antibodies against GS, S100β, and HuC/D. When positively labeled cell types could not be correlated with our above classification scheme as a result of the staining methods used for immunolabeling of ultrathin sections, cells were classified as "unknown." A total of 57 GS+ cells were identified and analyzed across tissue sections, with cytoplasmic labeling of this marker restricted almost exclusively to type IIa cells (91.2%) as evidenced by the density of gold particles within these cells (Fig. 14A,B). Type IIa cells could easily be distinguished by their abundant cytoplasm, numerous mitochondria and vacuoles, and position adjacent to the lumen (Fig. 14C–F). DAB labeling additionally revealed GS+ cell bodies with cytoplasmic processes extending from the soma of type IIa cells into the deeper layers of the PVZ (Fig. 14G,H), suggestive of putative radial glial cells. Moreover, in rare instances, GS+ staining could also be detected on the walls of proximal blood vessel (Fig. 14I).

By contrast, as predicted, S100β+ labeling appeared more widespread across cell types. Of the 46 S100β+ cells detected, a subpopulation of both type IIa cells (50%; Fig. 15B,C) and less frequently ciliated type IIb cells (4.3%; Fig. 15D) displayed gold labeling in the cytoplasm, with scant labeling also seen in the nucleus (Fig. 15A). A smaller number of putative type III (13%) and type IVa (32.6%) cells were also S100β+ (Fig. 15E,F); however, S100β+ labeling in these cell types was notably less than type IIa. Finally, DAB labeling using the neuronal marker HuC/D confirmed the presence of neurons both interspersed within PVZs and bordering these zones laterally adjacent to the parenchyma, following examination of 152 positively labeled cells (Fig. 15G–I).

To next identify which of the above cell types were mitotically active, we used antibodies against BrdU conjugated to 10-nm gold particles to label and visualize cells in the S-phase of the cell cycle. We analyzed a total of 95 BrdU-positive cells across ultrathin sections following labeling (Table 7). Three morphologically distinct cell types were BrdU+ across PVZs, with the percentage of BrdU+ labeling between cell types evenly distributed among subpopulations of type IIa (26.3%), type III (26.3%), and type IVa cells (21.1%; Fig. 16). All cell types displayed gold labeling localized specifically to the nucleus (Fig. 16A). Type IIa BrdU+ cells were identified mainly at the ventricular surface (Fig. 16B–D); their morphological profile was confirmed by the extensive cytoplasm surrounding the positively labeled nucleus. Proliferative type III (Fig. 16E–H) and type IVa (Fig. I–L) cells were observed both at the lumen and at deeper cell layers, and appeared to be more frequently labeled within the ventral aspect of the PVZ of Vv. Multiciliated type IIb and IVb cells could not be detected in the tissue, and thus it remained undetermined whether these cells contribute to the proliferative population. These findings indicate the presence of at least three proliferative

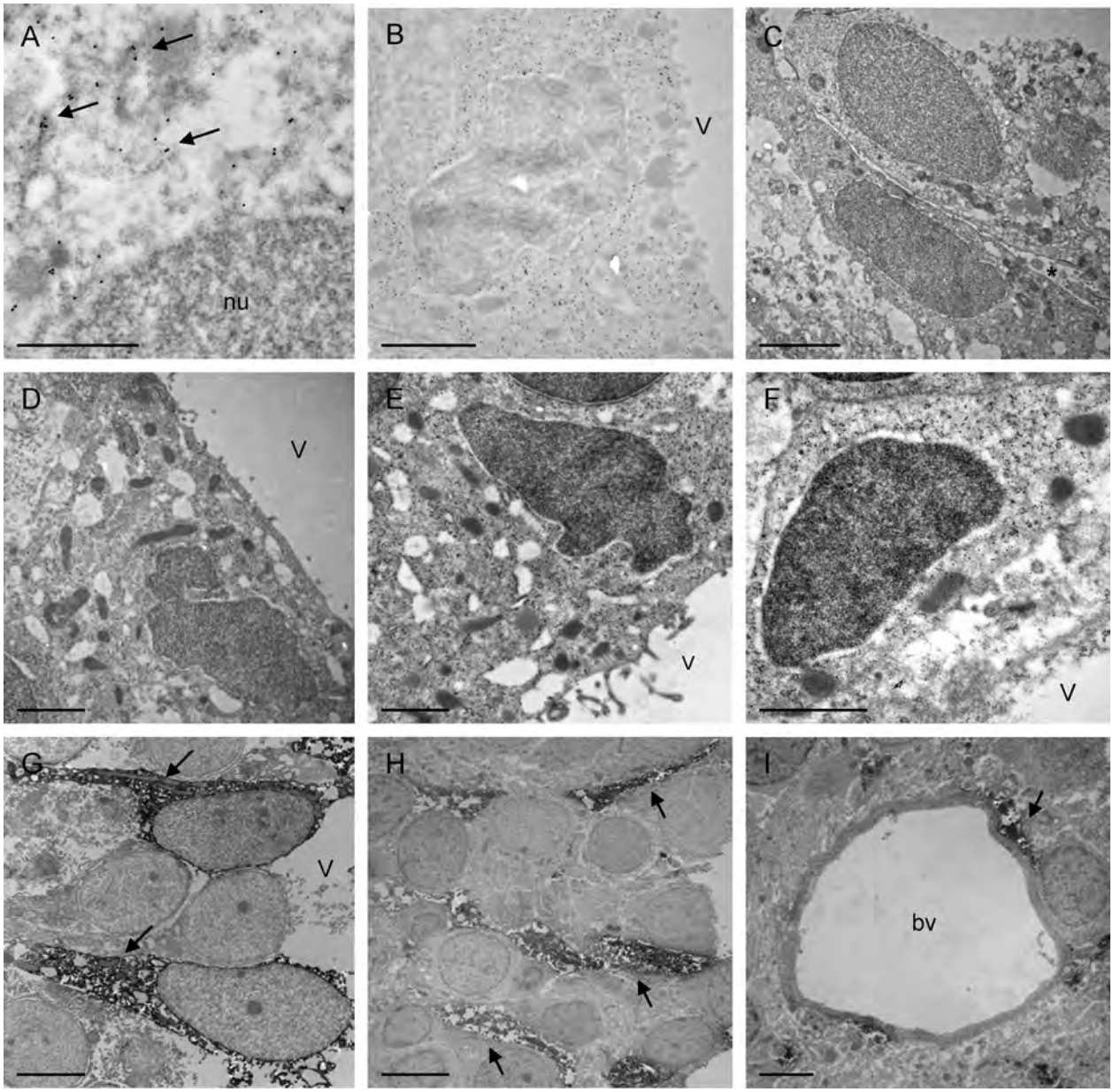

Figure 14. Glutamine synthetase-positive immunogold labeling of type IIa cells. **A,B:** High (A) and low (B) magnification image showing the specificity of gold particles to the cytoplasm (black arrow in A) of type IIa cells in the absence of contrast staining. **C–F:** Examples of GS+ labeling in subpopulations of type IIa cells situated at the ventricular surface distinguished by their large nuclei, abundant cytoplasm containing many mitrochondria and vacuoles, and a small number of microvilli projecting into the lumen. **G–I:** Using DAB labeling, the cytoplasmic processes of type IIa cells are seen extending into the deeper cell layers of the PVZ (G,H, black arrows), and in some instances these processes (black arrows in I) were detected on the walls of surrounding blood vessels. See also Table 7 for a summary of immuno-TEM labeling across all cell types. In all images dorsal is up. GS, glutamine synthetase; DAB, 3,3′-diaminobenzidine; nu, nucleus; bv, blood vessel; v, ventricle. Scale bar = 500 nm in A; 1 μm in B,D–F; 4 μm in G,H; 2 μm in C,I.

subpopulations with distinct cell morphologies within forebrain PVZs of the mature zebrafish: BrdU+ type IIa, type III, and type IV cells. Moreover, by comparing the ultrastructural phenotype of S100β+ and GS+ cells with those displaying BrdU+ labeling following single immunostaining with these antibody markers, our EM data suggest that subpopulations of S100β+/BrdU+ and GS+/BrdU+ type IIa cells, S100β+/BrdU+ type III cells, and S100β+/BrdU+ type IVa cells also likely exist within the PVZs investigated here, similar to that described in our co-labeling studies using cryosectioned tissue. However, future co-expression experiments for these and other markers at the EM level are required to confirm this hypothesis.

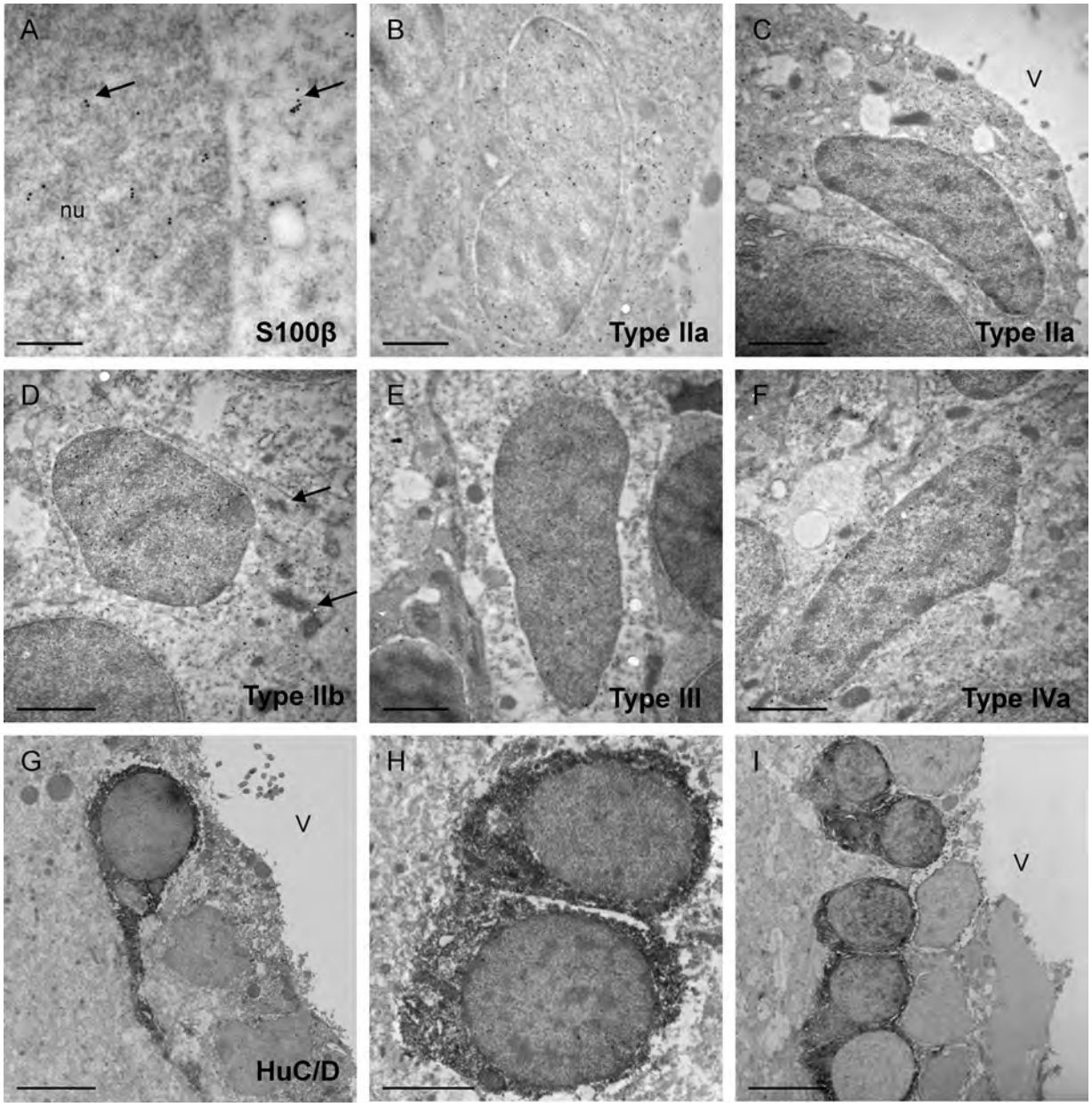

Figure 15. Immunolabeling of resin-embedded tissue used to identify the morphological profile of cells with a general glial (S100β) or neurononal (HuC/D) phenotype. **A,B:** High (A) and low (B) magnification images showing the localization of immunogold labeling of S100β overlapping in both the nucleus and cytoplasm (black arrows in A) in type IIa cells in the absence of contrast staining. **C–F:** Examples of S100β+ immunogold labeling of subpopulations of type IIa (C), type IIb (D, black arrows denote cilia), type III (E), and type IVa (F) cell types across different PVZs. **G–I:** Immunopositive DAB labeling for the mature neuronal marker HuC/D confirming the morphological phenotype of neurons located within PVZs, and typically divided from the ventricular surface by cytoplasmic processes of surrounding cells. Mature neurons could often be easily detected by their large, ovoid nucleus. Note that the staining pattern was specifically localized to the cytoplasm and processes of these cells. See also Table 7 for a summary of immuno-TEM labeling across all cell types. In all images dorsal is up. nu, nucleus; v, ventricle; DAB, 3,3′-diaminobenzidine. Scale bar 200 nm in A; 1 μm in B,D,E,F; 2 μm in H; 4 μm in G,I.

The number of newborn neurons peaks 2 weeks after birth, accounting for nearly half of the BrdU+ cell population, although at 4 weeks few neuronal subtypes are detected

In order to determine the timeline of neuronal differentiation across PVZs, we next performed an immunohistochemical labeling study in which animals were pulsed with BrdU and sacrificed 1, 2, or 4 weeks later. Co-labeling of BrdU with PSA-NCAM to identify newly differentiated, migrating neurons revealed a notable increase in the number of BrdU+/PSA-NCAM+ cells between 1 and 2 weeks (Fig. 17A,B); however, a significant difference

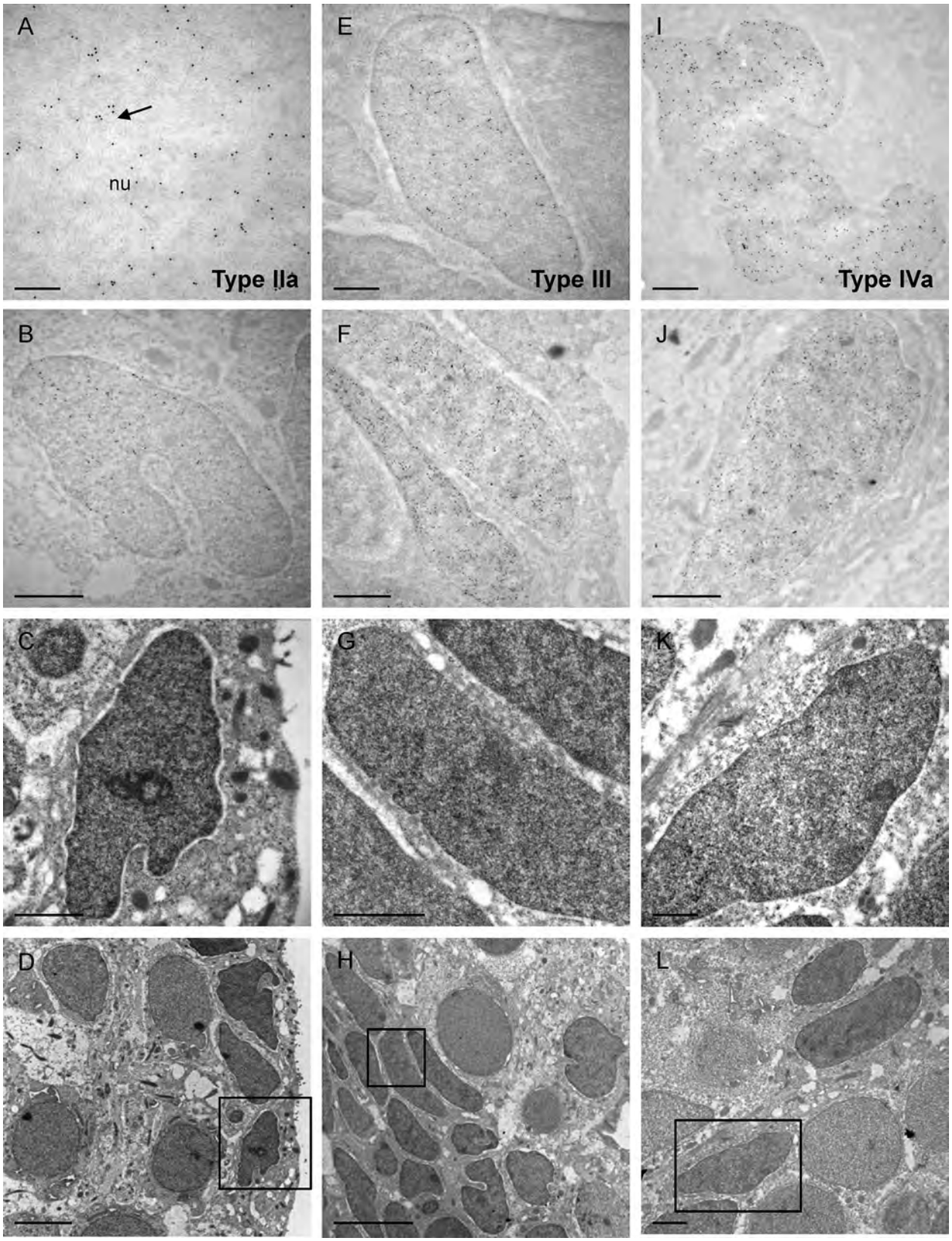

Figure 16

was reported only for the PVZ of D (independent samples t-test). Four weeks following BrdU injections, BrdU+/GS+ labeling showed that in some niches (Dm, Dl) nearly 35% of BrdU+ cells had given rise to radial glia cells (Fig. 17C,E). Considerable variation in the size of the BrdU+/GS+ cell population across PVZs could be seen, mainly between the pallial and subpallial zones (Fig. 17E). No BrdU+/GS+ co-labeling was found within the PVZ of Vv (Fig. 17D), whereas Ppa had less than 10% of the population BrdU+/GS+ (Fig. 17E). As a result, a significant difference in the percentage of BrdU+/GS+ cells was revealed between the subpallial zone of Vv and the pallial zone of Dm and Dl (one-way ANOVA; post hoc test). Moreover, by tracking the number of BrdU+/HuC/D+ cells at multiple time points, we were able to assess what percentage of the niche-specific BrdU+ cell population gave rise to de novo neurons and when differentiation rates began to vary between PVZs (Fig. 17F,G). Our data demonstrated a consistent rate of increase in neuronal differentiation across all PVZs from 2 hours to 1 week, after which time zones appeared to either increase (Dm, Ppa) or decrease (Vd, D) the rate of neuronal production, or the rate remained approximately the same (Vv, Dl; Fig. 17G). We found that with the exception of Vd, all forebrain PVZs reached the maximum number of newborn neurons by 2 weeks, with the number of BrdU+/HuC/D+ cells typically decreasing thereafter.

To assess the phenotype of newborn neurons across PVZs, a series of labeling experiments using neuronal subtype-specific markers were further executed over the same 4-week pulse-chase timeline as above. Co-labeling with BrdU and the calcium-binding protein calbindin, or the dopaminergic marker tyrosine hydroxylase (TH), revealed a near absence of co-labeled populations following the 4-week differentiation period. Less than 2% of BrdU+ cells were also positively labeled for calbindin in the PVZ of Ppa (Fig. 17H). Calbindin+ labeling was observed in all other PVZs; however, no co-labeling was detected. No co-labeling of BrdU+/TH+ cells was observed across any of the PVZs investigated, with TH+ cells typically localized to the lateral aspect of most niches (Fig. 17I). Similarly, positive co-labeling of BrdU and expression of GFP from the transgene *Tg[dlx5a/6aIG:gfp]*, which marks a large fraction of GABAergic neurons during late embryonic and early larval development, could not be detected in any PVZs, despite the presence of a relatively high number of GFP+ cells within and surrounding some PVZs (Fig. 17J).

Finally, to obtain positional data related to the migration pattern of differentiating BrdU+ cells arising from within the PVZ over the long term, we examined the position of BrdU+ cell populations after 2 hours, 4 weeks, and 10 months (Fig. 17K). The displacement of BrdU+ cells was determined by measuring the cell from the center of the nucleus to the edge of the ventricle at each time point. The movement of BrdU+ cells shows that across all PVZs this population migrated away from the ventricle over the first 4 weeks, albeit at different rates. After only 4 weeks many of the BrdU+ cells sampled were positioned outside the lateral borders of the PVZ. With the exception of Vv, it appeared that at 10 months post-BrdU injection, cells had displaced between 10 and 20 μm from their original position within the boundaries of the niche at 2 hours, some resembling a near plateau. In contrast, BrdU+ cells within the PVZ of Vv displayed a marked increase in cell migration between 4 weeks and 10 months, with the curve suggesting migratory behavior of these cells well beyond the maximum 10-month time point used here. These findings suggest that at least one common mode of cell migration of newborn neurons is to exit the boundaries of the PVZ over time by radial migration toward the parenchyma. We did not evaluate the possibility of rostrocaudal migration in these experiments. However, whether the rate of migration and position of newborn neurons over time can indicate the phenotypic fate of these cells remains to be tested.

DISCUSSION

Studies of the adult neurogenic niche of vertebrate (Garcia-Verdugo et al., 2002) and invertebrate (Schmidt and Derby, 2011) species have reported a range of different cellular organizations since the composition of the mammalian SEZ niche was first proposed over a decade

Figure 16. Bromodeoxyuridine-positive immunogold labeling in type IIa (A–D), type III (E–H), and type IVa (I–L) cells. **A–D:** High (A) and low (B) magnification images showing the specificity of gold particles to the nucleus (black arrow in A) in a subpopulation of proliferative type IIa cells in the absence of contrast staining. Morphological features of type IIa cells observed following contrast staining (C) and their position among adjacent cell types in the PVZ (D). **E–H:** A subpopulation of proliferative type III cells without (E,F) and with (G,H) contrast staining showing their morphological features and position in the PVZ. **I–L:** A subpopulation of proliferative type IVa cells without (I,J) and with (K,L) contrast staining displaying their characteristic morphological features and position in the PVZ. Black boxes in D, H, and L indicate the same cell type shown at higher magnification in C, G, and K respectively. See also Table 7 for a summary of immuno-TEM labeling across all cell types. In all images dorsal is up. nu, nucleus. Scale bar = 200 nm in A; 1 μm in B,C,F,G,J,L; 4 μm in D,H; 500 nm in E,I,K.

ago (Doetsch et al., 1997). To advance our understanding of niche-specific differences across vertebrates, the present study has documented the cytoarchitectural organization of six distinct forebrain neurogenic niches (periventricular zones [PVZs]) in a model teleost species, the zebrafish, by comparing the cellular composition between niches. Based on this work, we present a novel classification scheme of the niche-specific cell types and propose a model of the organization of these cells between pallial and subpallial zones of the adult zebrafish forebrain. We

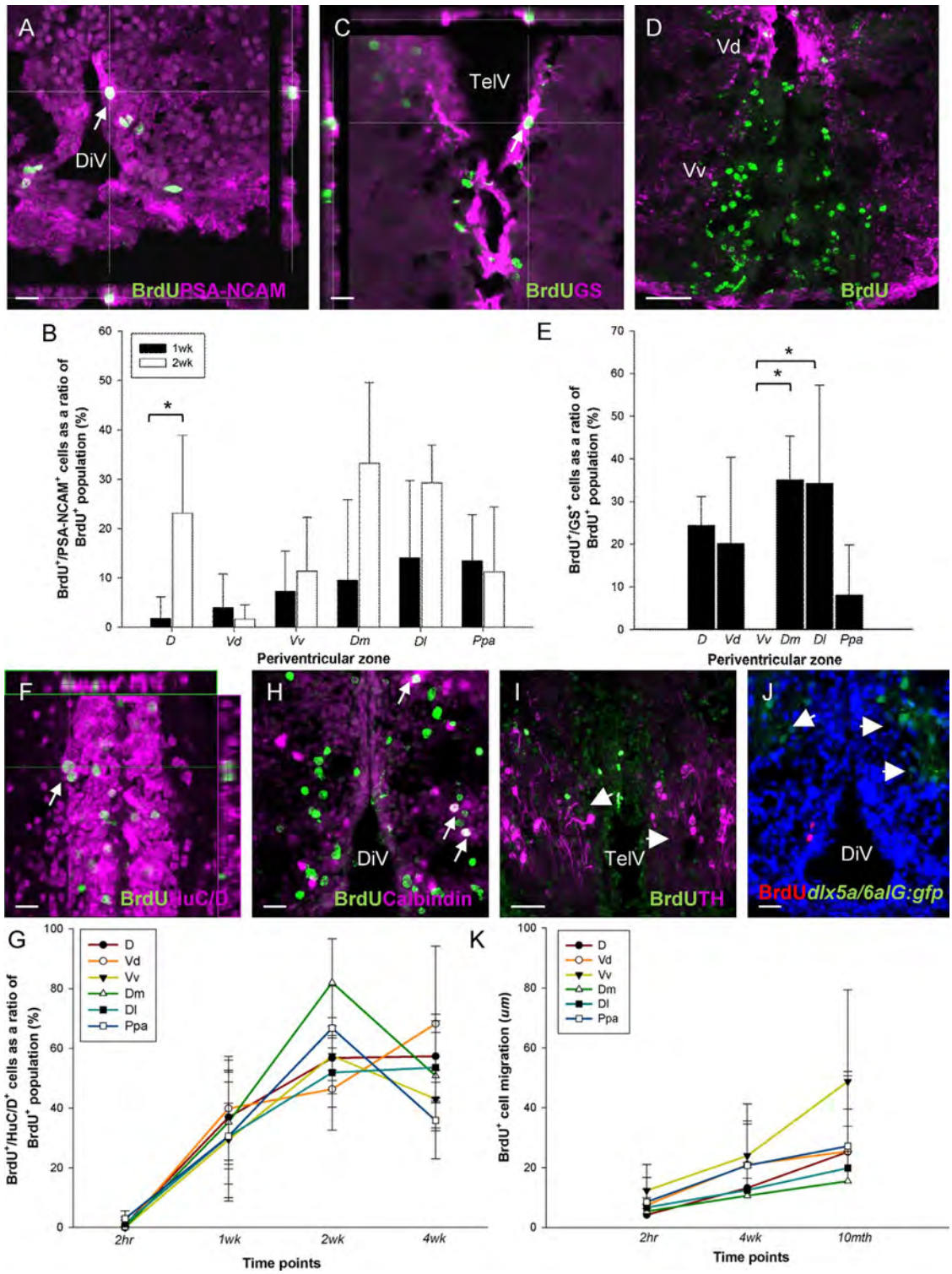

Figure 17

further complemented these morphological studies with comparisons of the density of proliferative cells, the cell cycle kinetics, the phenotype of proliferative cells, and the rate of neuronal differentiation between PVZs to gain insight into the fundamental cell parameters regulating neuronal production in the adult brain.

Model of the ultrastructural composition of adult zebrafish forebrain neurogenic niches

A central aim of the present study was to provide a detailed account of the ultrastructural composition of the major forebrain PVZs in the adult zebrafish. Here, we propose two cytoarchitectural models summarizing our descriptive analysis of six distinct neurogenic PVZs (Fig. 18). Detailed TEM across PVZs revealed seven morphologically distinct cell types, all of which display varying frequencies between zones. Of these cell types only two were multiciliated (type IIb, type IVb), whereas four nonciliated cell profiles were observed in addition to neurons. Figure 18A shows the common cellular composition of the PVZs of D, Vd, Dm, Dl, and the dorsal zone of Ppa, with type IIb and IVb cells exclusive to the niche of Ppa. Type IIa cells, with extensive cytoplasmic processes, along with neurons, were typically most abundant in these niches, with a lesser number of type III, IVa, and V cells observed. In contrast, the subpallial ventral zone of Ppa and the PVZ of Vv shared a similar composition, comprised primarily of type III and type IVa cells, and neurons (Fig. 18B).

These findings reveal that the subpallial niche of Vd and the dorsal zone of Ppa more closely resemble the ultrastructural organization of pallial PVZs. This may imply that a similar set of cellular and noncellular cues regulating the pallial niches overlaps within the niche of Vd and the dorsal zone of Ppa. Immunolabeling of resin-embedded tissue exposed three proliferative cell types, including subpopulations of BrdU+ type IIa, type III, and type IVa cells. By correlating the morphological signature of these cell types with those observed to be S100β+ and GS+, our EM data suggest that putative subpopulations of S100β+/BrdU+ and GS+/BrdU+ type IIa cells, S100β+/BrdU+ type III cells, and S100β+/BrdU+ type IVa cells likely also contribute to the overall cell population comprising PVZs. Nevertheless, we found that neighboring populations of type IIa, III, and IVa cells immunonegative for proliferative and glial markers appear to also exist within neurogenic zones, warranting further investigation as to the phenotype of these cells. These findings suggest a dichotomy not only between the cellular makeup of pallial and subpallial PVZs, but additionally the proliferative phenotypes of cells, with pallial PVZs (including the dorsal zone of Ppa) containing three different mitotic populations, compared with only two in the subpallial PVZs of Vv and Ppa (ventral zone).

Forebrain neurogenic niches in the adult zebrafish share intermediate features with the ultrastructural composition of the ventricular niche of their vertebrate relatives

The number of neurogenic niches in teleosts outnumbers those described in mammals, although the mechanisms regulating this difference are still not well understood. Few studies have examined the cellular composition of neurogenic niches of telost fishes or amphibians, two anamniotic vertebrate classes distinguished for both their regenerative and their neurogenic

Figure 17. Phenotype of BrdU-positive cells and displacement of this population following BrdU pulse-chase experiments compared between PVZs. **A,B:** BrdU+/PSA-NCAM+ co-labeling (A) quantified 1 and 2 weeks post-BrdU injection (B). Significance (*) was determined by using independent samples t-tests ($P \leq 0.05$). **C–E:** BrdU+/GS+ co-labeling (C) quantified 4 weeks post-BrdU injection (E). Note that with the exception of the PVZ of Ppa and Vv, this population comprises nearly 20–30% of the phenotype of BrdU+ cells. The absence of co-labeling detected in the PVZ of Vv is a result of little to no GS+ staining within this region (D). Significance (*) was determined by using a one-way ANOVA and Tukey's HSD post hoc tests ($P \leq 0.05$). **F,G:** BrdU+/HuC/D+ co-labeling (F) quantified at 2 hours and 1, 2, and 4 weeks post-BrdU injection to examine the percentage of newborn BrdU+/HuC/D+ cells composing the BrdU+ cell population (G). Notice that within all PVZs a steady increase in the number of co-labeled cells is seen from 2 hours to 1 week, and that this trend continues until 2 weeks, when the number of BrdU+/HuC/D+ cells reaches a maximum, with the exception of the niche of Vd. The number of newborn neurons between PVZs was most variable between the chase period of 2–4 weeks, at which time this cell population could be seen to decrease (Dm, Ppa, Vv), plateau (D, Dl), or continue to increase (Vd). **H:** BrdU+/calbindin+ staining observed in the PVZ of Ppa 4 weeks following birth. This population was only detected in Ppa, and consisted of less than 2% of the BrdU+ cells. **I:** BrdU+/TH− labeling in the PVZ of Vv after 4 weeks. In most PVZs the TH+ cells could be seen near the lateral boundary (white arrowheads), but no co-labeling was observed. **J:** Dlx5a/6aIG/gfp+ labeling of a subpopulation of GABAergic cells detected within and bordering (white arrowheads) the different PVZs. No co-labeling of this cell population with BrdU+ cells was observed. Nuclear counterstaining was done by using Hoechst 33258 (blue). **K:** Migration of BrdU+ cells from their original position within the boundaries of the PVZs at 2 hours, and examined following 4-week and 10-month BrdU chase periods. All PVZs demonstrated radial displacement ranging from 15 to 20 μm after 10 months relative to their original, with the exception of the PVZ of Vv, which showed a considerably higher rate of migration over time. In all images dorsal is up. For abbreviations, see list. Scale bar = 8 μm in A,C,F,H,J; 50 μm in D,I.

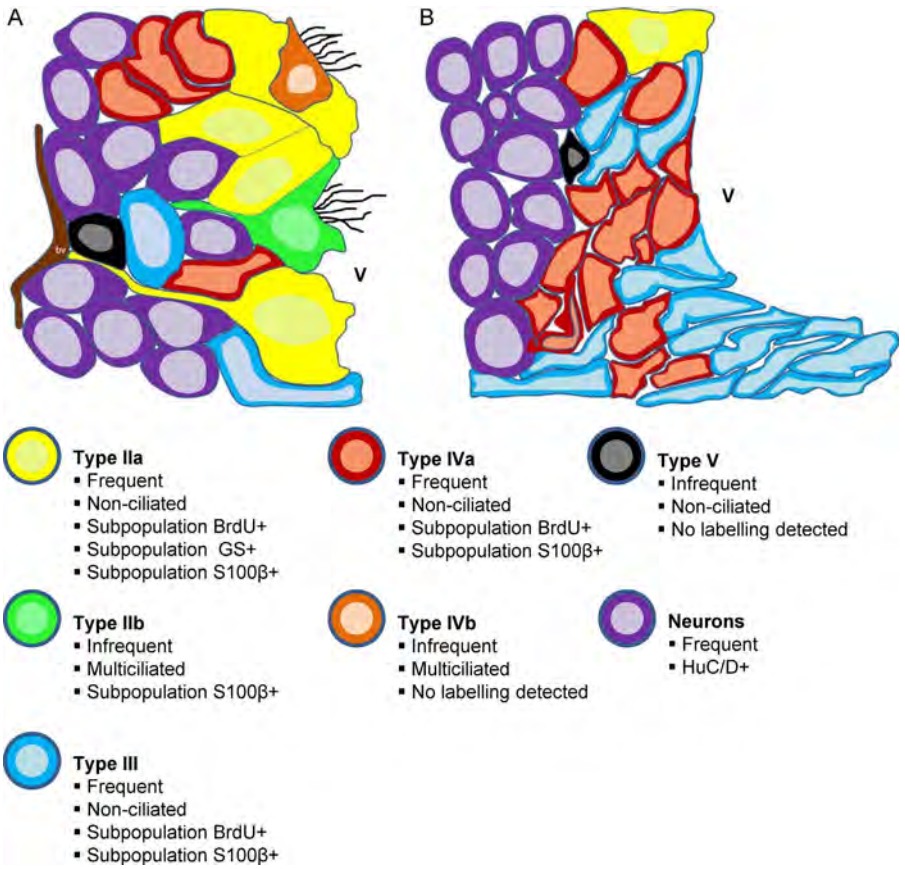

Figure 18. Model of the ultrastructural organization and cell types composing the six neurogenic PVZ niches described in this study. **A:** Schematic representation of the cellular composition of the PVZ of D, Vd, Dm, Dl, and the dorsal zone of Ppa. Note that multiciliated type IIb and IVb cells were only observed in the dorsal zone of the PVZ of Ppa, whereas all other cell types were commonly observed across PVZs. The processes of type IIa cells could be observed extending into the deeper layers of the PVZ and at times contacting proximal blood vessels (bv). Note that the subpallial PVZ of Vd and the dorsal zone of Ppa appear to contain a cytoarchitectural organization more closely resembling pallial PVZs. **B:** Schematic representation of the cellular composition of the PVZ of Vv and the ventral zone of the PVZ of Ppa. These two ventrally located niches consisted almost exclusively of a density of type III and type IVa cells, with a number of neurons forming the deeper layers of the niche. The main features of each cell type are denoted in the legend. For all cell types immunopositive for subpopulations of BrdU, S100β, or GS, subpopulations immunonegative for these markers were also present. v, ventricle.

capacities throughout life (reviewed in Lindsey and Tropepe, 2006). Uncovering the constituent cell types composing the neurogenic microenvironment remains an essential starting point to elucidate the manner by which active proliferation and neurogenesis are maintained throughout maturity in these species. Given the phylogenetic position of teleost fishes, the notion that the ultrastructural features of niches may more closely resemble those of their nonmammalian relatives might be expected compared with mammals; however, from our studies we find that these niches demonstrate intermediate cellular features of both groups. We show that the composition of periventricular niches in the adult zebrafish forebrain is made up of a complexity of cell morphologies creating distinct neurogenic compartments, similar to the numerous cell types present in the SEZ of mammals. The seven cell types described in these compartments show both niche-specific pallial and subpallial differences, in addition to regionally specific variation in cell types within a single niche (i.e., PVZ of Ppa).

A key finding of this work was the paucity of classical ependymal cells within any of the niches examined (Fig. 7), unlike the continuous ependymal lining observed along the ventricular surface of the SEZ of mammals (Doetsch et al., 1997; Gil-Perotin et al., 2009; Sawamoto et al., 2011) or the fragmented ependymal lining seen in the neurogenic niches of reptiles and birds (reviewed in Garcia-Verdugo et al, 2002). Ependymal cells were exclusively observed forming the roof of the telencephalic ventricle and covering the forebrain hemispheres a short distance dorsolaterally in the pallial niches of D and Dm.

Within the neurogenic PVZs themselves, GS+ radial glial-like type IIa cells seem to resemble the type B1

astrocytes previously described in mammals (Doetsch et al., 1997) and the homologous type B radial glia of birds and reptiles (Garcia-Verdugo et al., 2002). The use of DAB labeling of GS+ cells at the EM level provided suggestive evidence of the characteristic radial processes extending from the cell soma into the parenchyma (Fig. 14G,H), similar to that seen in cryosectioned tissue immunolabeled for this same marker (Fig. 6D). However, the apparent absence of a single cilium in type IIa cells described in our study may indicate a modified form of radial glia or that these went undetected during our analysis. A small number of cilia could often be seen in the ventricle adjacent to all PVZs; however, unless cilia could be reliably traced back to the corresponding cell type, cells were classified as lacking cilia. Additional serial reconstructions studies of immunolabeled GS+ populations of type IIa cells at the EM level would allow processes to be more faithfully tracked and further elucidate the radial glial-like nature of this phenotype.

Based on the occurrence of cell types between niches, a clear dichotomy in the cellular composition between select pallial and subpallial niches was apparent. The subpallial rostral niche of Vv and the ventral zone of the caudal niche of Ppa surrounding the diencephalic ventricle were composed almost exclusively of a number of tightly packed type III and type IVa cells. The ultrastructural features and BrdU+ labeling of type III and type IVa cells are reminiscent of morphological profile of type A and type C cells in mammals (Garcia-Verdugo et al., 2002), respectively. However, in the forebrain niches of the adult zebrafish these cell types are seen both at the ventricular surface in addition to the deeper layers of the niche, in contrast to the position of type A cells in mammals, birds, and reptiles, and type C cells in mammals, which are divided from the luminal surface by type B cells. Furthermore, type III cells in zebrafish express S100β, which is not expressed in the type A neuronal progenitors in the mammalian forebrain.

In one of the first studies to investigat the proliferative ventricular zone of a teleost, Zupanc and Zupanc (1992) revealed a density of cells with medium to darkly staining nuclei with elongate/irregular nuclear contours and lightly staining cytoplasm within the central posterior prepacemaker nucleus situated in the third ventricle of the weakly electric knifefish (*Eigenmannia* sp.). Similar to the localization of type III and IVa cells in our study, the elongated cells with more lightly staining nuclei were more often situated at the lumen, whereas the darkly staining cells, which appeared to have more irregular nuclear contours, were located one to two layers deep. This earlier study also showed evidence of multiciliated subpopulations of cells intermingled with the above cell types along the third ventricle, which is in line with the multiciliated type IIb and type IVb cells detected specifically in the PVZ of Ppa in our study. The restricted localization of type IIb and IVb cell types to the niche of Ppa was a surprising finding, given the proposed role of cilia in cerebrospinal fluid flow to provide directional migration of differentiating neurons (Mirzadeh et al., 2010; Amador-Arjona et al., 2011). Whether these multiciliated cell types present only in the subpallial niche of Ppa surrounding the diencephalic ventricle have developed specialized functions or serve as the ependymal-like cells of this ventricle to provide fluid flow in the absence of an ependymal lining, as seen in the roof of the telencephalic ventricle, remains to be determined.

More recently, studies in the adult zebrafish forebrain have revealed the compact cellular nature of the subpallial neurogenic compartment of Vv. Ganz et al. (2010) used resin-embedded semithin sections to display the general composition of this niche and the presence of mitotic profiles at the ventricular surface, similar to the location of mitoses seen in the niche of Vv and Ppa here. In line with this, we have confirmed the proliferative nature of subpopulations of type III and type IVa cells at the ultrastructural level by using immunogold labeling for BrdU+ cells. We have shown that these two cell types, which are most prevalent in niches surrounding the ventral telencephalic and diencephalic ventricles, are immunopositive for BrdU and the general glial marker S100β. However, in contrast to the type IIa cells discussed above, these two populations did not label with the radial glial/astrocytic marker GS. Interestingly, a recent study examining the putative rostral migratory stream in the adult zebrafish forebrain proposed the presence of three morphologically distinct cell types in the niche of Vv, identified by having either round nuclei, nonelongated nuclei, or elongated nuclei with a single cilium extending into the ventricle; these authors proposed that the cell with the elongated morphology was the radial glial cell resident in the niche (Kishimoto et al, 2011).

The elongated cell morphology described by Kishimoto et al. (2011) is in agreement with the type III cells based on our classification scheme across PVZs; however, our data do not support the notion that these cells are radial glia. First, across all PVZs examined, we did not convincingly detect cilia projecting from this cell type, nor were these cells immunopositive for GS at the ultrastructural level. Moreover, immunolabeling studies of cryosectioned tissue corroborated these ultrastructural results, showing an almost complete lack of BrdU+/GS+ co-labeling in cells located in the subpallial niches of Vv and Ppa 2 hours (Fig. 6F) and 4 weeks (Fig. 17C–E) post-BrdU injections; the niches were composed mainly of type III and type IVa cells. Finally, we never saw radial glia-like processes extending into the deeper layers of the niche while

examining type III cells, whereas this was most commonly detected in type IIa cells (Fig. 11E). We do not dispute that the elongated profile of type III cells is suggestive of a proliferating progenitor phenotype, although the multiple lines of evidence shown here do not support the view that these cells have a radial glial morphology.

Specifying the boundaries of the neurogenic niche and evaluating its proliferative capacity

A hallmark feature of adult neurogenesis is the existence of an actively dividing proliferative pool of stem/progenitor cells from which de novo neurons can be generated over time. The size of the proliferative pool and their associated cell cycle kinetics directly influence the neurogenic output of the niche, and thus defining the niche boundaries where this mitotic population is maximal is crucial to uncovering the phenotype of adult neural stem/progenitor cells. Here, we show that along the rostrocaudal axis of each of the six neurogenic PVZs examined there exists a narrow range in which the density of mitotic cells is greatest, which can be used to more stringently specify the niche boundaries in this plane (Figs. 2, 3). In all instances, cycling cells were located proximal to the forebrain ventricles following the 2-hour BrdU pulse-chase period, rather than in the deeper parenchymal regions of PVZs. Nevertheless, we cannot rule out a small contribution of parenchymal derived cells toward the adult neurogenic population, although parenchymal neurogenesis was not explicitly examined in this study. Only following longer chase periods (i.e., 2 and 4 weeks) were proliferative cells seen displaced toward the parenchyma, providing evidence that the major source of de novo neurons arises from mitotic stem/progenitor cells bordering the midline forebrain ventricles.

In defining the rostrocaudal boundaries, we found that niches could be categorized into three groups: niches showing a fairly even distribution of BrdU+ cells between the rostral- and caudalmost levels (D, Dm); niches displaying significantly denser populations of BrdU+ cells more rostrally (Vd, Vv); and niches demonstrating a significantly higher density of BrdU+ cells at the caudalmost extent of the neuroanatomical region in which they reside (Dl, Ppa). The density of BrdU+ cells situated rostrally in the PVZ of Vv reported here agrees well with other studies examining the subpallial niche of Vv as the source of proliferative cells migrating along a putative rostral migratory stream toward the olfactory bulbs (Adolf et al., 2006; Marz et al., 2010; Kishimoto et al, 2011). The localization of niche boundaries along the rostrocaudal axis of the forebrain nuclei in which they reside appears in most cases to be positively correlated with the size of the forebrain ventricle. For instance, the size of the telencephalic ventricle along the rostrocaudal axis of D and Dm shows little variation, whereas this same ventricle in the subpallium is most prominent at the rostral aspect of Vd and Vv, with the diencephalic ventricle adjacent to Ppa showing a more caudal enlargement. This trend may in part be explained by the need for ventricular fluid flow to provide trophic support to the stem/progenitor populations residing in the niche in order to maintain an active state for proliferation (Buddensiek et al., 2010). Additionally, the vascular environment is likely to play a role in the regionalization of neurogenic niches in the zebrafish forebrain, as demonstrated in the mammalian SEZ (Tavazoie et al., 2008).

The cell cycle kinetics of proliferative stem/progenitor cells initiate the process of adult neurogenesis within the boundaries of the niche and provide a method of identifying different proliferative populations based on their cell cycle parameters. Earlier studies using cumulative BrdU labeling in the SEZ of mammals have shown that within a single adult niche regional variation exists, demonstrating the greatest growth fraction of BrdU+ cells in the dorsolateral region of the SEZ with a total cell cycle time of 12.7 hours and S-phase length of 4.2 hours (Morshead and van der Kooy, 1992). We found that the number of proliferating BrdU+ cells labeled in the PVZ of D, Vv, Dm, and Dl continued to increase in size (i.e., growth fraction) beyond the endpoint of our study (12.5 hours), with the niche of Vv having the greatest estimated minimum growth fraction ($\sim$29%). From the minimum growth fraction estimates of these niches, our findings indicate the presence of relatively slowly cycling cell populations, with the total length of the cell cycle ranging from $\sim$15 to 23 hours. In contrast, the niche of Ppa and the first of two potential cell populations within Vd displayed properties suggestive of relatively fast cycling cells, with cell cycle lengths of $\sim$7.5 hours and 11 hours, respectively.

Our results are in partial agreement with one previous study using co-labeling of BrdU+/PCNA+ cells to detect slow and fast mitotic populations across similar niches as examined here (Adolf et al., 2006). These authors propose the existence of fast dividing cells within the subpallial niches of Vv and Ppa, with the remaining niches consisting of slow dividing cells and also propose that this latter population continues to increase over 10 days. However, because only the growth fraction was reported from the different niches assessed in the previous study, it is difficult to make direct comparisons with the cell cycle kinetics revealed in our study. Furthermore, a limitation in our analysis is that we cannot precisely identify which cell type is cycling at a given estimated cell cycle time within the different PVZs. Nonetheless, our data suggest that in D, Vv, Dm, and Dl all three proliferative cell

types present (type IIa, III, IVa) are cycling at similar rates, whereas this may not be the case in the niche of Vd that demonstrated possible evidence of two different proliferative populations. Future studies aimed at tracking specific cell type are required to gain a richer understanding of the population kinetics of the niche.

Toward a more comprehensive view of the phenotype of cells composing neurogenic niches and regulating neuronal output in the adult zebrafish forebrain

The ability to classify the cell types within the microenvironment of the niche by phenotype and lineage is critical to permit comparisons with the cellular organization of different species and to understand differences in the molecular control of these cells. In line with earlier studies (Ganz et al., 2010; Marz et al., 2010), our work has shown the presence of at least two separate glial cell populations within PVZs, including morphologically distinct cell populations immunopositive for BrdU and S100β or BrdU and GS, some demonstrating the presence of cilia. Similar to Ganz and colleagues (2010), we showed a complete absence of the canonical radial glia marker GS in the subpallial niches of Vv and Ppa, and only minimal BrdU+/GS+ expression in Vd, compared with the pallial niches of D, Dm, and Dl. Moreover, all pallial niches also showed larger BrdU+/S100β+ populations. The above studies align well with our classification scheme based on the morphological cell phenotypes identified at the ultrastructural level across PVZs. First, subpopulations of BrdU+, S100β+, or GS+ type IIa cells were absent within the niche of Vv, and the ventral zone of the niche of Ppa, but could be detected in all other niches examined displaying features of radial glial cells. Second, populations of type III and IVa cells, a subset that is immunopositive for BrdU and S100β, almost exclusively composed the PVZ of Vv and Ppa (ventral zone), but could be observed in all niches.

In this study we also discovered rare proliferative pools of cells immunopositive for BrdU/Sox2 and BrdU/Pax6. The pattern of Sox2 staining seen here is in line with *sox2* mRNA and protein expression previously shown by using in situ hybridization and additional Sox2 antibodies within the medial niches of the rostral forebrain, with subpopulations of this marker co-labeling with cycling cells (Adolf et al. 2006; Lam et al., 2009; Marz et al., 2010). A notable difference however, was the more limited Sox2 labeling seen in our experiments, which might be related to the older adult age of fish used in the current study. Unlike the small degree of Sox2 labeling observed, populations of Pax6-labeled cells were more widespread, although in most cases these cells were detected adjacent to the boundaries of PVZs where few BrdU+ cells were situated following a 2-hour chase period. Expression of the transcription factor Pax6 is well known to play a critical role during teleostean (Wullimann and Rink, 2002) and mammalian (Sakara and Osumi, 2008) forebrain development. Given the highly conserved nature of the Pax6 antibody used here, the expression pattern of Pax6 is likely indicative of Pax6a labeling. Nevertheless, we cannot rule out the possibility that a fraction of Pax6b+ cells are also being labeled. Earlier work by Adolf and colleagues (2006) used in situ hybridization to demarcate the expression of *pax6a* mRNA lateral to, and *pax6b* mRNA within, the medial forebrain proliferative zones of the adult zebrafish. These findings suggest that the Pax6+ cell populations detected here may in fact be a combination of both Pax6a- and Pax6b-expressing cell types, at least in corresponding niches, including the medial PVZ of D and Dm and the PVZ of Vd and Vv.

However, here we additionally documented a small number of Pax6-labeled cells within the PVZ of Dl and Ppa, and also observed BrdU+/Pax6+ cells exclusively within the boundaries of the niche. Both Sox2 and Pax6 have been used extensively as stem cell markers, and in the adult zebrafish forebrain Sox2 expression has been associated with defining progenitor cell types within neurogenic zones (Marz et al., 2010). The infrequent detection of cycling Pax6+ (PVZ of Dl) and Sox2+ (PVZ of Ppa) cells makes these phenotypes potential candidates for slow cycling stem/progenitor populations.

Marz and colleagues (2010) reported the phenotype of four progenitor cell types within niches lining the telencephalic ventricle, consisting of nondividing radial glia (type I), dividing radial glia (type II), dividing radial glia with PSA-NCAM expression (type IIIa), and nonglial PSA-NCAM+ progenitors (type IIIb). With the exception of type IIIb, all other cell types were seen to exhibit strong nestin+ expression. In fitting our ultrastructural classification in with the above progenitor phenotypes, it would appear that our type IIa cells align most closely with type II progenitors as evidenced both by immunolabeling and by the location of these cells in the dorsomedial (Vd, D, Dm) and lateral niches (Dl). These cells were immunopositive for the two glial markers (S100β, GS) as well as the S-phase marker BrdU. Long processes could further be seen radiating into the deeper cell layers in medially located niches, and a high occurrence of type IIa cells could be observed in the PVZs of D, Vd, Dm, Dl and the dorsal zone of Ppa. More challenging is correlating BrdU+ and S100β+ type III and IVa cells with the above progenitor classification given that the location of these cells agrees with the subpallial position of progenitor cells in the niche of Vv and Ppa.

However, the difficulty of successfully immunolabeling these cell types with multiple markers at the

ultrastructural level limits the degree to which we may infer their phenotype. The positive immunogold labeling for S100β and BrdU for both type III and IVa cells seen in our data likely suggests one of these two cell types as candidates for the type IIIa progenitor phenotype proposed by Marz et al. (2010). From the above comparisons between immunolabeling and ultrastructural studies, we propose that type IIa cells, or at least a subpopulation of these, is of a radial glial phenotype. However, the lineage relationship of the cell types identified within the adult forebrain neurogenic niches of the zebrafish remains an open question that will require further detailed analyses before comparisons of the different cell phenotypes proposed between laboratories can be accurately presented.

Adult-born neurons commonly undergo radial or tangential migration to arrive at locations outside the boundaries of the niche and become committed to a specific neurotransmitter-expressing phenotype. Because our findings showed that approximately 50% or more BrdU+ cells give rise to newborn neurons across PVZs (Fig. 17G), by tracking proliferative cells over time we were able to evaluate the displacement of differentiating cells. Our data show that cell displacement continues up until 8 months, with newborn neurons in most PVZs having migrated radially toward the parenchyma from their initial position by this time. Whether the rate of displacement by newborn cells is correlated with the time required for a neuronal-specific phenotype to become specified during the process of migration remains unknown. However, only 1 week post-BrdU injections, co-labeling of BrdU+/HuC/D+ cells could be detected in all niches. Adolf et al. (2006) showed that as early as 3 days post-BrdU injection, newborn neurons could be detected, with proportions reaching a maximum after 2 weeks. Our experiments investigating the timeline of neuronal differentiation revealed a nearly identical pattern, with PVZs displaying the greatest proportion of differentiated neurons at 2 weeks and consisting of 40–80% of the BrdU+ cell population. By 4 weeks, however, a drop in the percentage of newly differentiated neurons was noted across most niches.

Furthermore, these data show that the number of differentiated neurons between 2 and 4 weeks decreases by approximately 20% in the niches of Dm and Ppa, which may be a result of greater apoptotic activity. To our surprise, at 4 weeks only a small number of calbindin+/BrdU+ cells were detected in the niche, with no co-labeling of BrdU with TH or a transgenic marker of GABAergic neurons, *Tg[dlx5a/6aIG:gfp]*. Long-term chase experiments of up to 270 days in related proliferative zones have shown a complete absence of calbindin+/BrdU+ labeling (Zupanc et al., 2005). However, newly differentiated subtypes of TH+ and *gad67*+ neurons have been identified 2 months after BrdU injections in the rostral telencephalon (Adolf et al., 2006), and indicate that these neuronal subpopulations require a longer time period than used here, in order to become committed to one of these two subtypes. Aside from the length of the differentiation period, our data suggest that mitotic cells arising from PVZs might instead give rise to alternative neuronal phenotypes than those examined here, such as glutamatergic or cholinergic neurons. Determining the neuronal-specific phenotype of cells generated from neurogenic niches will be an important step in elucidating their functional role in the mature CNS.

CONCLUSIONS

We propose a model illustrating differences in the cellular organization of forebrain neurogenesis in zebrafish niches and a novel classification scheme of the seven morphologically distinct cell types composing these niches. Of these cell types, our data suggest that cycling type IIa cells are a likely candidate for the morphological phenotype of radial glial-like stem cells. Our studies also revealed that pallial and subpallial niches harbor differences in their cellular organization. Finally, by investigating the cell cycle characteristics and rates of neuronal differentiation between niches, we show that although similar cell types are distributed among forebrain niches, the frequency of these cells and how they are regulated within the niche to give rise to adult born neurons vary widely. The findings presented here should serve as a foundation for investigating the lineage relationships of cells within these niches as well as the degree to which they undergo neurogenic plasticity.

ACKNOWLEDGMENT

The authors thank Gunther Zupanc (Northeastern University, Boston, MA) for technical advice on zebrafish perfusions; Marc Ekker (University of Ottawa, Canada), and Ian Scott (University of Toronto, Canada) for transgenic zebrafish lines; Robert Temkin and Henry Hong (University of Toronto, Canada) for their assistance with immuno-TEM, SEM, and confocal imaging; Bryan Stewart (University of Toronto, Canada) for statistical advice; and Sabrina Hossain and Bonnie Chu for general technical assistance.

LITERATURE CITED

Adolf B, Chapouton P, Lam CS, Topp S, Tanhauser B, Strahle U, Gotz M, Bally-Cuif L. 2006. Conserved and acquired features of adult neurogenesis in the zebrafish telencephalon. Dev Biol 295:278–293.

Alvarez-Buylla A, Lim DA. 2004. For the long run: maintaining germinal niches in the adult brain. Neuron 41:683–686.

Amador-Arjona A, Elliott J, Miller A, Ginbey A, Pazour GJ, Enikolopov G, Roberts AJ,TerskikhAV. 2011. Primary cilia

regulate proliferation of amplifying progenitors in adult hippocampus: implications for learning and memory. J Neurosci 31:9933–9944.

Broglio C, Gomez A, Duran E, Ocana FM, Jimenez-Moya F, Rodriguez F, Salas C. 2005. Hallmarks of a common forebrain vertebrate plan: specialized pallial areas for spatial, temporal and emotional memory in actinopterygian fish. Brain Res Bull 66:277–281.

Buddensiek J, Dressel A, Kowalski M, Runge U, Schroeder H, Hermann A, Kirsch, Storch A, Sabolek M. 2010. Cerebrospinal fluid promotes survival and astroglial differentiation of adult human neural progenitor cells but inhibits proliferation and neuronal differentiation. BMC Neurosci 11:48.

Castro A, Becerra M, Manso MJ, Anadon R. 2006. Calretinin immunoreactivity in the brain of the zebrafish, *Danio rerio*: distribution and comparison with some neuropeptides and neurotransmitter-synthesizing enzymes. II. Midbrain, hindbrain, and rostral spinal cord. J Comp Neurol 494: 792–814.

Chapouton P, Skupien P, Hesl B, Coolen M, Moore JC, Madelaine R, Kremmer E, Faus-Kessler T, Blader P, Lawson ND, Bally-Cuif L. 2010. Notch activity levels control the balance between quiescence and recruitment of adult neural stem cells. J Neurosci 30:7961–7974.

Crosnier C, Vargesson N, Gschmeisser S, Ariza-McNaughton L, Morrison A, Lewis J. 2005. Delta-Notch signalling controls commitment to a secretory fate in the zebrafish intestine. Development 132:1093–1104.

Dimitrov E, Usdin TB. 2010. Tuberoinfundibular peptide of 39 residues modulates the mouse hypothalamic-pituitary-adrenal axis via paraventricular glutamatergic neurons. J Comp Neurol 518:4375–4394.

Doetsch F, Garcia-Verdugo JM, Alverez-Buylla A. 1997. Cellular composition and three-diemensional organization of the subventricular germinal zone in the adult mammalian brain. J Neurosci 17:5046–5061.

Doetsch F, Caille I, Lim DA, Garcia-Verdugo JM, Alverez-Buylla A. 1999. Suventricular zone astrocytes are neural stem cells in the adult mammalian brain. Cell 97:703–716.

Font E, Desfilis E, Perez-Canellas MM, Garcia-Verdugo JM. 2001. Neurogenesis and neuronal regeneration in the adult reptilian brain. Brain Behav Evol 58:276–295.

Ganz J, Kaslin J, Hochmann S, Fredenreich D, Brand M. 2010. Heterogeneity and Fgf dependence of adult neural progenitors in the zebrafish telencephalon. Glia 58: 1345–1363.

Garcia-Verdugo JM, Ferron S, Flames N, Collado L, Desfilis E, Font E. 2002. The proliferative ventricular zone in adult vertebrates: a comparative study using reptiles, birds, and mammals. Brain Res Bull 57:765–775.

Geuna S. 2005. The revolution of counting "tops": two decades of the disector principle in morphological research. Microsc Res Tech 66:270–274.

Gil-Perotin S, Duran-Moreno M, Belzunegui S, Luquin MR, Garcia-Verdugo JM. 2009. Ultrastructure of the subventricular zone in *Macaca fascicularis* and evidence of a mouse-like migratory stream. J Comp Neurol 514:533–554.

Gotz M, Hartfuss E, Malatesta P. 2002. Radial glial cells as neuronal precursors: a new perspective on the correlation of morphology and lineage restriction in the developing cerebral cortex of mice. Brain Res Bull 57:777–788.

Grandel H, Kaslin J, Granz J, Wenzel I, Brand M. 2006. Neural stem cells and neurogenesis in the adult zebrafish brain: origin, proliferation dynamics, migration and cell fate. Dev Biol 295:263–277.

Grupp L, Wolburg H, Mack AF. 2010. Astroglial structures in the zebrafish brain. J Comp Neurol 518:4277–4287.

Hinsch K, Zupanc GKH. 2007. Generation and long-term persistence of new neurons in the adult zebrafish brain: a quantitative analysis. Neuroscience 146:679–696.

Kam M, Curtis MA, McGlasha SR, Connor B, Nannmark U, Faull RL. 2009. The cellular composition and morphological organization of the rostral migratory stream in the adult human brain. J Chem Neuroanat 37:196–205.

Kaslin J, Ganz J, Geffarth M, Grandel H, Hans S, Brand M. 2009. Stem cells in the adult zebrafish cerebellum: initiation and maintenance of a novel stem cell niche. J Neurosci 29:6142–6153.

Kee N, Sivalingam S, Boonstra R, Wojtowicz JM. 2002. The utility of Ki-67 and BrdU as proliferative markers of adult neurogenesis. J Neurosci Methods 115:97–105.

Kim W-Y, Shen J. 2008. Presenilins are required for maintenance of neural stem cells in the developing brain. Mol Neurodegener 3:2.

Kishimoto N, Alfaro-Cervello C, Shimizu K, Asakawa K, Urasaki A, Nonaka S, Kawakami K, Garcia-Verdugo JM, Sawamoto K. 2011. Migration of neuronal precursors from the telencephalic ventricular zone into the olfactory bulb in adult zebrafish. J Comp Neurol 519:3549–3565.

Lam CS, Marz M, Strahle U. 2009. Gfap and nestin reporter lines reveal characteristics of neural progenitors in the adult zebrafish brain. Dev Dyn 238:475–486.

Lindsey BW, Tropepe V. 2006. A comparative framework for understanding the biological principles of adult neurogenesis. Prog Neurobiol 80:281–307.

MacDonald RB, Debiais-Thibaud M, Talbot JC, Ekker M. 2010. The relationship between dlx and gad1 expression indicates highly conserved genetic pathways in the zebrafish forebrain. Dev Dyn 239:2298–2306.

Marquardt T, Ashery-Padan R, Andrejewski N, Scardigli R, Guillemot F, Gruss P. 2001. Pax6 is required for the multipotent state of retinal progenitor cells. Cell 105:43–55.

Marusich MF, Furneaux HM, Henion PD, Weston JA. 1994. Hu neuronal proteins are expressed in proliferating neurogenic cells. J Neurobiol 25:143:155.

Marz M, Chapouton P, Diotel N, Vaillant C, Hesl B, Takamiya M, Lam CS, Kah O, Bally-Cuif L, Strahle U. 2010. Heterogeneity in progenitor cell subtypes in the ventricular zone of the zebrafish adult telencephalon. Glia 58:870–888.

Mirzadeh Z, Merkle FT, Soriano-Navarro M, Garcia-Verdugo JM, Alvarez-Buylla A. 2008. Neural stem cells confer unique pinwheel architecture to the ventricular surface in neurogenic regions of the adult brain. Cell Stem Cell 3: 265–278.

Mirzadeh Z, Han Y-G, Soriano-Navarro M, Garcia-Verdugo JM, Alvarez-Buylla A. 2010. Cilia organize ependymal planar polarity. J Neurosci 30:2600–2610.

Morrison SJ, Spradling AC. 2008. Stem cells and niches: mechanisms that promote stem cell maintenance throughout life. Cell 132:598–611.

Morshead CM, Garcia D, Sofroniew MV, van der Kooy D. 2003. The ablation of glial fibrillary acidic protein-positive cells from the adult central nervous system results in the loss of forebrain neural stem cells but not retinal stem cells. Eur J Neurosci 18:76–84.

Morshead CM, van der Kooy D. 1992. Postmitotic death is the fate of constitutively proliferating cells in the subependymal layer of the adult mouse brain. J Neurosci 12: 249–256.

Nowakowski RS, Lewin SB, Miller MW. 1989. Bromodeoxyuridine immunohistochemical determination of the lengths of the cell cycle and the DNA-synthetic phase for an anatomically defined population. J Neurocytol 18:311–318.

Pellegrini E, Mouriec K, Anglade I, Menuet A, Le Page Y, Gueguen M-M, Marmignon M-H, Brion F, Pakdel F, Kah O.

2007. Identification of aromatase-positive radial glial cells as progenitor cells in the ventricular layer of the forebrain in zebrafish. J Comp Neurol 501:150–167.
Perez-Canellas MM, Garcia-Verdugo JM. 1996. Adult neurogenesis in the telencephalon of a lizard: a [^{3}H]thymidine autoradiographic and bromodeoxyuridine immunocytochemical analysis. Dev Brain Res 93:49–61.
Perez-Sanchez F, Molowny A, Garcia-Verdugo JM, Lopez-Garcia C. 1989. Postnatal neurogenesis in the nucleus sphericus of the lizard, *Podarcis hispanica*. Neurosci Lett 106:71–75.
Roesch K, Jadhav AP, Trimarchi JM, Stadler MB, Roska B, Sun BB, Cepko CL. 2008. The transcriptome of retinal muller glial cells. J Comp Neurol 509:225–238.
Rothenaigner I, Krecsmarik M, Hayes JA, Bahn B, Lepier A, Fortin G, Gotz M, Jagasia R, bally-Cuif L. 2011. Clonal analysis by distinct viral vectors identifies bona fide neural stem cells in the adult zebrafish telencephalon and characterizes their division properties and fate. Dev Stem Cell 138:1459–1469.
Rougon G, Dubois C, Buckley N, Magnani JL, Zollinger W. 1986. A monoclonal antibody against meningococcus group B polysaccharides distinguishes embryonic from adult N-CAM. J Cell Biol 103:242924–232937.
Rousselot P, Nottebohm F. 1995. Expression of polysialylated N-CAM in the central nervous system of adult canaries and its possible relation to function. J Comp Neurol 356: 629–640.
Sakurai K, Osumi N. 2008. The neurogenesis-controlling factor, Pax6, inhibits proliferation and promotes maturation in murine astroctyes. J Neurosci 28:4604–4612.
Salas C, Broglio C, Duran E, Gomez A, Ocana FM, Jimenez-Moya F, Rodriguez F. 2006. Neuropsychology of learning and memory in teleost fish. Zebrafish 3:157–171.
Sanai N, Nguyen T, Ihrie RA, Mirzadeh Z, Tsai H-H, Wong M, Gupta N, Berger MS, Huang E, Garcia-Verdugo J-M, Rowitch DH, Alvarez-Buylla A. 2011. Corridors of migrating neurons in the human brain and their decline during infancy. Nature 478:382–387.
Sawamoto K, Hirota Y, Alfaro-Cervello C, Soriano-Navarro M, He X, Hayakawa-Yano Y, Yamada M, Hikishima K, Tabata H, Iwanami A, Alvarez-Buylla A, Garcia-Verdugo JM, Okano H. 2011. Cellular composition and organization of the subventricular zone and rostral migratory stream in the adult and neonatal common marmoset brain. J Comp Neurol 519:690–713.
Schmidt C, Hof PR. 2005. Design-based stereology in neuroscience. Neuroscience 130:813–831.
Schmidt M, Derby CD. 2011. Cytoarchitecture and ultrastructure of neural stem cell niches and neurogenic complexes maintaining adult neurogenesis in the olfactory midbrain of spiny lobsters, *Panulirus argus*. J Comp Neurol 519: 2283–2319.
Seki T, Arai Y. 1995. Age-related production of new granule cells in the adult dentate gyrus. Neuroreport 6:2479–2482.
Seri B, Garcia-Verdugo JM, McEwen B, Alvarez-Buylla A. 2001. Astrocytes give rise to new neurons in the adult mammalian hippocampus. J Neurosci 21:7153–7160.
Seri B, Garcia-Verdugo J-M, Collado-Morente L, McEwen BS, Alvarez-Buylla A. 2004. Cell types, lineage, and architecture of the germinal zone in the adult dentate gyrus. J Comp Neurol 478:359–378.
Shen Q, Wang Y, Kokovay E, Lin G, Chuang S-M, Goderie SK, Roysam B, Temple S. 2008. Adult SVZ stem cells lie in a vascular niche: a quantitative analysis of niche cell-cell interactions. Cell Stem Cell 3:289–300.
Silvestroff L, Bartucci S, Soto E, Gollo V, Pasquini J, Franco P. 2010. Cuprizone-induced demyelination in CNP::GFP transgenic mice. J Comp Neurol 518:2261–2283.
Sofroniew MV, Vinters HV. 2010. Astrocytes: biology and pathology. Acta Neuropathol 119:7–35.
Souza BR, Romano-Silva MA, Tropepe V. 2011. Dopamine D_2 receptor activity modulates Akt signalling and alters GABAergic neuron development and motor behaviour in zebrafish larvae. J Neurosci 31:5512–5525.
Steiner B, Klempin F, Wang L, Kott M, Kettenmann H, Kempermann G. 2006. Type-2 cells as link between glial and neuronal lineage in adult hippocampal neurogenesis. Glia 54:805–814.
Taupin P. 2007. BrdU immunohistochemistry for studying adult neurogenesis: paradigms, pitfalls, limitations, and validation. Brain Res Rev 53:198–214.
Tavazoie M, Van der Veken L, Silva-Vargas V, Loussaint M, Colonna L, Zaida B, Garcia-Verdugo JM, Doetsch F. 2008. A specialized vascular niche for adult neural stem cells. Cell Stem Cell 3:279–288.
Topp S, Stigloher C, Kormisarczuk AZ, Adolft B, Becker TS, Bally-Cuif L. 2008. Fgf signalling in the zebrafish adult brain: association of Fgf activity with ventricular zones but not cell proliferation. J Comp Neurol 510:422–439.
Tseng Y-Y, Gruzdeva N, Li A, Chuang J-Z, Sung C-H. 2010. Identification of the Tctex-1 regulatory element that directs expression to neural stem/progenitor cells in developing and adult brain. J Comp Neurol 518:3327–3342.
Uyttebroek L, Shepherd IT, Harrisson F, Hubens G, Blust R, Timmermans J-P, Van Nassauw L. 2010. Neurochemical coding of enteric neurons in adult and embryonic zebrafish (*Danio rerio*). J Comp Neurol 518:4419–4438.
Wainwright MS, Craft JM, Griffin WS, Marks A, Pineda J, Padgett KR, Van Eldik LJ. 2004. Increased susceptibility of S100β transgenic mice to perinatal hypoxia-ischemia. Ann Neurol 56:61–67.
Wang T-W, Stromberg GP, Whitney JT, Brower NW, Klymkowsky MW, Parent JM. 2006. Sox3 expression identified neural progenitors in persistent neonatal and adult mouse forebrain germinative zones. J Comp Neurol 496:88–100.
West MJ. 1999. Stereological methods for estimating the total number of neurons and synapses: issues of precision and bias. Trends Neurosci 22:51–61.
Wong K, Weadick CJ, Kuo C, Chang BSW, Tropepe V. 2010. Duplicate dmbx1 genes regulate progenitor cell cycle and differentiation during zebrafish midbrain and retinal development. BMC Dev Biol 10:100
Wullimann MF, Rink E. 2002. The teleostean forebrain: a comparative and developmental view based on early proliferation, *Pax6* activity and catecholaminergic organization. Brain Res Bull 57:363–370.
Wullimann MF, Rupp B, Reichert H. 1996. Neuroanatomy of the zebrafish brain: a topological atlas. Basel: Birkhauser. p 1–144.
Yang M, Cagle MC, Honig MG. 2010. Identification of cerebellin2 in chick and its preferential expression by subsets of developing sensory neurons and their targets in the dorsal horn. J Comp Neurol 518:2818–2840.
Zhao C, Deng W, Gage FH. 2008. Mechanisms and functional implications of adult neurogenesis. Cell 132:645–660.
Zupanc GKH. 2001. A comparative approach towards the understanding of adult neurogenesis. Brain Behav Evol 58:246–249.
Zupanc GKH, Zupanc MM. 1992. Birth and migration of neurons in the central posterior/prepacemaker nucleus during adulthood in weakly electric knifefish (*Eigenmannia* sp.). Proc Natl Acad Sci U S A 89:9539–9543.
Zupanc GKH, Hinsch K, Gage FH. 2005. Proliferation, migration, neuronal differentiation, and long-term survival of new cells in the adult zebrafish brain. J Comp Neurol 488:290–319.
Zupanc GKH, Wellbrock UM, Sirbulescu RF, Rajendran RS. 2009. Generation, long-term persistence, and neuronal differentiation of cells with nuclear aberrations in the adult zebrafish brain. Neuroscience 159:1338–1348.